Parameter Estimation and Application for Static Nonlinear and Dynamic Linear Systems

Lin Ye

Supervisor: A/Prof. Steven W. Su

Faculty of Engineering and Information Technology
University of Technology Sydney

This dissertation is submitted for the degree of
Doctor of Philosophy

May 2018

Declaration

I hereby declare that except where specific reference is made to the work of others, the contents of this dissertation are original and have not been submitted in whole or in part for consideration for any other degree or qualification in this, or any other university. This dissertation is my own work and contains nothing which is the outcome of work done in collaboration with others, except as specified in the text and Acknowledgements.

Production Note:

Signature: Signature removed prior to publication.

Date: 17/05/2018

Acknowledgements

I would like to express my sincere gratitude to my supervisor A/Prof. Steven W. Su for his continual support, guidance, help and encouragement during my PhD study. A/Prof. Steven W. Su has brought me into the topics of parameter estimation and system identification, and provided brilliant insights in my research work. It is my honor to have a supervisor who always inspires me to achieve higher targets and overcome difficulties. His conscientious and meticulous attitude on research has significant influence on my work.

I am grateful to Prof. Hung T. Nguyen (Swinburne University of Technology) for his kind support. I would also like to thank Dr. Ying Guo (Commonwealth Scientific and Industrial Research Organisation), and Prof. Branko G. Cellar (University of New South Wales) for their support.

I am also grateful to my colleagues in A/Prof. Steven W. Su' research group, in particular, Ahmadreza Argha, Tao Zhang, Wentian Zhang, Hairong Yu, Yao Huang, etc., for their selfless help. Working together with them will be a good memory. I am also grateful to my friends, Zhichao Sheng, Ye Shi, Haimin Zhang, Zhiyuan Shi, Daniel Roxby.

My deepest gratitude goes to my parents for their immeasurable support and encouragement throughout my graduate studies.

Abstract

General issues associated with parameter estimation have been extensively studied. During the past several decades, a vast number of methods have been developed for solving different parameter estimation issues in different areas. Thanks to numerous newly-introduced areas, the parameter estimation and its related techniques still play important roles and need to be expanded to solve new challenges. Since the research topics of parameter estimation are extremely wide, this dissertation is concerned with two topics within parameter estimation related to calibration of MEMS accelerometer and modelling of oxygen uptake.

It is challenging to obtain the unknown parameters of tri-axial accelerometer accurately based on auto-calibration as the cost function is nonlinear and non-convex. Furthermore, it is more challenging to solve this nonlinear and non-convex cost function online to overcome the variation of parameter caused by the external change of environment. To overcome these challenges, an iterative parameter estimation method with the experimental design to solve the accelerometer model is proposed. Furthermore, two algorithms are explored based damped recursive estimation and expectation maximum algorithm to online estimate the unknown parameter in the model. This topic can be summarised as a parameter estimation problem of a special nonlinear static system. Over the past decades, the modelling of oxygen uptake response to exercise has always been a challenging topic due to measurement noise, insufficient stimulations of the system and individual differences of human beings. To overcome these difficulties, a nonparametric estimation method is investigated for the modelling of oxygen uptake response and ensure its accuracy and reliability. The second topic can be summarised as a parameter estimation problem of a noisy dynamic linear system

with limited stimulation. These two topics are highly prized for academic significance but also remained open due to their challenges in mathematics.

First, for parameter estimation problem of the offline auto-calibration of accelerometer, a 6-orientation G-optimal experimental scheme is proposed for a special second-degree model based on the statistical experimental design. Then, a new linearisation approach is developed to apply the proposed G-optimal experimental scheme. Then, a convergence-guaranteed recursive parameter estimation algorithm is developed that can be easily implemented in a portable wearable device. The region of convergence of the proposed algorithm is proved. Numerous simulations and experiments are carried out to validate the efficiency of the proposed method.

Second, for parameter estimation problem of the online auto-calibration of accelerometer, a linearisation method of the 6-parameter tri-axial accelerometer model is explored. Then, a modified damped recursive least square (MDLRS) estimation method is proposed to estimate the unknown parameters in real time. Meanwhile, the MDRLS can iteratively remove the bias caused by the linearisation during the online estimation process. The convergence speed and estimation effectiveness of the proposed method are discussed based on both simulations and experiments. The results show that the proposed method can achieve similar accuracy with significantly fewer measurements. In the end, the region of convergence of the proposed online estimation method is analysed and discussed based on Monte Carlo simulation. Simulations and experiments also demonstrate the performance of the proposed method.

Third, in real life, the misalignments exist between axes for some tri-axial accelerometers. Therefore, the 9-parameter model can achieve higher accuracy for those accelerometers. However, this model will reduce accuracy for those accelerometers without misalignments. To online estimate the unknown parameter with automatic model selection of tri-axial accelerometer, a sparse least square (SPARLS) estimation is explored. To apply this SPARLS, a linearisation method of the 9-parameter model is proposed. Based on the linearised method, the SPARLS is modified to solve the unknown parameter in real time while penalising the insufficient parameters. Therefore, the model of tri-axial accelerometer can be adjusted automatically in real time to remove the insignificant parameters caused by noise. Then, the conditions for the con-

vergence of this iterative approach are identified and investigated based on simulations for different situations. A self-designed device is also used to validate the performance of the proposed algorithm.

Forth, for modelling oxygen uptake response to exercise system, a nonparametric estimation method for impulse response is developed to identify any order systems. To estimate the impulse response based on a simple step input signal, a novel kernel-based estimation method is investigated. The proposed method can efficiently reduce the order of impulse response model by incorporating a $\mathcal{L}_1$ norm penalty term. Furthermore, the overall penalty terms can be converted into a special elastic net to simplify the calculation procedure. Then, to consider the prior information, kernels are investigated by extensive simulations, and the stable spline (SS) kernel is recommended as the best candidate. It is demonstrated by experiments and simulations that the proposed method is efficient for the modelling of impulse response of oxygen uptake to dynamic exercise, which often confronts a highly noised measurement under the stimulation of a simple input signal. Finally, an averaged impulse response model is established, which can quantitatively describe the oxygen uptake on-kinetics for treadmill exercise.

Publications

The contents of this thesis are based on the following papers that have been published, accepted, or submitted to peer-reviewed journals and conferences.

Journal Papers:

1. Lin Ye, Ying Guo, and Steven W. Su, "An Efficient Autocalibration Method for Triaxial Accelerometer," *IEEE Transactions on Instrumentation and Measurement*, vol. 66, no. 9, pp. 2380-2390, June 2017.

2. Lin Ye, Ahmadreza Argha, Branko G Celler, Hung T. Nguyen and Steven W, Su, "Online Auto-calibration of Triaxial Accelerometer with time-variant model structures," *Sensors and Actuators A: Physical*, vol. 266, pp. 294-307, October 2017.

3. Lin Ye, Ahmadreza Argha, Branko G Celler, Hung T. Nguyen and Steven W, Su, "Dynamic Characteristics of Oxygen Uptake," *BioMedical Engineering OnLine*, vol. 17, no. 1, pp. 44-62, April 2018

4. Lin Ye, et al, "A Fast-Converge Real-time Auto-Calibration Algorithm for Triaxial Accelerometer," under second round of review at *IEEE Transactions on Instrumentation and Measurement*, 2017.

5. Hairong Yu, Lin Ye, et al "Nonparametric Dynamical Model of Cardiorespiratory Responses at the Onset and Offset of Treadmill Exercises," under second round of review at *Medical & Biological Engineering & Computing*, 2017.

Conference Papers:

1. Lin Ye, Ahmadreza Argha, Branko G Celler, Yi Zhang, Hung T. Nguyen and Steven W, Su, "Nonparametric modelling of VO 2 response to exercise," in *Proc. 2017 39th International Conference of IEEE Engineering in Medicine and Biology Society*, pp. 1525-1528, July 2017.

2. Lin Ye, et al, "An online recursive autocalibration of triaxial accelerometer," in *Proc. 2016 38th International Conference of IEEE Engineering in Medicine and Biology Society*, pp. 2038-2041, July 2016.

3. Lin Ye, et al, "Inertial Sensor based Post Fall Analysis for False Alarming Reduction," in *Proc. 2016 Telehealth and Assistive Technology*, pp. 864-011, October 2016.

4. Lin Ye, and Steven W. Su "Experimental design for the calibration of tri-axial Magnetometers," in *Proc. 2015 9th International Conference on Sensing Technology* , pp. 864-011, October 2016.

5. Lin Ye, and Steven W. Su "Optimum Experimental Design applied to MEMS accelerometer calibration for 9-parameter auto-calibration model," in *Proc. 2015 37th International Conference of IEEE Engineering in Medicine and Biology Society*, July 2015.

6. Admadreza Argha, Lin Ye, Steven W. Su, and Branko G. Celler "Real-time modelling of heart rate response during exercise using a novel constrained parameter estimation method," in *Proc. 2016 38th International Conference of IEEE Engineering in Medicine and Biology Society*, July 2016.

7. Admadreza Argha, Lin Ye, Steven W. Su, and Branko G. Celler "Heart rate regulation during cycle-ergometer exercise using damped parameter estimation method," in *Proc. 2016 38th International Conference of IEEE Engineering in Medicine and Biology Society*, July 2016.

Table of contents

List of figures

List of tables

Chapter 1

Introduction

This chapter starts with the motivation and scope of this thesis, then introduces some related research topics, and finally shows outlines of this thesis.

1.1 Motivation and Scope

General issues associated with parameter estimation have been extensively studied for decades. In the past years, a vast number of methods have been developed for tacking parameter estimation issues in different areas. Generally, the model of parameter estimation can be considered from different points of view, from linear model to nonlinear model, and from static model to dynamic model. Due to extensive researches on parameter estimation, the theoretical solutions of parameter estimation for linear static systems and linear dynamic systems have been well developed. Although the methods for linear systems are well developed, there still exist lots of problems related to nonlinear parameter estimation. And some questions are difficult to solve by conventional parameter estimation methods. As we know, parameter estimation is an extremely wide research area including a massive number of topics. Therefore, for this research, we focused on two parameter estimation problems and their related topics. The first part is related to the calibration of tri-axial accelerometer, which can be formulated as a parameter estimation problem for a nonlinear non-convex function. The second part is a parameter estimation problem related to the modelling of oxygen

uptake response to exercise, which can be considered as a parameter estimation problem with insufficient stimulations and large measurement noise.

Recently, engineers and researchers from industries and academics have raised lots of interests in MEMS type inertial measurement unit (IMU), as it can provide important information for health morning devices [1–4], navigation systems [5, 6], fault detection systems [7, 8], etc. All applications mentioned above required accurate readings from IMU. However, due to the limitation of manufacturing techniques, the reading of accelerometer is often suffered from large bias and instability. Therefore, to obtain accurate measurements from MEMS accelerometer, calibration is always necessary. Traditional, the calibration of accelerometer requires a precise turntable which is normally difficult to access by most researchers and engineers.

In order to calibrate the accelerometer without sophisticated equipment, recently, a new calibration method called auto-calibration has been proposed. The idea of this auto-calibration is based on the fact that the overall acceleration of tri-axial accelerometer is the local acceleration ('1g') in the static state. Based on this method, the tri-axial accelerometer only needs to be orientated to several different orientations. Based on the measurements from those orientations, the accelerometer can be calibrated without extra equipment. Comparing with classical calibration methods, the auto-calibration can also achieve the deserved accuracy. However, there are several aspects can be improved by for the auto-calibration method. Generally, the auto-calibration methods can be categorised as offline method and online method: 1) Offline method, the estimated parameters are computed based on all the necessary measurements; 2) Online method, the estimated parameters will be updated whenever a valid new measurement is obtained. For the offline auto-calibration, the selection of orientations has not been theoretically discussed based on the theory of experimental design. Furthermore, due to the difficulty of online parameter estimation of the nonlinear non-convex model, there lacks discussion of the online calibration. Last but not least, the automatic model selection of online calibration can remove the incorrect estimation caused by noise. An online parameter estimation with the automatic model selection can furthermore improve the accuracy of calibration. In general, the goals of the research in this part of the dissertation can be summarised as:

- To implement the experimental design in the accelerometer calibration, the accelerometer calibration problem and experimental design are studied. Then, a suitable experimental scheme is proposed based on selected index of design of experiment (DoE), and the constraint of the input signal should be considered. Modified the model of accelerometer so that the proposed experimental scheme can be applied. The unknown parameter can then be solved by a proposed iterative algorithm without bias.

- To study the online calibration of the accelerometer, a suitable model is selected and the linearisation method is explored. Based on the linearised model, a recursive estimation method should be studied and improved for the linearised model. To stabilise the estimated parameters, a proper penalty should be embedded into the cost function. Eventually, the new cost function should be addressed by the proposed recursive method. The estimated response should be stable and accurate.

- To investigate the automatic model selection of online calibration, a comprehensive model is selected at the first place. To achieve the fast rate of convergence and the online estimation, an expectation maximum algorithm based least square estimation is explored and studied. The proposed algorithm includes a $\mathcal{L}_1$ penalty term to shrink the model. Therefore, the proposed method can achieve the automatic model selection during online calibration in this case.

Secondly, the modelling of oxygen consumption is a typical problem of dynamic system identification. Oxygen uptake (VO_2) on-kinetics is an important physiological parameter for the determination of functional health status and muscle energetics during physical exercise [9]. In addition, the VO_2 provides a useful assessment of the body's ability to support a change in metabolic demand and insights into the circulatory and metabolic response to exercise. So far, several studies confirmed that oxygen uptake is mainly controlled by the intramuscular factor related metabolic system [10]. Different from the heart rate, the oxygen uptake is not affected by mood, stress, etc., and is generally considered as the most accurate measurement of the fitness of cardiorespiratory system instead of the heart rate. Previous researches conducted on the oxygen uptake modelling can be divided into two main categories: static status

modelling and dynamic status modelling. For the dynamic modelling, the existed studies mainly based on classical system identification approaches, e.g. the least square (LS), maximum likelihood (ML) and prediction error method (PEM). Due to the fact that most of the measurements of VO_2 are noisy and the stimulations of the system are insufficient, the dynamic model of this system is always considered as a first-order system. Furthermore, it is likely that due to the individual difference, a higher order system can obtain a better fit. Therefore, this part of the research will focus on new modelling technique of this oxygen uptake response to exercise. The goals of the research in this part of the dissertation can be summarised as:

- Nonparametric system identification method is proposed to avoid the influence of the order of the system. Based on the kernel-based estimation method, the parameter of the impulse response of the oxygen uptake response to exercise is estimated.
- To consult the prior information, a proper kernel is selected and fine tuned to achieve optimum results. In this case, the required input signal can be simplified.
- To further reduce the number of parameters in the estimated finite impulse response, a $\mathcal{L}_1$ norm penalty is embedded in the cost function to form a special elastic net.

1.2 Problems in Parameter Estimation of Tri-Axial Accelerometer Calibration

In order to meet the demanded accuracy of acceleration measurement from researchers and engineers, many methods have been applied in the calibration of the accelerometer. In this dissertation, the problems in different scenarios are investigated to ensure reliability and effectiveness of the calibration of tri-axial accelerometer.

1.2.1 Offline Auto-calibration of Tri-Axial Accelerometer

A new calibration method for the MEMS tri-axial accelerometer is developed in several recent papers [11, 12], named as auto-calibration. This auto-calibration method can be implemented without using sophisticated equipment in non-experimental conditions. However, the quality, especially the assessment of each individual calibration, has not received the attention it deserves. To author's best knowledge, unlike traditional calibration methods, no paper systemically discussed the issues of DoE yet. Previous, most studies focused on the parameter estimation algorithms and its feasibility investigations. Few papers [13, 14] qualitatively described the selections of experimental observations without explaining the reason.

Classical accelerometer calibration, normally carried out in a well-controlled laboratory environment, can be formulated as a static linear parameter identification problem, for which DoE theory has been well established [15–18]. However, the models associated with the auto-calibration are often nonlinear. This makes the existed linear DoE approaches, which are effective and theoretically rigorous in traditional accelerometer calibration, invalid for auto-calibration. Without the optimum orientation, auto-calibration cannot achieve the best performance. Therefore, it is worth paying attention to a parameter estimation method based on auto-calibration with proper experimental design for the tri-axial accelerometer. With the advantages from auto-calibration and DoE, the calibration acceleroemter should achieve deserve performance and the method will be relativity easy to implement.

1.2.2 Online Auto-Calibration of Tri-Axial Accelerometer

Auto-calibration method were developed recently [11, 13, 19] for the tri-axial accelerometer calibration without using sophisticated laboratory equipment. [20–22] proposed an effective linearisation method and consummated the auto-calibration by considering the quality of each individual calibration. The selection of experimental observations is well discussed based on the theory of DoE and several experimental schemes were proposed based on different indices of DoE. However, the output of MEMS accelerometer still depends on environmental conditions [23, 24], such as temperature and pressure. If the

accelerometer is used in an environment with drastically changed in temperature, it is necessary to frequently re-calibrate the accelerometer to obtain the accurate measurements. However, frequently re-calibration of the accelerometer will be time-consuming for users. Hence, the online calibration is also necessary.

To the author's best knowledge, most studies are focusing on offline calibrations so far. The Kalman filter and other filtering methods based methods were developed by few papers [12, 25, 26], in which the linearised state space model is derived by Taylor expansion about an operating point. Furthermore, some of the online methods [25, 26] were not based on auto-calibration. The cost functions of 6- and 9-parameter models of tri-axial accelerometer based on auto-calibration are nonlinear and nonconvex. They are generally impractical to apply the nonlinear programming method directly. So far, the best solution is to apply the unscented Kalman filter for online auto-calibration. However, the rate of convergence is very slow. Therefore, this problem deserves more attention. It is important to propose a method to solve this parameter estimation problem that the rate of convergence is fast.

1.2.3 Online Auto-Calibration of Tri-Axial Accelerometer with Automatic Model Selection

Based on the idea of auto-calibration of tri-axial accelerometer, researchers proposed several methods to calibrate the MEMS type tri-axial accelerometer without sophisticated equipment. So far, several papers, including [11, 13, 19, 27], proposed the offline calibration methods based on the idea of auto-calibration. Furthermore, [20–22] consummated the auto-calibration method by paying attention to the quality of each individual measurement of auto-calibration, in which the selection of individual measurement is based on the theory of experimental design. However, the output of MEMS accelerometer still suffers from the drifting caused by ambient temperature [23, 24]. To overcome this shortage, online calibration is also proposed to improve the performance of calibration. During the online calibration, the estimated parameters are varying, and it is likely that some parameters are actually zero. Hence, the value of estimation of those parameters is caused by noise. It will improve the accuracy of calibration if only when the significant parameters are selected and estimated.

To the author's best knowledge, most papers selected pre-defined models, such as 6-, 9-, and 12- parameter models without theoretically explaining the reason for selecting such models. Only [28] discussed the selection of model based on Aakaike information criterion (AIC) [29, 30]. The results proved that the proper model can improve the accuracy of measurement after calibration. However, the AIC based method is proposed for offline calibration instead of online calibration. Therefore, an online parameter estimation method for tri-axial accelerometer with automatic model selection is important as it can further improve the accuracy of measurement after calibration.

1.3 Problems in Modelling of Oxygen Uptake Response to Exercise

Modelling methods are widely used in biological signal analysis [31–33]. Several research studies for the modelling of the dynamics of physiological signal in response to treadmill exercise were also conducted [2, 34, 35]. Since [10], the modelling of oxygen uptake response to exercise has been widely studied. From previous researches, it was proved that the oxygen uptake is not affected by mood, stress, etc. It is considered as one of the best indices to indicate the fitness of the cardiorespiratory system. The modelling of oxygen uptake response to exercise can be divided into two categories: static status modelling and dynamic status modelling. Recently, dynamic status modelling of oxygen uptake response attracted lots of attentions. Previously, most papers approximated the oxygen uptake response as a first order system, such as [36, 37], etc. For the input signal, those researches always used simple step signal as input. To the best of author's knowledge, most of the previous studies only utilised traditional system identification methods, e.g. the least square estimation (LS), maximum likelihood estimation (ML) and prediction error method (PEM).

For classical approaches, if only the simple step signal is considered as the input, the stimulation of the system may be insufficient in some cases. Hence, the classical methods, such as maximum likelihood and prediction error method, may fail to obtain an model with the desired accuracy and robustness for this cardiorespiratory response

estimation. To overcome this shortage, [38] and [39] applied the Pseudo Random Binary Signal (PRBS) as input to better stimulate the system. And [34] proposed a modeling method based on the Hammerstein model instead of the classic first order system.

In some cases, it is hard for some people to follow the PRBS as the input, and it is hard to obtain accurate systems without sufficient inputs. Particularly, it is unpractical to identify a higher system without enough stimulation of the system. Meanwhile, the prior information of the system has never been used in previous researches. Therefore, the modelling of oxygen uptake response to exercise is always a challenging topic. Furthermore, if the individual difference of human is considered, it is likely that the oxygen uptake responses of some people are high-order systems. Furthermore, it is also necessary to consider the prior information as it can reduce the demand for complex input signals.

1.4 Thesis Contribution

This thesis presents the investigation of parameter estimation and system identification with applications in the accelerometer calibration and the oxygen uptake modelling. For the parameter estimation, this thesis explores offline parameter estimation with experimental design, online parameter estimation with different penalties. For modelling of oxygen uptake response to exercise, nonparametric modelling technique related to parameter estimation with kernel penalty being explored. The contribution of this thesis can be summarised as follows:

- First, for the parameter estimation problem of offline auto-calibration of the accelerometer , a 6-orientation G-optimal experimental scheme is proposed for a special second-order model based on the theory of statistical experimental design. Then, in order to apply the proposed G-optimal experimental scheme, a new linearisation approach has been proposed, which can simplify the auto-calibration model in the desired second-order form so that the proposed G-optimality is achievable. Then, a convergence-guaranteed recursive parameter estimation algorithm has been developed that can be easily implemented in a wearable

device with limited computational power. The region of convergence is proved for the proposed method. In addition, to the author's best knowledge, for most of the cases, the proposed approach is the most efficient auto-calibration scheme that can reach the maximum G-efficiency for the tri-axial accelerometer.

- Second, for the parameter estimation problem of online auto-calibration of the accelerometer, a linearisation method of 6-parameter tri-axial accelerometer model has been explored for online calibration. Then, a damped recursive least square estimation method has been modified to estimate the unknown parameters in real-time. Meanwhile, the modified damped recursive least square (MDRLS) method can iteratively remove the bias caused by linearisation during online estimation process. It is worth to notice that the convergence speed and estimation effectiveness of the proposed method have been discussed based on not only simulation but also experiment with a self-designed health monitoring device. Comparing to the existing methods, the proposed method can achieve similar accuracy with significantly fewer measurements. In the end, based on Monte Carlo simulation, the region of convergence of the proposed online estimation method has been analysed and discussed. The results also demonstrate that the proposed method is also unbiased which is an important factor in the accelerometer calibration.

- Third, to online estimate unknown parameter with automatic model selection, a sparse least square (SPARLS) estimation method is explored. To apply the proposed algorithm, a linearisation method of 9-parameter model is developed. Based on the linearised model, the proposed algorithm is modified to solve unknown parameters in real time. The penalty term can help to remove insufficient parameters. Therefore, the model of tri-axial accelerometer can change in real time to remove the insignificant parameters caused by noise. The convergence conditions of the iterative approach are identified and investigated based on simulations for different situations. Finally, the effectiveness of the proposed approach is also demonstrated and verified by experiment.

- Forth, for modelling oxygen uptake response to exercise system, a nonparametric estimation method for impulse response is developed to identify any order systems.

To estimated the impulse response based on a simple step input as the input signal, a novel kernel-based estimation method is investigated which can efficiently estimate the impulse response model by incorporating a kernalised $\mathcal{L}_2$ norm penalty term. Furthermore, to overcome the large measurement noise of oxygen uptake and reduce the number of unknown parameters, a $\mathcal{L}_1$ penalty term is added to convert the overall penalty term to a special elastic net. Particularly, to include the prior information, the kernel selection is investigated by using extensive simulations, and the stable spline (SS) kernel is recommended as the best candidate. It is demonstrated by simulations and experiments that the proposed method is efficient for the modelling of the impulse response of oxygen uptake response to exercise in the dynamic state, even when the input signal is simple and the measurements are noisy. Finally, an averaged impulse response model is established, which is able to quantitatively describe the oxygen uptake on-kinetics for treadmill exercise.

1.5 Dissertation Outline

The outline of the dissertation is listed as follows:

Chapter 1

This chapter presents the motivation and scope, the research topics and contribution, and the outline of the dissertation.

Chapter 2

A literature review of parameter estimation in the calibration of the tri-axial accelerometer and oxygen uptake modelling is presented.

Chapter 3

To provide a systematic investigation of DoE for auto-calibration method, a major focus of DoE is to optimally design suitable input signals to stimulate the system significantly so that the information about the system can be extracted from the experiments. For the identification of a static model of an inertial sensor, a well selected/designed set of

experimental observations with desired properties, regarding DoE, can significantly improve the accuracy of parameter estimation [15].

In this chapter, a 6-observation G-optimal experimental design is proposed. To apply the proposed experimental scheme, a new linearisation method for auto-calibration [11] is explored and developed. A recursive method has been developed to solve the unkown parameter without bias. Furthermore, a posterior type G-efficiency [17] is introduced to evaluate a specific experiment. With the linearised model, a convergence-guaranteed iterative and recursive parameter estimation method is proposed. Simulations and experiments are carried based on proposed calibration method.

The work in this chapter has been published in:

- Lin Ye, Ying Guo, and Steven W. Su, "An Efficient Autocalibration Method for Triaxial Accelerometer," *IEEE Transactions on Instrumentation and Measurement*, vol. 66, no. 9, pp. 2380-2390, June 2017.
- Lin Ye, and Steven W. Su "Optimum Experimental Design applied to MEMS accelerometer calibration for 9-parameter auto-calibration model," in *Proc. 2015 37th International Conference of IEEE Engineering in Medicine and Biology Society*, July 2015.
- Lin Ye, and Steven W. Su, "Experimental design and its posterior efficiency for the calibration of wearable sensors.," *Journal of Intelligent Learning Systems and Applications*, vol. 7, no. 1, pp. 11-20, February 2015.

Chapter 4

In this chapter, to improve the accuracy of the accelerometer measurement and reduce the influence caused by enviromental variation, an online calibration method is developed. First of all, a linearisation method based on the commonly used 6-parameter MEMS TAs model [11, 22] is adopted. After that, to online estimate the unknown parameter, a modified version of damped recursive least square (MDRLS) estimation method is investigated. Noticeably, this method can converge to true value rapidly even when the parameters are varying. With a proper balance between error term and penalty term in the cost function, the estimation can be stable and fast-converge. And the unwanted fluctuation of parameter estimation can be efficiently reduced by

the damping penalty term. Besides, since this method is relatively simple, it can be implemented in a standard commercial grade embedded Micro Controller Unit (MCU) easily as the memory required to record the intermediate results that is in small size and fixed. The results from simulation and experiment are recorded, which demonstrate the effectiveness of the proposed online calibration method. In the end, the convergence conditions of the proposed method have been analysed and discussed based on Monte Carlo simulation.

The work in this chapter has been published in:

- Lin Ye, Ying Guo, Lei Dong, Hung T. Nguyen, and Steven W. Su, "A Fast-Converge Real-time Auto-Calibration Algorithm for Triaxial Accelerometer," under submission to *IEEE Transactions on Instrumentation and Measurement*, 2017.
- Lin Ye, Steven W. Su, Lei Dong, and Nung T. Nguyen, "An online recursive autocalibration of triaxial accelerometer," in *Proc. 2016 38th International Conference of IEEE Engineering in Medicine and Biology Society*, pp. 2038-2041, July 2016.

Chapter 5

This chapter firstly introduces a new linearisation method based on the most commonly used 9-parameter auto-calibration model [11, 22]. After that, a sparse recursive least square (SPARLS) estimation method [40] is utilised to solve the unknown parameters. Particularly, this method is effective while the model parameters are varying. Furthermore, based on the characteristic of $\mathcal{L}_1$-norm penalised expectation-maximum (EM) algorithm, this method can automatically determine the model complexity in an optimal manner. Besides, this method is implemented in an embedded Micro Control Unit (MCU) for online calibration in real time. Simulation and experiments demonstrate the effectiveness of the proposed approach.

The work in this chapter has been published in:

- Lin Ye, Ahmadreza Argha, Branko G Celler, Hung T. Nguyen and Steven W, Su, "Online Auto-calibration of Triaxial Accelerometer with time-variant model

structures," *Sensors and Actuators A: Physical*, vol. 266, pp. 294-307, October 2017.

Chapter 6

In this chapter, the nonparametric modeling method [41, 42] is applied and improved to identify the the model of oxygen uptake response to the treadmill exercise. Instead of using the classical ARX model, this nonparametric modelling method is based on the impulse response. Therefore, the order of the system does not need extra consideration. Furthermore, to overcome the large measurement noise and reduce the number of unknown parameters. A $\mathcal{L}_1$ norm is added to shrink the system and remove the parameters caused by noise.

With this kernel-based estimation method, a simple step function is enough as input since the kernel can provide prior information of the system. Several different kernels are introduced and tested. The results from simulation and experiment show that the stable spline (SS) kernel can achieve the best result. The data are collected from 20 untrained and healthy participants in treadmill exercises. With the estimated impulse response from 20 participants , we make a statistical comparison between the results from the proposed method and prediction error method. An average model based on the data of 20 participants is given at the end.

The work in this chapter has been published in:

- Lin Ye, Ahmadreza Argha, Branko G Celler, Hung T. Nguyen and Steven W, Su, "Dynamic Characteristics of Oxygen Uptake," *BioMedical Engineering OnLine*, vol. 17, no. 1, pp. 44-62, April 2018
- Hairong Yu, Lin Ye, et al, "Nonparametric Dynamical Model of Cardiorespiratory Responses at the Onset and Offset of Treadmill Exercises," under submission to *Medical & Biological Engineering & Computing*, 2017.
- Lin Ye, Ahmadreza Argha, Branko G Celler, Yi Zhang, Hung T. Nguyen and Steven W, Su, "Nonparametric modelling of VO 2 response to exercise," in *Proc. 2017 39th International Conference of IEEE Engineering in Medicine and Biology Society*, pp. 1525-1528, July 2017.

Chapter 7

This chapter summarises the works of this PhD dissertation and presents the potential future research developments.

Chapter 2

Literature Review

In this chapter, we introduce some related knowledge about the parameter estimation in accelerometer calibration and VO_2 modelling. Then, some parameter estimation methods, as a mathematical foundation for solving the problems in this dissertation, are introduced.

2.1 Parameter Estimation in Accelerometer Calibration

In 1979, the first MEMS type accelerometer was developed[43]. Then, several different types of MEMS accelerometer have been developed, including piezoresistive[44], piezoelectric[45], capacitive[46], etc[47, 48]. With the development of the Micro-Electro-Mechanical Systems (MEMS) technology, recently, the MEMS based accelerometer has been used widely in different applications. Generally, the MEMS accelerometer is small, less expensive and power saving. Hence, the MEMS accelerometer is extensively utilised in wearable health monitoring devices, motion tracking systems, and fault detection system, etc.

For example, for health monitoring devices, [1] proposed an unsupervised machine-learning method for a fall-detection system. In this system, the measurement from tri-axial accelerometer (TA) was included and played an important role in the measurement

of body movement. In [3], the accelerometer was mounted on the lower back to synchronised body measurement and electrocardiography (ECG) signal so that the authors can identify and control the heart rate regulation system.

For those motion tracking systems, the tri-axial accelerometer is widely used as a part of the inertial measurement unit. Based on different data fusion methods, the orientation of the inertial measurement unit can be calculated by the acceleration, angular velocity and magnetic field. [49] developed a Quaternion-Based Kalman filter for motion tracking with a tri-axial accelerometer. [50] developed an indirect Kalman filter based attitude estimation method with a tri-axial acclerometer. It is clear that the tri-axial accelerometer is important in motion tracking or navigation system.

Furthermore, the MEMS type tri-axial accelerometer is also widely used in consumer electronic devices. For most of the smart phone, an accelerometer is included to estimate the orientation. And it is also found in the smart watch to provide information for step count calculation.

Although the MEMS types tri-axial accelerometer are widely used in different applications, precise measurements are always required. However, due to the limitation of modern MEMS technology, the measurement of the MEMS type accelerometer still suffers from large bias and instability with relatively large noise. Therefore, the calibration of accelerometer is a necessary step in order to obtain the accurate measurement.

2.1.1 The 6-Parameter Model of Tri-axial Accelerometer

For the calibration of tri-axial accelerometer, a 6-parameter model is popular, paper [28], [22] and [13] selected the 6-parameter model in their researches. For the 6-parameter model, let us define $\boldsymbol{V} = [v_x, v_y, v_z]^T$ as the measurements of tri-axial accelerometers. Then, the mathematical model of local acceleration (local gravity) $\boldsymbol{A} = [a_x, a_y, a_z]^T$ with measurement $\boldsymbol{V}$ as input can be expressed as:

$$\begin{bmatrix} a_x \\ a_y \\ a_z \end{bmatrix} = \begin{bmatrix} S_x & 0 & 0 \\ 0 & S_y & 0 \\ 0 & 0 & S_z \end{bmatrix} \left(\begin{bmatrix} v_x \\ v_y \\ v_z \end{bmatrix} + \begin{bmatrix} O_x \\ O_y \\ O_z \end{bmatrix} \right), \tag{2.1}$$

where S_x, S_y, S_z and O_x, O_y, O_z represent scale factors and offsets. Therefore, the resulting model has six independent parameters. For the measurement $\boldsymbol{V}$, the unit is the gravity (g) in this work.

2.1.2 9-Parameter Model of Tri-Axial Accelerometer

Another popular model of the tri-axial accelerometer is the 9-parameter model, it was also selected in several researches, including [14, 11, 51], etc. Similar to the 6-parameter model, only three additional misalignment factors $\phi_{xy}, \phi_{xz}, \phi_{yz}$ for the 9-parameter model are included to represent the correlations between each axis. Hence, a matrix $\boldsymbol{T}$ can be described as:

$$\boldsymbol{T} = \begin{bmatrix} 1 & 0 & 0 \\ \phi_{xy} & 1 & 0 \\ \phi_{xz} & \phi_{yz} & 1 \end{bmatrix}, \tag{2.2}$$

The complete scale factor matrix $\boldsymbol{K}$ is the dot product of $\boldsymbol{S}$ and $\boldsymbol{T}$:

$$\boldsymbol{K} = \begin{bmatrix} S_x & 0 & 0 \\ S_x\phi_{xy} & S_y & 0 \\ S_z\phi_{xz} & S_z\phi_{yz} & S_z \end{bmatrix} \triangleq \begin{bmatrix} k_{xx} & 0 & 0 \\ k_{xy} & k_{yy} & 0 \\ k_{xz} & k_{yz} & k_{zz} \end{bmatrix}. \tag{2.3}$$

The 9-parameter model can then be expressed as:

$$\begin{bmatrix} a_x \\ a_y \\ a_z \end{bmatrix} = \begin{bmatrix} k_{xx} & 0 & 0 \\ k_{xy} & k_{yy} & 0 \\ k_{xz} & k_{yz} & k_{zz} \end{bmatrix} \left(\begin{bmatrix} v_x \\ v_y \\ v_z \end{bmatrix} + \begin{bmatrix} O_x \\ O_y \\ O_z \end{bmatrix} \right), \tag{2.4}$$

2.1.3 Classical Calibration Method

Classical calibration methods require the position information of the accelerometer. Normally, the position information is provided by a precise turntable, and the value of the position is considered as the reference value. Then, the measurement from the accelerometer is compared with the reference value. Based on the above 6- or 9-parameter model, the scale factor, misalignment, and offset can then be easily calculated. For the classical method, the accuracy of calibration is highly depended on the accuracy of the turntable. Therefore, a precise turntable is always required in the classical calibration method. The theory of this method is easy and straightforward. However, it is hard to implement this method as a precise turntable is hard to access by most researchers and engineers.

2.1.4 6-Position Calibration Method and Related Methods

In paper [52], a calibration method based on six positions was developed. For this method, the accelerometer is required to place on the surface with each axis of the sensors facing up and down alternately. For each axis, the scale factor and the offset can be calculated as:

$$S_x = \frac{v_{x,up} - v_{x,down}}{2 * g}, \tag{2.5}$$

$$S_y = \frac{v_{y,up} - v_{y,down}}{2 * g}, \tag{2.6}$$

$$S_z = \frac{v_{z,up} - v_{z,down}}{2 * g}, \tag{2.7}$$

$$O_x = \frac{v_{x,up} + v_{x,down}}{2}. \tag{2.8}$$

$$O_y = \frac{v_{y,up} + v_{y,down}}{2}. \tag{2.9}$$

$$O_z = \frac{v_{z,up} + v_{z,down}}{2}. \tag{2.10}$$

where $v_{x,up}$, $v_{y,up}$, $v_{z,up}$ are the measurements of x, y, z-axis when it is pointing up and $v_{x,down}$, $v_{y,down}$, $v_{xz,down}$ are the measurements of x, y, z-axis when it is pointing down.

Although this method is efficient, paper [14] pointed out that this method depends on how well the axes are aligned. The misalignment is not considered in this method and the box for measurement must be perfectly cube-shaped. Furthermore, Paper [14] improved the method by considering 3 extra misalignment factors. And a 18-position calibration method was proposed.

2.1.5 Auto-Calibration Method

In order to overcome the disadvantages of previous calibration methods, recently, the idea of auto-calibration was developed to solve the calibration of the tri-axial accelerometer effectively [28, 11, 53] without sophisticated equipment. The key concept of the auto-calibration method can be summarised as that the overall measurements of tri-axial accelerometers in the static state should be equal to the local gravity acceleration ('1g'),

$$g = \sqrt{a_x^2 + a_y^2 + a_z^2}. \tag{2.11}$$

Mathematically speaking, the auto-calibration method is more difficult than classical methods. For the auto-calibration, the expansion of Eq.(2.11) based on the 6- or 9-parameter model from Eq.(2.1) or Eq.(2.4) is normally nonlinear and non-convex. However, this method does not need the precise turntable which can be considered as a huge advantage comparing with classical methods. Therefore, most researchers and engineers tend to apply the auto-calibration method to calibrate the MEMS tri-axial accelerometer.

Cost function of Auto-Calibration

Based on (2.11), the error $\tilde{\epsilon}_i$ of the 6-parameter model for the i-th measurement can be expressed as follows [11],

$$\begin{aligned}\tilde{\epsilon}_i =& a_{x,i}^2 + a_{y,i}^2 + a_{z,i}^2 - g^2 \\ =& \sum_{j=x,y,z} \left[S_j \cdot (v_{j,i} + O_j)\right]^2 - g^2, i = 1, 2, \cdots, n,\end{aligned} \tag{2.12}$$

where $v_{j,i}$ $(j = x, y, z)$ is a component of the i-th measurement. For the 9-parameter model, the error $\tilde{\epsilon}_i$ of the i-th measurement can then be expressed as [51]:

$$\begin{aligned}\tilde{\epsilon}_i = & \left[k_{xx}\left(v_{x,i} + o_x\right)\right]^2 + \left[k_{xy}\left(v_{x,i} + o_x\right) + k_{yy}\left(v_{y,i} + o_y\right)\right]^2 \\ & + \left[k_{xz}\left(v_{x,i} + o_x\right) + k_{yz}\left(v_{y,i} + o_y\right) + k_{zz}\left(v_{z,i} + o_z\right)\right]^2 - g^2, i = 1, 2, \cdots, n,\end{aligned} \tag{2.13}$$

Thus, if we assume that $\boldsymbol{\beta}$ is the vector of the unknown parameters of the model, the cost function can be defined as:

$$J(\boldsymbol{\beta}) = \sum_{i=1}^{n} \left(|| \boldsymbol{f}_{\boldsymbol{\beta}}(\boldsymbol{V}_i) - g^2 || \right), \tag{2.14}$$

where $\boldsymbol{V}_i = [v_{x,i}, v_{y,i}, v_{z,i}]^T$ $(i = 1, 2, \cdots, n)$ is the i-th measurement, $\boldsymbol{f}_{\boldsymbol{\beta}}(\boldsymbol{V}_i)$ is a function of $\boldsymbol{V}_i$. Based on the above cost function, the parameter estimation can be formulated as a nonlinear non-convex parameter estimation problem. Therefore, the calibration of the tri-axial accelerometer can be considered as a parameter estimation problem.

Existing Method for Auto-Calibration

Based on the above cost functions for the 6- and 9-parameter models, extensive researches have been carried out to solve the parameters in an optimum way. Some popular papers are listed below:

- Frosio et. al [11] proposed a Newton's optimisation method based on the 9-parameter model.

- Cai et. al [51] proposed a particle swarm optimisation method based on the 9-parameter model with measurements from 24 orientations.
- Skog et. al [53] proposed a Newton's optimisation method for the 9-parameter model with measurements from 18 orientations. However, the 18 orientations were not provided.
- Zhang et. al [54] proposed a least square method based solution for the 9-parameter model with measurements from 9 orientations.
- Glueck et. al [12] proposed an unscented Kalman filter based method for the 6-parameter model which required lots of measurements.

Besides, to solve the unknown parameters based on the auto-calibration, several numerical methods, such as the Downhill simplex optimisation method [55], maximum likelihood estimation [56], graph optimisation [57], and Levenberg-Marquardt minimisation method [58, 59], were also developed to solve the unknown parameter.

2.1.6 Offline Auto-Calibration with Design of Experiment

For classical calibrations, the orientations were well selected [52, 14]. However, for the auto-calibration method, few papers discussed the selection of orientations for measurements. For example:

- Won et. al [13] proposed a 6-orientation experimental scheme for the auto-calibration method.
- Cai et. al [51] proposed a 24-orientation experimental scheme for the auto-calibration method.
- Zhang et. al [54] proposed a 9-orientation experimental scheme for the auto-calibration method.

These three experimental schemes are presented in Fig.2.1, Fig.2.2 and Fig.2.3 respectively.

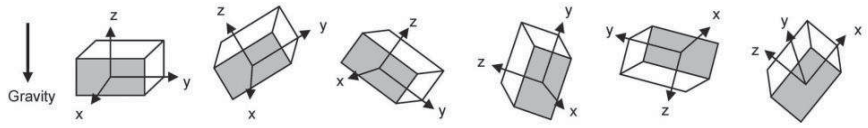

Fig. 2.1 6-orientation experimental scheme from Won et al, 2010

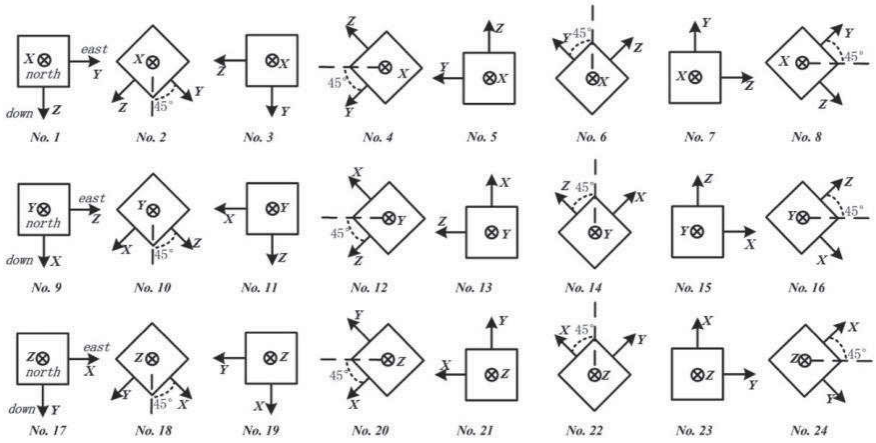

Fig. 2.2 24-orientation experimental scheme from Cai et al, 2013

Posture no.	1	2	3
Description	*x*-upward	*x*-downward	*y*-upward
Illustration			
Posture no.	4	5	6
Description	*y*-downward	*z*-upward	*z*-downward
Illustration			
Posture no.	7	8	9
Description	*x*-east, *y*-north-upward with 45° pitch, *z*-south-upward with 45° pitch	*y*-east, *z*-north-upward with 45° pitch, *x*-south-upward with 45° pitch	*z*-east, *x*-north-upward with 45° pitch, *y*-south-upward with 45° pitch
Illustration			

Fig. 2.3 9-orientation experimental scheme from Zhang et al, 2014

Besides, most researchers, including [60, 61], etc., did not mention the exact number of orientations. And for the papers above, the selections of orientations have not been discussed based on the theory of experimental design (DoE). Therefore, for the first part of the research, a method based on the auto-calibration shall be proposed and the optimum experimental scheme shall be discussed. Since the nonlinear experimental

design is very complex, a linearisation method shall also be proposed to reduce the difficulty when designing the optimum experiment for auto-calibration. In the next section, the background of experimental design will be reviewed.

Review of Experimental Design

Theoretically, experimental design is a mathematical and statistical method used in the development of an adequate functional relationship between the response of interest $y \in R$ and a number of associated input variables $x_1, x_2, \cdots, x_k$. As part of DoE, the optimum DoE is constructed on the basis of certain variance-related optimality. In general, to apply the technique from DoE, low order polynomial models are widely used [15, 17]:

$$y = \boldsymbol{f}^T(\boldsymbol{x})\boldsymbol{\beta} + \epsilon, \tag{2.15}$$

where $\boldsymbol{x} = [x_1, x_2, \cdots, x_k]^T$, $\boldsymbol{f}(\boldsymbol{x}) \in \boldsymbol{R}^{p\times 1}$ is a vector function of p elements consisting of powers and cross products of powers of $x_1, x_2, \cdots, x_k$ up to a certain degree denoted by $d \geq 1$, $\boldsymbol{\beta}$ is the vector of parameters to be estimated, and ϵ is assumed to be a random experimental error with zero mean.

In order to achieve the optimum estimation of parameters, a series of n experiments should be implemented first. In each experiment, the response y is observed for specified settings of the control variables. These settings are considered as the design for obtaining the optimum estimation of parameters, which can be expressed as $\boldsymbol{\mathcal{D}} \in \boldsymbol{R}^{n\times k}$:

$$\boldsymbol{\mathcal{D}} = \begin{bmatrix} x_{11} & x_{12} & \dots & x_{1k} \\ x_{21} & x_{22} & \cdots & x_{2k} \\ \vdots & \vdots & \ddots & \vdots \\ x_{n1} & x_{n2} & \dots & x_{nk} \end{bmatrix}, \tag{2.16}$$

where x_{ui} $(i = 1, 2, \cdots, k, u = 1, 2, \cdots, n)$ represents the uth design setting of x_i and each row of $\boldsymbol{\mathcal{D}}$ represents a design point in a k-dimensional Euclidean space. Assuming that y_u represents the response value of design setting $\boldsymbol{x_u} = [x_{u1}, x_{u2}, \cdots, x_{uk}]^T$, from (2.15), we have:

$$y_u = \boldsymbol{f}^T(\boldsymbol{x_u})\boldsymbol{\beta} + \epsilon_u, u = 1, 2, \cdots, n, \tag{2.17}$$

where ϵ_u represents the error from the uth observations. Then, (2.17) can be expressed in matrix from as:

$$\boldsymbol{y} = \boldsymbol{X}\boldsymbol{\beta} + \boldsymbol{\epsilon}, \tag{2.18}$$

where $\boldsymbol{y} = [y_1, y_2, \cdots y_n]^T$, the u-th row of matrix $\boldsymbol{X} \in \boldsymbol{R}^{n\times p}$ is $\boldsymbol{f}^T(\boldsymbol{x_u})$ and $\boldsymbol{\epsilon} = [\epsilon_1, \epsilon_2, \cdots, \epsilon_n]^T$.

For (2.18), let us assume that $\boldsymbol{\epsilon}$ has a zero mean and a variance-covariance matrix given by $\sigma^2\boldsymbol{I}_n$. Then, the variance-covariance matrix of the least-square estimator $\hat{\boldsymbol{\beta}}$ for (2.18) can be expressed as [62]:

$$var(\hat{\boldsymbol{\beta}}) = \sigma^2(\boldsymbol{X^T X})^{-1}. \tag{2.19}$$

The variance of the predicted response $\hat{y}$ can be calculated as:

$$var(\hat{y}) = \sigma^2\boldsymbol{f}^T(\boldsymbol{x})(\boldsymbol{X^T X})^{-1}\boldsymbol{f}(\boldsymbol{x}). \tag{2.20}$$

Then, the scaled prediction variance (SPV) which is defined as:

$$d(\boldsymbol{x}, \boldsymbol{\xi}_n) = \boldsymbol{f}^T(\boldsymbol{x})\boldsymbol{M}^{-1}(\boldsymbol{\xi}_n)\boldsymbol{f}(\boldsymbol{x}) = \frac{n \cdot var(\hat{y}(\boldsymbol{x}))}{\sigma^2}, \tag{2.21}$$

where $\boldsymbol{\xi}_n$ is the experimental scheme with n observations and $\boldsymbol{M}$ is the Fisher information matrix defined as:

$$\boldsymbol{M} = \frac{\boldsymbol{X}^T\boldsymbol{X}}{n}. \tag{2.22}$$

Suppose a special case of the second-order polynomial model can then be expressed as:

$$y = \sum_{i=1}^{2}\beta_i x_i + \sum_{i=1}^{2}\beta_{ii}x_i^2 + \epsilon. \tag{2.23}$$

Then, assume that we have a 6-observation experimental scheme, and the design matrix $\boldsymbol{\mathcal{D}}$ is:

$$\boldsymbol{\mathcal{D}} = \begin{array}{c} \begin{matrix} x_1 & x_2 \end{matrix} \\ \begin{bmatrix} 1 & 0 \\ -1 & 0 \\ 0 & 1 \\ 0 & -1 \\ 0.5 & 0 \\ 0 & 0.5 \end{bmatrix} \end{array}. \tag{2.24}$$

For experimental scheme (2.24), the model matrix $\boldsymbol{X}$ of model (2.23) is:

$$\boldsymbol{X} = \begin{array}{c} \begin{matrix} x_1 & x_2 & x_1^2 & x_2^2 \end{matrix} \\ \begin{bmatrix} 1 & 0 & 1 & 0 \\ -1 & 0 & 1 & 0 \\ 0 & 1 & 0 & 1 \\ 0 & -1 & 0 & 1 \\ 0.5 & 0 & 0.25 & 0 \\ 0 & 0.5 & 0 & 0.25 \end{bmatrix} \end{array}, \tag{2.25}$$

and $\boldsymbol{f}(\boldsymbol{x}) = \begin{bmatrix} x_1, & x_2, & x_1^2, & x_2^2 \end{bmatrix}^T$.

Most Important Indices of Optimum Experimental Design

In the optimum experimental design, several indices have been proposed to evaluate an experiment from various aspects.

The optimum experimental design focuses on proposing the special experimental scheme with different aspects. Based on the proposed experimental scheme, the estimated responses or estimated parameters should have some special characteristics. Most of the indices used to evaluate an optimum experimental scheme are related to the estimation variances from the Eq.(2.19) and Eq.(2.20), such as D-, G-, A-, and V-optimality [62].

- D-optimality: For the parameter estimation, D-optimality is aiming to minimise the general variance of the estimated parameters.
- G-optimality: For the estimation of response, G-optimality is aiming to minimise the maximum variance of the scaled prediction variance.
- A-optimality: For the parameter estimation, A-optimality is aiming to minimise the sum of the variance of estimated parameters.
- V-optimality: For the estimation of response, V-optimality is aiming to minimise the sum of the scaled prediction variance.

Generally, for an experimental scheme $\boldsymbol{\xi}_{n^*}$, if Eq.(2.22) is maximised, then the experimental scheme $\boldsymbol{\xi}_{n^*}$ is D-optimal.

Furthermore, for the scaled prediction variance in Eq.(2.21), if

$$\max \ d(x, \boldsymbol{\xi}_{n^*}) = p, \tag{2.26}$$

where p is the number of unknown parameters, then this experimental scheme $\boldsymbol{\xi}_{n^*}$ is G-optimal.

Besides, D_S-optimality is developed to optimise the variance of the subset of the unknown parameters [62]. c-optimality is developed to estimate the linear combination of the unknown parameter with minimum variance [62].

In real-life, for applications with different backgrounds, different types of indices should be selected to design the special experiment scheme based on the model.

2.1.7 Online Auto-Calibration

According to the datasheet of most accelerometers which are developed recently, the estimated parameters from offline calibration will change due to the variation of environment. Therefore, an online calibration is also necessary to further improve the accuracy.

Most researches, such as [11, 13, 19] etc, are offline solution. Based on Eq. (2.12), Eq.(2.13) and Eq.(2.14), it is obvious that the cost function is nonlinear and non-

convex. Practically, the online estimation of unknown parameters from the nonlinear and non-convex cost function is difficult and challenging. Only a few papers tackled this problem with online solutions. Most papers for online calibration, such as [25, 26], still require sophisticated equipment. So far, [60, 12] developed an unscented Kalman filter (UKF) based online auto-calibration method which can solve the problem if the parameters are varying extremely slow. Some popular researches that focused on online calibration can be summarised as:

- Beravs et. al [26] proposed a UKF based algorithm to online calibrate the tri-axial accelerometer. However, extra equipment is required to provide reference value.
- Batista et. al [25] proposed a time-varying Kalman filter to online calibrate the tri-axial accelerometer. However, the proposed method needs a motion table.
- Glueck et. al [60] proposed a UKF based algorithm to online calibrate the tri-axial accelerometer based on auto-calibration without additional equipment.
- Glueck et. al [12] improved the proposed UKF based method from [60] and lots of observations were required.

UKF Based Online Calibration

For the online calibration of tri-axial accelerometer, it is clearly shown in previous section that Kalman filter based methods are widely used. It is worth mentioned a study based on unscented Kalman filter from papers [12, 60] which can be summarised as below. For a 6-parameter model, let us assume that the state vector $\hat{w}_k$ is defined as [12]:

$$\hat{w}_k = \begin{bmatrix} \hat{S}_x & \hat{S}_y & \hat{S}_z & \hat{O}_x & \hat{O}_y & \hat{O}_z \end{bmatrix}^T. \tag{2.27}$$

For Unscented Kalman Filter part, it can be expressed as the follow [63].

Initial:

$$\hat{w}_0 = E[w], \tag{2.28}$$

$$P_{\hat{w}_0} = E[(w - \hat{w}_0)(w - \hat{w}_0)^T], \tag{2.29}$$

$$w_0^{(m)} = \frac{\lambda}{L + \lambda}, \tag{2.30}$$

$$w_0^{(c)} = \frac{\lambda}{L+\lambda} + (1 - \alpha^2 + \beta), \tag{2.31}$$

$$w_i^{(m)} = w_i^{(c)} = \frac{\lambda}{2(L+\lambda)}, \quad i = 1, \cdots, 2L, \tag{2.32}$$

where $\lambda = \alpha^2(L + \kappa)$ is a scaling parameter, L is the dimension of w, $\alpha \in [0, 1]$ determines the spread of the sigma point, $\kappa = 0$ is another scaling parameter.

Algorithm 1 UKF based On-Line Auto-Calibration

For $k = 1, 2, 3, \cdots, \infty$

Calculate Sigma Points:

$$\mathcal{X}_{k|k-1} = [\hat{w}_k^- \quad \hat{w}_k^- \pm \sqrt{(L+\lambda)P_{w_k}^-}], \tag{2.33}$$

Time Update:

$$\hat{w}_k^- = \hat{w}_{k-1}, \tag{2.34}$$

$$P_{w_k}^- = P_{w_k} + R_{r_{k-1}}, \tag{2.35}$$

Measurement Update

$$Y_{k|k-1} = g(U_k, \mathcal{X}_{k|k-1}), \tag{2.36}$$

$$\hat{d}_k^- = \sum_{i=0}^{2L} w_i^{(m)} Y_{i,k|k-1}, \tag{2.37}$$

$$S_{\tilde{d}_k} = \sum_{i=0}^{2L} w_i (Y_{i,k|k-1} - \hat{d}_k^-)(Y_{i,k|k-1} - \hat{d}_k^-)^T + R_{e_k}, \tag{2.38}$$

$$P_{w_k d_k} = \sum_{i=0}^{2L} w_i (\mathcal{X}_{k|k-1} - \hat{w}_k^-)(\mathcal{X}_{k|k-1} - \hat{w}_k^-)^T, \tag{2.39}$$

$$K_k = P_{w_k d_k} S_{\tilde{d}_k}^{-1}, \tag{2.40}$$

$$\hat{w}_k = \hat{w}_k^{-1} + K_k(d_k - \hat{d}_k^-), \tag{2.41}$$

$$P_{w_k} = P_{w_k}^- - K_k S_{\tilde{d}_k,} K_k^T. \tag{2.42}$$

Although this method can online auto-calibrate accelerometer without additional equipment. From paper [12], around 1000 measurements are required for the estimated

parameters to converge to the final values. Therefore, if the parameters are varying relatively fast due to the change of environments, this method cannot achieve the best performance.

Damped Recursive Least Square Estimation

To overcome the disadvantages of UKF in this problem, a new online calibration method is required. Inspired by the linearised method proposed in [22], a modified damped recursive least square method shall be able to solve the unknown parameters based on the linearised 6-parameter model.

For damped recursive least square estimation, if we assume that vector $\boldsymbol{\beta}$ is the vector of unknown parameter. Then, the cost function can be defined based on Eq.2.12 as:

$$J(\hat{\boldsymbol{\beta}}) = (\sum_{k=1}^{t} \lambda^{t-k} \epsilon_k^2) + \mu ||\hat{\boldsymbol{\beta}}_t - \hat{\boldsymbol{\beta}}_{(t-1)}||_2^2, \tag{2.43}$$

where μ is the forgetting factor. Comparing to classical recursive least square estimation, the damping penalty term $||\hat{\boldsymbol{\beta}}_t - \hat{\boldsymbol{\beta}}_{(t-1)}||_2^2$ can help to stabilise the estimated parameter. Generally, the rate of convergence of recursive least square estimated based algorithm is fast. With the damping penalty term, the damped recursive least square estimation can also be stable. Due to its simplicity, it can be easily implemented into a micro controller unit with limited computation power.

2.1.8 Online Calibration with Model Selection

In the previous studies, most researchers selected the 6- or 9-parameter models. A few papers selected the 12-parameter models. A brief summary is listed below:

- 6-parameter model: [13], [60], [12], [58], etc.
- 9-parameter model: [28], [51], [53] [54], [11], [26], etc.
- 12-parameter model: [64], [55], [25], etc.

For paper [11], although the authors selected the 12-parameter model at the first place, the authors assumed that the scale factor was symmetric later on. Therefore,

paper [11] actually selected the 9-parameter model instead of the 12-parameter model. Based on the results, most researchers selected the 9-parameter model, the rest selected the 6- or 12-parameter model.

However, most of the researchers did not theoretically explain the reason of selecting such model in their researches. If the authors from previous researches assumed that the misalignment did not exist, the 6-parameter model was selected. If they assumed the existence of the misalignment, then the 9- or 12-parameter model was selected.

Model Selection Based on Akaike Information Criterion

So far, only paper [28] explained the model selection of the auto-calibration of MEMS type tri-axial accelerometer based on Akaike information criterion (AIC) [29, 30]. The AIC index for the auto-calibration model is defined as:

$$AIC_{C,P} = 2P - 2\ln L_p + 2P(P+1)/(N-P-1), \tag{2.44}$$

where P is the number of unknown parameter, L_p is the likelihood function, N is the number of measurements and it must be larger than $P+1$.

Based on this, several experiments have been carried out and the authors of [28] concluded that 6- and 9-parameter models are sufficient for the auto-calibration of MEMS tri-axial accelerometer.

Regularisation in Cost Function

Although AIC can determine the optimum number of parameters in the model, it is developed for offline calibration [28]. During the online calibration, some parameters may change to zero. In this case, the pre-defined model can not be adjusted automatically. Some estimated parameters are actually caused by noise. It is necessary to modify the model real time. In this case, those parameters caused by noise can be removed during online calibration. So far, none of the researchers tackled this problem yet.

For the author's best knowledge, the penalty term in the cost function can provide extreme important characteristics in parameter estimation. As we know, without

penalty term, the parameter estimation often suffers from some drawbacks. A proper penalty term may help to stabilise or shrink the number of unknown parameters. There are several types of penalty terms that are quite popular, such as the $\mathcal{L}_1$ norm penalty [65], the $\mathcal{L}_2$ norm penalty, or the combination of the $\mathcal{L}_1$ and $\mathcal{L}_2$ norm penalty [66], etc.

Assuming $\boldsymbol{x}$ is the vector of unknown parameters, some penalty terms based on $\boldsymbol{x}$ can be summarised as:

- $\mathcal{L}_1$ norm penalty, $||x||_1$
- $\mathcal{L}_2$ norm penalty, $||x||_2^2$
- damping penalty, $||\boldsymbol{x}_{n+1} - \boldsymbol{x}_n||_2^2$
- elastic net, $a||\boldsymbol{x}|| + (1-a)||\boldsymbol{x}||_2^2$

For this specific problem, to automatically adjust the model of tri-axial accelerometer, the $\mathcal{L}_1$ norm penalty is selected as it can be used to shrink the number of unknown parameters. It was first introduced as LASSO in [65] which is a significant improvement in parameter estimation area.

Based on the above theory, the online calibration with model selection can be converted to a parameter estimation problem that required parameter shrinkage. It can be solved by the proper combination and development of above theory. In Chapter 5, the details of online EM algorithm with $\mathcal{L}_1$ norm penalty will be given to solve this specific parameter estimation.

Penalised Expectation Maximum Algorithm

To handle parameter estimation problem with missing data or incomplete data, expectation maximum (EM) algorithm is widely used. Due to the characteristic of measurements from accelerometer. EM algorithm can be considered as an ideal solution for parameter estimation in the calibration of acceleroemter.

The EM algorithm is developed based on the maximum likelihood estimation in [67]. For EM algorithm, assuming that we have an observation set $\boldsymbol{y}$, an unobserved data (laten variable) $\boldsymbol{v}$, and the unknown parameter $\boldsymbol{\beta}$, the *complete log-likelihood*

of EM algorithm can be expressed as $\log p(\boldsymbol{y}_n, \boldsymbol{v}_n|\boldsymbol{\beta}_n)$, which can be achieved in two steps. For the expectation step, the conditional expectation is calculated. For the maximisation step, the parameters are computed to maximise conditional expectation [67]. However, in order to shrink the number of the unknown parameters, a proper penalty term shall be included. The EM algorithm, which can be modified to the penalised EM algorithm to solve this particular problem [68]. It can be summarised into the following two steps:

- E-step: Calculate the conditional expectation $\log p(\boldsymbol{y}_n|\boldsymbol{\beta}_n)$, which is defined as Q-function $Q(\boldsymbol{\beta}_n, \hat{\boldsymbol{\beta}}_n^{(l)})$ in the l-th iteration:

$$Q(\boldsymbol{\beta}_n, \hat{\boldsymbol{\beta}}_n^{(l)}) = E\left[\log p(\boldsymbol{y}_n, \boldsymbol{v}_n|\boldsymbol{\beta}_n)|\boldsymbol{y}_n, \hat{\boldsymbol{\beta}}_n^{(l)}\right], \tag{2.45}$$

- M-step: Updates the estimated $\hat{\boldsymbol{\beta}}_n^{(l+1)}$ based on:

$$\hat{\boldsymbol{\beta}}_n^{(l+1)} = \arg\max_{\beta_n}\left(Q(\boldsymbol{\beta}_n, \hat{\boldsymbol{\beta}}_n^{(l)}) - penalty(\hat{\boldsymbol{\beta}}_n^{(l)})\right). \tag{2.46}$$

2.2 Parameter Estimation in Modelling of VO_2

Oxygen uptake (VO_2) on-kinetics is an important physiological parameter for the determination of functional health status and muscle energetics during physical exercise [69, 9, 70, 71]. Several studies confirmed that oxygen uptake is mainly controlled by intramuscular factors related metabolic system [72–74]. Different from the heart rate, the oxygen uptake is not affected by mood, stress, etc., and it is generally considered as the most accurate index of the cardiorespiratory system fitness.

2.2.1 VO_2 in Cardiorespiratory System

Respiratory action, also known as cell respiration, is a chemical process that biological cells oxidatively decompose organic matters and emit energy. The most commonly used organic matter to supply energy for cells is glucose. There are two ways to convert glucose into energy: aerobic respiration and anaerobic respiration. Aerobic respiration

refers to the cells, which is under the condition of oxygen as well as the participation of a variety of enzymes that act as catalytic and makes organic matter completely oxidative decompose. This process produces carbon dioxide and water, results in the release of energy and the generation of a large amount of Adenosine Triphosphate which is known as ATP. ATP can transport chemical energy within cells for metabolism. Under normal conditions, only considering the case of glucose for energy, the products are carbon dioxide and water in aerobic respiration. During intensive exercises, there is no oxygen in cells; the anaerobic respiration is in progress. The product is mainly lactic acid in this case. The cell neither consume oxygen, nor produce carbon dioxide. The total reaction of aerobic respiration can be expressed as [75],

$$\begin{aligned} &6O_2 + 6H_2O + C_6H_{12}O_6 \overset{enzyme}{\longrightarrow} \\ &6CO_2 + 12H_2O + \ energy. \end{aligned} \tag{2.47}$$

Furthermore, the pathway of oxygen in human body is shown in Fig.2.4[76].

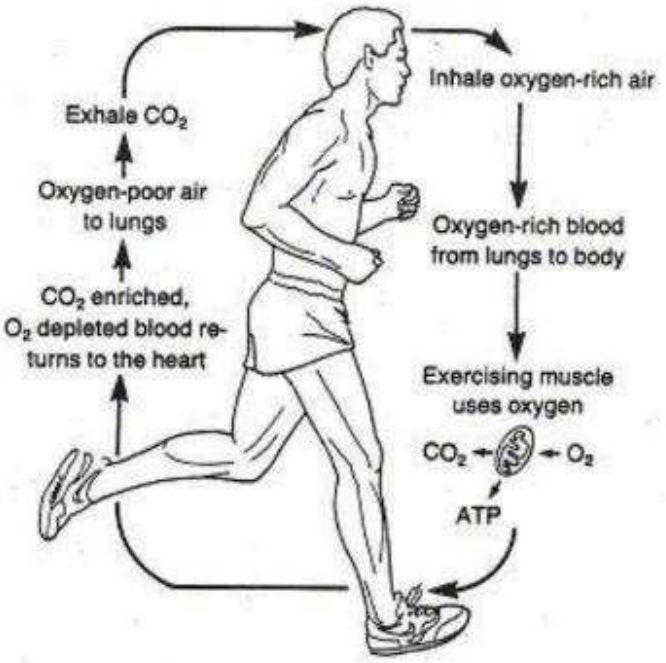

Fig. 2.4 The oxygen pathway from Sharma, 2014

2.2.2 Conventional Method of VO_2 Modelling

Due to the important characteristic of oxygen uptake in exercises, several studies for the modelling of physiological signal in response to treadmill exercise were also conducted. So far, for the dynamic modelling of oxygen uptake, several different modelling methods have been proposed. [10] first introduced the oxygen uptake kinetic for onset and offset of leg work. Then, lots of researchers studied on this area in order to obtain an accurate model. Previously, most researches, such as [36, 37], approximated the oxygen uptake response to cycling as first order system [74]:

$$VO_2(t) = VO_2^0 + \beta \times [1 - e^{(t-TD)/\tau_p}], \tag{2.48}$$

where TD is the time delay, τ_p is the time constant, and VO_2^0 is the baseline value of oxygen uptake. Normally, the time delay can be ignored. Then, the above model can be transformed into a first order ARMA model which is:

$$y(k) = a_1 x(k-1) + b_1 y(k-1) + \epsilon_1, \quad k = 2, 3, \cdots, M, \tag{2.49}$$

where $y(k)$ and $x(k)$ are the value of measurement and the value of input at time k respectively. Predicted error method (PEM) [77] is normally considered as the best method for solving this kind of ARMA model.

Later on, [38] and [39] applied Pseudo Random Binary Signal (PRBS) as the input signal to better stimulate the system. From results of spectrum analysis, the dynamic linearity of oxygen uptake at low frequency with work load was proved. Recently, paper [34] proposed a modelling method based on the Hammerstein model. It showed that the estimated response is better than previous methods.

The disadvantages of previous methods are clear. Normally, it is still quite difficult for users to follow the PRBS signal as input. Meanwhile, although the oxygen uptake response to exercise system can be roughly modelled as first-order dynamics systems under single step response, it is likely that the oxygen uptake response to exercise systems are actually a high-order system for some people under complex input signals due to the individual difference. Therefore, a nonparametric model will be an ideal

solution for this system identification task. However, due to the large number of parameters in the impulse response (FIR) of nonparametric model, it was impossible to estimate the parameters of the FIR without enough stimulations. Recently, [41, 42, 78] proposed a novel kernel based parameter estimation method to solve this problem.

2.2.3 Kernal Based Estimation Method

In this section, a new kernel based nonparametric model estimation method [41, 42, 78] is reviewed.

Let us select t as the current time and T as the sampling time, the relationship between the output (y, oxygen uptake) and input (u, speed) can be considered as a simple single input single output (SISO) dynamic system. Therefore, the discrete time output based on the impulse response of this system can be then expressed as[42]:

$$y(t) = \sum_{\tau=0}^{N} u(t-\tau)g(\tau) + \epsilon(t), \quad t = 1, 2, \cdots N \tag{2.50}$$

where $g(\cdot)$ represents the parameters of the finite impulse response (FIR), $\epsilon(t)$ is the Gaussian white noise and N is the total sampling number.

To obtain the unknown parameter $g(\cdot)$, a widely used cost function of Eq.(2.50) can be expressed as:

$$\sum_{t=1}^{N}(y(t) - L_t[g])^2, \tag{2.51}$$

where $L_t[g]$ is defined as:

$$L_t[g] = \sum_{\tau=0}^{\infty} u(t-\tau)g(\tau). \tag{2.52}$$

Now, assuming that a function $g \in R^m$, in regularisation term can be projected into a reproducing kernel Hilbert space (RKHS), i.e., $g \to g_{\mathcal{H}}$ ($R^m \times R^m \to R^{m\times m}(\mathcal{H})$). Based on this projection, the high frequency components in function g can be penalised, which can lead to smooth estimation of g. Furthermore, different from support vector regression (SVR) [79], the inputs and the unknown parameters from the error term are not projected into a higher dimension. Hence, the original system parameters are easy to be obtained directly. Eventually, the impulse response model can be identified by

minimizing the cost function:

$$\min_{g\in\mathcal{H}}\left(\sum_{t=1}^{N}(y(t)-L_t[g])^2+\gamma||g||_{\mathcal{H}}^2\right). \tag{2.53}$$

2.2.4 Review of Kernels

The projection $\gamma||g||_{\mathcal{H}}^2$ of function $g(\cdot)$ in 2.53 is based on kernel fucntion. Recently, several kernels were developed for this kernel based parameter estimation method. Four popular kernels are listed below [80]:

- Diagonal/Incorrelated (DI) kernel:

$$P(i,j)=\begin{cases}c\lambda^i, & i=j\\ 0\end{cases}, \tag{2.54}$$

  where $c,\lambda>0$.

- Tuned/Correlated (TC) kernel:

$$P(i,j)=c\min(\lambda^i,\lambda^j) \tag{2.55}$$

  where $c>0$, $1\geq\lambda\geq 0$.

- Diagonal/Correlated (DC) kernel:

$$P(i,j)=c\rho^{|i-j|}\lambda^{|i+j|/2}, \tag{2.56}$$

  where $c>0$, $0<\lambda\leq 1$ and $|\rho|\leq 1$.

- Stable Spline (SS) kernel:

$$P(i,j)=\begin{cases}c\dfrac{\lambda^{2i}}{2}\left(\lambda^i-\dfrac{\lambda^j}{3}\right), & i\geq j\\ c\dfrac{\lambda^{2j}}{2}\left(\lambda^j-\dfrac{\lambda^i}{3}\right), & j\geq i\end{cases}, \tag{2.57}$$

  where $c,\lambda>0$.

2.2.5 Optimum Kernel

Recently, [81, 82] proposed several optimisation methods to obtain an optimum kernel based on previous measurements.

From [81], the optimum kernel is considered as the linear combination of several pre-defined kernels (P). The optimum kernel can be expressed as:

$$P(\mu) = \sum_{i=1}^{k} a_i P_i, \quad \mu = [a_1, \cdots, a_k]^T \tag{2.58}$$

Then, with several assumptions and approximations, the estimation of μ can be considered as a difference of convex programming (DCP) problem [81, 83]. With several transformations, a majorisation minimsation (MM) [84] algorithm and a semidefinite programming (SDP) algrotihm [85] were proposed to solve the optimum μ. Based on paper [81], the DC, TC and SS kernels were selected as the pre-defined kernels. From the results, with the optimum kernel, the goodness-of-fit of estimated response can be increased slightly.

2.3 Summary

First of all, this chapter reviews the calibration of tri-axial and its relationship with parameter estimation. Secondly, this chapter reviews the previous knowledge of the modelling of oxygen uptake response to exercise. From the literature reviews, it is obvious that the auto-calibration of the tri-axial accelerometer can be considered as a parameter estimation problem of a nonlinear and nonconvex system. Furthermore, the modelling of oxygen uptake response to exercise can also be formulated as a parameter estimation problem without sufficient stimulations nor clean measurements.

According to the literature review, it indicates that the MEMS accelerometer is widely used nowadays, and the MEMS accelerometer cannot output accurate measurements without calibration due to the limitation of technologies. From the literature review, it indicates that several aspects of the auto-calibration of accelerometer still need to be improved. From the literature review, it indicates that the MEMS ac-

celerometer is widely used nowadays. However, due to the limitation of technologies, the MEMS acceleroemter required

For modelling of oxygen uptake response to exercise, previous studies did not pay enough attentions to individual differences. Furthermore, the system cannot be accurately estimated with insufficient stimulations and noise measurements due to the limitation of previous methods. A new method is expected to improve the accuracy of the dynamic modelling of oxygen uptake.

Chapter 3

An Efficient Auto-Calibration Method for Tri-Axial Accelerometer

3.1 Introduction

To reduce the dependency on high precision laboratory equipment, in recent years, gravity-based auto-calibration methods have been developed [11–13, 23, 26, 56, 86]. The principle of auto-calibration is built on the fact that the vector sum of tri-axial measurements should theoretically be equal to local gravity in the static state. Auto-calibration, in contrast with the classical calibration approach, does not need to precisely align TA to ensure that the projection of gravity on each axis is accurate. It only requires the TA to be *statically*, not necessarily accurately, placed in a number of distinct orientations.

Previous studies [11, 13, 55] for auto-calibration did not pay enough attention to calibration efficiency. In [14, 52, 87], only a brief discussion of direction selection for the entire IMU is given. They have not systematically investigated the selection of optimal orientations for parameter estimation, and often have only provided empirical advices. As examples, auto-calibration approaches discussed in [11, 13] have not given a specific number of initial observations, but have assumed that the number of experiments is

sufficient. These methods are not cost-effective for the users lacking the calibration apparatus because *stably* placing TA in a relatively *large* number of different directions is often time-consuming.

Instead of empirically selecting the initial orientation, a guide for optimal orientation selection with favourable calibration statistical properties deserves careful study. To this end, DoE has been developed, which is particularly useful in finding the maximum information about parameter calibration by means of a limited number of experiments. For classical inertial sensor calibration, the variance of estimated responses should be considered before calibration. This has led to the introduction of G-optimality to minimise the maximum estimation variance over the entire design region. However, since the auto-calibration model of the TA is highly nonlinear, the DoE cannot easily be directly applied to auto-calibration.

Until recently, [20] discussed the orientation selection for automatic calibration with the 9-parameter model based on DoE. In order to be more efficient, this chapter attempts to develop a new six-position auto-calibration method for MEMS TA based on the most commonly used 6-parameter model. Besides the advantages of all auto-calibration approaches, it should be emphasised that the proposed method will take the advantages of DoE to achieve best estimation accuracy in the sense of minimising the maximum estimation variance over the entire measurement range. In addition, due to its simplicity, the proposed method can be easily implemented in an embedded microcontroller, i.e. the proposed calibration can be implemented in *real time* in a wearable device with limited computational power.

In regard to parameter estimation, papers [11, 51, 55] applied nonlinear estimation methods, for which the convergence cannot be always guaranteed. Unlike most of the existing methods, the proposed calibration approach is based on a new linearisation method for the 6-parameter model. To reduce the error caused by linearisation, a convergence-guaranteed recursive linear least square estimation has been proposed to remove bias. In this work, DoE [17, 62] is used to optimally select the best orientations to minimise the maximum variance of the estimation error in the whole design region. Furthermore, the effectiveness and robustness of the method have been validated by both simulation and experiments, which shows that the desired estimation accuracy

of scale factors, offsets and responses are achieved. In addition, the results indicate that the estimation of the unknown parameters can often converge within 3 steps of iterations by using the proposed linear iterative parameter estimation method.

The major contributions of this chapter can be summarised as follows. Firstly, a six-point G-optimal experiment is proposed for a special second-degree model based on DoE. Secondly, a new linearisation approach has been proposed, which can simplify the auto-calibration model in the desired second-degree form so that the G-optimality is achievable. Thirdly, a convergence-guaranteed recursive parameter estimation algorithm has been developed. It can be easily implemented in a wearable device with limited computational power. In addition, to the best of the author's knowledge, the proposed approach is the most efficient auto-calibration scheme that can reach the maximum G-efficiency for six-parameter TA.

This chapter is organised as follows. In section 3.2, an experimental scheme is proposed and evaluated for a specific second-degree model based on DoE. In section 3.3, the linearisation method and the iterative parameter estimation algorithm are presented. In section 3.4, both the simulation and experiment are presented. Section 3.5 summarises the chapter.

3.2 A G-optimal Experimental Design

DoE is a statistical method used in the development of an adequate functional relationship between the response of interest $y \in R$ and a number of associated input variables $x_1, x_2, \cdots, x_k$. As part of DoE, optimum DoE is constructed on the basis of certain variance-related optimality. In general, to apply the technique from DoE, low order polynomial models are widely used [15, 17]:

$$y = \boldsymbol{f}^T(\boldsymbol{x})\boldsymbol{\beta} + \epsilon, \tag{3.1}$$

where $\boldsymbol{x} = [x_1, x_2, \cdots, x_k]^T$, $\boldsymbol{f}(\boldsymbol{x}) \in \boldsymbol{R}^{p\times 1}$ is a vector function of p elements consisting of powers and cross products of powers of $x_1, x_2, \cdots, x_k$ up to a certain degree denoted

by $d \geq 1$, $\boldsymbol{\beta}$ is the vector of parameters to be estimated, and ϵ is assumed to be a random experimental error with zero mean.

For a special 3 variables second-order polynomial model without intercept and interaction terms, it can be expressed as:

$$y = \sum_{i=1}^{3} \beta_i x_i + \sum_{i=1}^{3} \beta_{ii} x_i^2 + \epsilon. \tag{3.2}$$

where y is the response of the system, x_i is the input and $\beta_i(\beta_{ii})$ is the unknown parameter. The error term ϵ is assumed to be a random experimental error with zero mean.

Generally, in order to achieve optimum estimation of parameters for model (3.2), a series of n experiments should be implemented first. In each experiment, the response y is observed for specified settings of the control variables. These settings are considered as the design for obtaining the optimum estimation of parameter. Assuming that x_{ui} $(i = 1, 2, \cdots, k, u = 1, 2, \cdots, n)$ represents the uth design setting of x_i with k variables and y_u represents the response value of design setting $\boldsymbol{x_u} = [x_{u1}, x_{u2}, \cdots, x_{uk}]^T$, for Eq. (3.1), we have:

$$y_u = \boldsymbol{f}^T(\boldsymbol{x_u})\boldsymbol{\beta} + \epsilon_u, u = 1, 2, \cdots, n, \tag{3.3}$$

where ϵ_u represents the error from the uth observations. Then, Eq.(3.3) can be expressed in matrix from as:

$$\boldsymbol{y} = \boldsymbol{X}\boldsymbol{\beta} + \boldsymbol{\epsilon}, \tag{3.4}$$

where $\boldsymbol{y} = [y_1, y_2, \cdots y_n]^T$, the uth row of matrix $\boldsymbol{X} \in \boldsymbol{R}^{n \times p}$ is $\boldsymbol{f}^T(\boldsymbol{x_u})$ and $\boldsymbol{\epsilon} = [\epsilon_1, \epsilon_2, \cdots, \epsilon_n]^T$.

In optimum DoE, several indices are proposed to evaluate an experiment from various aspects of parameter estimation. Most of the indices are related with estimation variance, such as D-, G-, and I-optimality [62]. For Eq.(3.4), let us assume that $\boldsymbol{\epsilon}$ has a zero mean and a variance-covariance matrix given by $\sigma^2 \boldsymbol{I}_n$, its G-optimality can be investigated by the value of the scaled prediction variance (SPV) which is defined as:

$$d(\boldsymbol{x}, \boldsymbol{\xi}_n) = \frac{n \cdot var(\hat{y}(\boldsymbol{x}))}{\sigma^2} = n \cdot \boldsymbol{f}^T(\boldsymbol{x})(\boldsymbol{X^T X})^{-1}\boldsymbol{f}(\boldsymbol{x}), \tag{3.5}$$

where $\boldsymbol{\xi}_n$ is the experimental scheme with n observations.

Suppose we have a 6-observation experimental scheme, and the design matrix $\boldsymbol{\mathcal{D}}$ is:

$$\boldsymbol{\mathcal{D}} = \begin{array}{c} \begin{matrix} x_1 & x_2 & x_3 \end{matrix} \\ \left[\begin{array}{ccc} 1 & 0 & 0 \\ -1 & 0 & 0 \\ 0 & 1 & 0 \\ 0 & -1 & 0 \\ 0 & 0 & 1 \\ 0 & 0 & -1 \end{array}\right] \end{array}. \tag{3.6}$$

For experimental scheme (3.6), the model matrix $\boldsymbol{X}$ of Eq.(3.2) is:

$$\boldsymbol{X} = \begin{array}{c} \begin{matrix} x_1 & x_2 & x_3 & x_1^2 & x_2^2 & x_3^2 \end{matrix} \\ \left[\begin{array}{cccccc} 1 & 0 & 0 & 1 & 0 & 0 \\ -1 & 0 & 0 & 1 & 0 & 0 \\ 0 & 1 & 0 & 0 & 1 & 0 \\ 0 & -1 & 0 & 0 & 1 & 0 \\ 0 & 0 & 1 & 0 & 0 & 1 \\ 0 & 0 & -1 & 0 & 0 & 1 \end{array}\right] \end{array}, \tag{3.7}$$

and $\boldsymbol{f}(\boldsymbol{x}) = \left[\begin{array}{cccccc} x_1, & x_2, & x_3, & x_1^2, & x_2^2, & x_3^2 \end{array}\right]^T$.

A G-optimal design is the one that minimises the maximum SPV over experimental region. From the definition of G-optimal experimental design [62], if

$$\underset{\boldsymbol{x}\in\boldsymbol{R}}{Max}\, d(\boldsymbol{x}, \boldsymbol{\xi}_n) = p, \tag{3.8}$$

where p is the number of unknown parameters, then this experimental design is G-optimal [17].

Theorem 3.1 below confirms the experimental scheme (3.6) for model (3.2) is G-optimal.

Theorem 3.1 *Experimental scheme (3.6) is the G-optimal design for model (3.2) in the spherical design region* $\sum_{i=1}^{3} x_i^2 = 1$.

Proof See Appendix A. ∎

Remark 3.1 *Based on the proof of Theorem 3.1, it is actually easy to see that the experimental scheme (3.6) is also G-optimal in the design region of the ball,* $\sum_{i=1}^{3} x_i^2 \leq 1$. *However, for gravity-based calibration, the experimental design region is a sphere rather than a ball. We therefore here only consider the case the design region is a sphere.*

3.3 Efficient Auto-calibration for MEMS Tri-Axial Accelerometer

3.3.1 Model Linearisation for the Proposed Experimental Scheme

The fabrication of MEMS evolved from the process technology in semiconductor device fabrication, i.e. the basic techniques are deposition of material layers, patterning by photolithography and etching to produce the required shapes [88]. According to [28], for most of the recent developed MEMS TAs, the accuracy of the 6-parameter and 9-parameter models are almost the same. More specifically, with current photolithography techniques, the cross-axis factors between the axes of most MEMS TAs are generally negligible. In such cases, it is reasonable for us to select the 6-parameter model, rather than the 9-parameter model, for further discussion.

For the 6-parameter model, let us define $\boldsymbol{V} = [v_x, v_y, v_z]^T$ as the measurements of TAs. The unit of these measurements is gravity (g) in this work. In practice, for the analog accelerometer, the original output unit $\boldsymbol{V_d}$ is voltage. Fortunately, the datasheet from accelerometer manufactory provides the typical sensitivity λ (the unit is V/g for analogy accelerometer); the measurements with unit g can be easily obtained by:

$$\boldsymbol{V} = \lambda^{-1}\boldsymbol{V_d}. \tag{3.9}$$

For the digital accelerometer, the output unit is the least significant bit (LSB). Eq.(3.9) can also be applied to the digital accelerometer with different sensitivity (LSB/g). Note that this procedure is necessary for the convergence of the proposed calibration method; details to be explained later in this section. At this point, the mathematical model of local acceleration $\boldsymbol{A} = [a_x, a_y, a_z]^T$ with measurement $\boldsymbol{V}$ as input can be expressed as:

$$\begin{bmatrix} a_x \\ a_y \\ a_z \end{bmatrix} = \begin{bmatrix} S_x & 0 & 0 \\ 0 & S_y & 0 \\ 0 & 0 & S_z \end{bmatrix} \left(\begin{bmatrix} v_x \\ v_y \\ v_z \end{bmatrix} + \begin{bmatrix} O_x \\ O_y \\ O_z \end{bmatrix} \right), \tag{3.10}$$

where S_x, S_y, S_z and O_x, O_y, O_z represent scale factors ($\boldsymbol{S}$) and offsets ($\boldsymbol{O}$). Therefore, the resulting model has six independent parameters.

The idea of the auto-calibration method is that the measurement of TA should be equal to local gravity acceleration in a static state, i.e.,

$$g = \sqrt{a_x^2 + a_y^2 + a_z^2}. \tag{3.11}$$

Based on Eq.(3.11), the error $\tilde{\epsilon}_i$ for the ith measurement can be expressed as follows [11],

$$\begin{aligned} \tilde{\epsilon}_i =& a_{x,i}^2 + a_{y,i}^2 + a_{z,i}^2 - g^2 \\ =& \sum_{j=x,y,z} \left[S_j \cdot (v_{j,i} + O_j) \right]^2 - g^2, i = 1, 2, \cdots, n, \end{aligned} \tag{3.12}$$

where $v_{j,i}$ $(j = x, y, z)$ is a component of the ith measurement.

Thus, if we assume that $\boldsymbol{\beta}$ is the vector of the unknown parameters of the model, the cost function is defined as:

$$J(\boldsymbol{\beta}) = \sum_{i=1}^{n} \left(|| \boldsymbol{f}_{\boldsymbol{\beta}}(\boldsymbol{V}_i) - g^2 || \right), \tag{3.13}$$

where $\boldsymbol{V}_i = [v_{x,i}, v_{y,i}, v_{z,i}]^T$ $(i = 1, 2, \cdots, n)$ is the ith measurement, $\boldsymbol{f}_{\boldsymbol{\beta}}(\boldsymbol{V}_i)$ is a vector function of $\boldsymbol{V}_i$. The parameter estimation can be formulated as a nonlinear non-convex optimisation problem:

$$\min_{\boldsymbol{\beta}} J(\boldsymbol{\beta}). \tag{3.14}$$

Several numerical optimisation methods, such as the Downhill simplex optimisation method [55], Newton method [11], maximum likelihood estimation [56], unscented Kalman filter [12], graph optimisation [57], and Levenberg-Marquardt minimisation method [58, 59], are applied to solve this problem. Although the existing methods are able to identify the unknown parameter accurately in most cases, the convergence cannot be always ensured, and they are relatively complex to be implemented with an embedded micro-controller unit (MCU).

Unlike previous solutions, in this work, the G-optimal experimental scheme (3.6) will be applied to minimize the maximum variance of the estimated response. A linearisation method is proposed to reduce the computational complexity. In order to achieve this goal, it is necessary to simplify (3.12) by ignoring some less significant terms first.

According to [28], for a TA with regular accuracy, $\tilde{\epsilon}_i$ in (3.12) is a summation of a normal distribution and a Chi-square distribution. Compared to the Chi-square distribution component, the normal distribution part is dominant [28]. The overall error $\tilde{\epsilon}_i$ can be approximated as normal distribution with a zero mean. Hence, let us expand Eq.(3.12) and rearrange it as:

$$g^2 = 2 \sum_{j=x,y,z} \underbrace{S_j^2 O_j}_{\beta_k} v_{j,i} + \sum_{j=x,y,z} \underbrace{S_j^2}_{\beta_{kk}} v_{j,i}^2 + \sum_{j=x,y,z} S_j^2 O_j^2 + \epsilon_i, \tag{3.15}$$

where the random noise ϵ_i is normal distribution with zero mean. The first and second terms in Eq.(3.15) are contributed by scale factors, offsets and measurements. The third term is a function of the square of scale factors and offsets. For most recently manufactured MEMS TAs, the scale factor error and offset for each axis are typically less than $0.1g$ and 10%, respectively. Taking a commonly used commercial grade accelerometer ADXL345 as an example, in some extreme cases, it is possible for the scale factor error and offset to reach 10% and $0.15g$ respectively. Correspondingly, the maximum value of γ can reach $0.0817g^2$. Besides that, the third term in Eq.(3.15) only consists of scale factor and offset. If we assume the scale factor and offset are

constants, in this case, we can define the third term in Eq.(3.15) as γ,

$$\gamma = \sum_{j=x,y,z} S_j^2 O_j^2. \tag{3.16}$$

Let us also redefine a new set of parameters as follows:

$$\begin{cases} 2S_x^2 O_x = \beta_1 \\ 2S_y^2 O_y = \beta_2 \\ 2S_z^2 O_z = \beta_3 \\ S_x^2 = \beta_{11} \\ S_y^2 = \beta_{22} \\ S_z^2 = \beta_{33}\,. \end{cases} \tag{3.17}$$

It should be noted that the polarity of scale factor of each axis should be predetermined for the proposed method. To see this, let us take β_{11} and S_x as example. The proposed method computes β_{11} instead of S_x first, and calculates S_x by taking the square root of β_{11}. Without the predetermined polarity of S_x, we often select positive scale factor from the square root of β_{11}, which might be incorrect in some cases. Fortunately, the polarity of the scale factor for each axis is usually available from the data sheet, or can be easily determined by some simple tests. In order to simplify our discussion, without loss of generality, we assume that S_j is positive in the following discussions.

Now, replacing v_x, v_y, v_z by x_1, x_2, x_3, Eq.(3.15) can be rewritten as a function of $\boldsymbol{x} = [x_1, x_2, x_3]^T$:

$$y_i = \beta_1 x_{1,i} + \beta_2 x_{2,i} + \beta_3 x_{3,i} + \beta_{11} x_{1,i}^2 + \beta_{22} x_{2,i}^2 + \beta_{33} x_{3,i}^2 + \gamma + \epsilon_i. \tag{3.18}$$

As γ is small constant, for the moment, temporarily assuming γ is zero, Eq.(3.18) can be written as:

$$y_i = \beta_1 x_{1,i} + \beta_2 x_{2,i} + \beta_3 x_{3,i} + \beta_{11} x_{1,i}^2 + \beta_{22} x_{2,i}^2 + \beta_{33} x_{3,i}^2 + \epsilon_i. \tag{3.19}$$

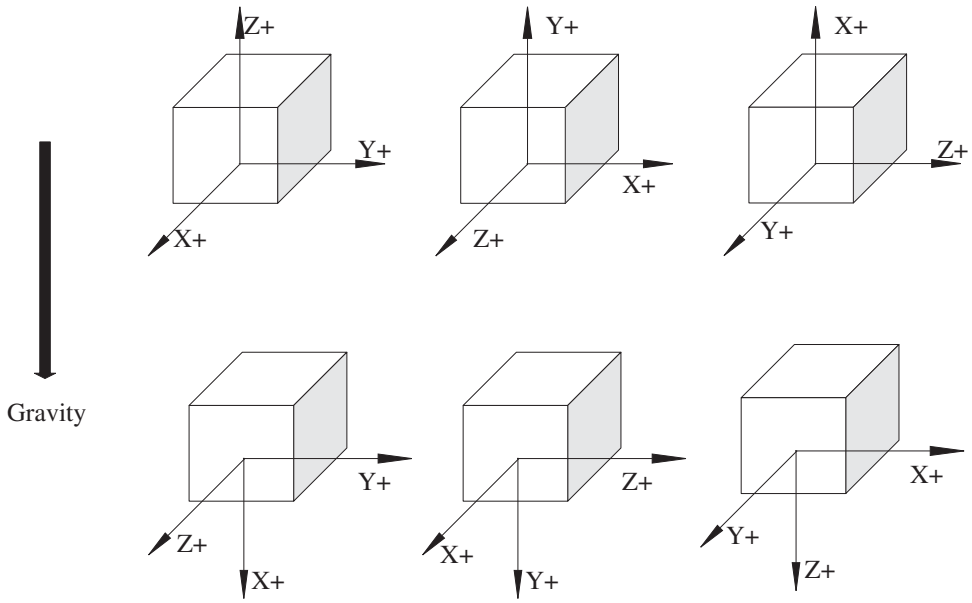

Fig. 3.1 The proposed 6-observation experimental scheme.

Now, let us recall the proposed 6-observation experimental scheme (3.7). Based on this experimental scheme, Eq.(3.19) can be expressed in matrix form as:

$$\boldsymbol{y} = \boldsymbol{X}\boldsymbol{\beta} + \boldsymbol{\epsilon}, \tag{3.20}$$

where $\boldsymbol{X} \in \boldsymbol{R}^{6\times 6}$ with its ith row as $[x_{1,i}, x_{2,i}, x_{3,i}, x_{1,i}^2, x_{2,i}^2, x_{3,i}^2]$, $\boldsymbol{y} = [y_1, y_2, \cdots, y_6]^T$, $\boldsymbol{\beta} = [\beta_1, \beta_2, \beta_3, \beta_{11}, \beta_{22}, \beta_{33}]^T$ and $\boldsymbol{\epsilon} = [\epsilon_1, \epsilon_2, \cdots, \epsilon_6]^T$.

In order to implement the experimental scheme (3.6), by projecting gravity on each axis of the three axes, the following relationship can be obtained:

$$\begin{bmatrix} x_1 \\ x_2 \\ x_3 \end{bmatrix} = \begin{bmatrix} g \cdot cos(\theta_x) \\ g \cdot cos(\theta_y) \\ g \cdot cos(\theta_z) \end{bmatrix}, \tag{3.21}$$

where θ_x, θ_y and θ_z are the tile angles between gravity and each axis. As shown in Fig. 3.1, the experimental scheme (3.6) requires each axis to be oriented upwards and downwards once.

So far, the analysis is based on the ideal situation, i.e., the offsets are 0. In this case, the neglected term γ from Eq.(3.18) is zero and Eq.(3.21) can be solved by LSE directly

without bias. In a practical situation, the measurement will be slightly different from the true value due to the scale factor errors and nonzero offsets. Now, we consider the bias caused by ignoring γ.

For experimental scheme (3.6), the matrix form of Eq.(3.18) can be expressed as:

$$\boldsymbol{y} = \boldsymbol{X}\boldsymbol{\beta} + \boldsymbol{\gamma} + \boldsymbol{\epsilon}, \tag{3.22}$$

where column vector $\boldsymbol{\gamma} \in \boldsymbol{R}^{6\times 1} = [\gamma, \gamma, \cdots, \gamma]^T$.

The expected value of estimator $\hat{\boldsymbol{\beta}}$ for Eq.(3.22) is given by,

$$\begin{aligned} E\left(\hat{\boldsymbol{\beta}}\right) &= \left(\boldsymbol{X}^T\boldsymbol{X}\right)^{-1}\boldsymbol{X}^T E\left[\boldsymbol{y}\right] \\ &= (\boldsymbol{X}^T\boldsymbol{X})^{-1}\boldsymbol{X}^T\left(\boldsymbol{X}\boldsymbol{\beta} + \boldsymbol{\gamma}\right) \\ &= \boldsymbol{\beta} + \left(\boldsymbol{X}^T\boldsymbol{X}\right)^{-1}\boldsymbol{X}^T\boldsymbol{\gamma}. \end{aligned} \tag{3.23}$$

Apparently, bias error also appears in the estimated response, and the expected value of the estimated response can be given by:

$$\begin{aligned} E\left(\hat{\boldsymbol{y}}\right) &= \boldsymbol{f}(\boldsymbol{X})E\left[\hat{\boldsymbol{\beta}}\right] \\ &= \boldsymbol{X}\left(\boldsymbol{\beta} + \left(\boldsymbol{X}^T\boldsymbol{X}\right)^{-1}\boldsymbol{X}^T\boldsymbol{\gamma}\right) \\ &= \boldsymbol{X}\boldsymbol{\beta} + \boldsymbol{X}\left(\boldsymbol{X}^T\boldsymbol{X}\right)^{-1}\boldsymbol{X}^T\boldsymbol{\gamma}. \end{aligned} \tag{3.24}$$

Thus, we have:

$$\begin{aligned} E(\hat{\boldsymbol{y}}) - E(\boldsymbol{y}) &= [\boldsymbol{X}\boldsymbol{\beta} + \boldsymbol{X}\left(\boldsymbol{X}^T\boldsymbol{X}\right)^{-1}\boldsymbol{X}^T\boldsymbol{\gamma}] - [\boldsymbol{X}\boldsymbol{\beta} + \boldsymbol{\gamma}] \\ &= [\boldsymbol{X}\left(\boldsymbol{X}^T\boldsymbol{X}\right)^{-1}\boldsymbol{X}^T\boldsymbol{\gamma} - \boldsymbol{\gamma}] \\ &= [\boldsymbol{H} - \boldsymbol{I}]\boldsymbol{\gamma}, \end{aligned} \tag{3.25}$$

where $\boldsymbol{H}$ is the hat matrix defined by $\boldsymbol{X}(\boldsymbol{X}^T\boldsymbol{X})^{-1}\boldsymbol{X}^T$.

From Eq.(3.25), it appears that the estimated response will be biased slightly due to the ignorance of γ.

In order to retain the advantages of DoE, a convergence guaranteed iterative LSE method has been proposed which can significantly reduce the bias of the estimated

parameter. From Eq.(3.22), we have:

$$\boldsymbol{y} - \boldsymbol{\gamma} = \boldsymbol{X}\boldsymbol{\beta} + \boldsymbol{\epsilon}. \tag{3.26}$$

For Eq.(3.26), the convergence-guaranteed iterative LSE method is summarised in Algorithm 2.

Algorithm 2 Iterative LSE Algorithm for Parameter Estimation

1: Assuming that the initial value of the neglected term $\boldsymbol{\gamma}^{(0)}$ is 0, for Eq.(3.26), the initial estimation of $\boldsymbol{\beta}$ can be computed directly by least square estimation,

$$\hat{\boldsymbol{\beta}}^{(1)} = (\boldsymbol{X}^T\boldsymbol{X})^{-1}\boldsymbol{X}^T(\boldsymbol{y} - \boldsymbol{\gamma}^{(0)}). \tag{3.27}$$

2: We solve the unknown parameters based on the estimated $\hat{\boldsymbol{\beta}}$ and Eq.(3.17). With the ith estimated $\hat{\boldsymbol{\beta}}^{(i)}$, the scale factors and offsets can be computed. Based on this new set of estimated scale factors and offsets, we estimate the new $\hat{\boldsymbol{\gamma}}^{(i)}$:

$$\begin{cases} \hat{S}_x^{(i)} = \sqrt{\hat{\beta}_{11}^{(i)}}, \\ \hat{S}_y^{(i)} = \sqrt{\hat{\beta}_{22}^{(i)}}, \\ \hat{S}_z^{(i)} = \sqrt{\hat{\beta}_{33}^{(i)}}, \\ \\ \hat{O}_x^{(i)} = \hat{\beta}_1^{(i)}/2\hat{\beta}_{11}^{(i)}, \\ \hat{O}_y^{(i)} = \hat{\beta}_2^{(i)}/2\hat{\beta}_{22}^{(i)}, \\ \hat{O}_z^{(i)} = \hat{\beta}_3^{(i)}/2\hat{\beta}_{33}^{(i)}, \\ \\ \hat{\gamma}^{(i)} = \sum\limits_{j=x,y,z} \hat{S}_j^{2(i)}\hat{O}_j^{2(i)}, \\ \hat{\boldsymbol{\gamma}}^{(i)} = \underbrace{[\hat{\gamma}^{(i)}, \hat{\gamma}^{(i)}, \cdots, \hat{\gamma}^{(i)}]}_{6}{}^T. \end{cases} \tag{3.28}$$

3: **repeat**

4: **until** the following convergence criteria is reached:

$$\max_{j=1,2,3} \left\{ |\hat{\beta}_{j(jj)}^{(n)} - \hat{\beta}_{j(jj)}^{(n)}| < \delta \right\}, \tag{3.29}$$

where δ equals to 1.0×10^{-6}.

5: Eventually, after n steps of iterations, the nearly unbiased estimator $\hat{\boldsymbol{\beta}}^{(n)}$ can be expressed as:

$$\hat{\boldsymbol{\beta}}^{(n)} = (\boldsymbol{X}^T\boldsymbol{X})^{-1}\boldsymbol{X}^T(\boldsymbol{y} - \hat{\boldsymbol{\gamma}}^{(n-1)}). \tag{3.30}$$

Theorem 3.2 below presents the conditions to guarantee the convergence of Algorithm 2.

Theorem 3.2 *Assume* $\boldsymbol{\beta}$ *is identifiable for a given experimental data set. If* $\gamma = \sum_{j=x,y,z} S_j^2 O_j^2$ *is less than 0.5, then* $\hat{\boldsymbol{\beta}}^{(n)}$ *in Algorithm 2 is convergent.*

Proof See Appendix B. ∎

The condition of Theorem 3.2 can ensure the convergency of Algorithm 2. Next, we briefly discuss the rate of convergence of this iterative algorithm. As discussed before, for the MEMS accelerometer, in some extreme cases, the maximum value of γ can reach $0.0817g^2$. To exam the efficiency of this iterative analysis, we simulate this procedure with different initial values for γ (0.1, 0.2, 0.3, 0.4) which is much larger than $0.0817g^2$. Fig. 3.2 shows the convergence rate of Algorithm 2 with different γ. Simulation results indicate that the estimated value converges to the real value within 3 iterations in most the cases ($\gamma = 0.1, 0.2, 0.3$). For those with extremely poor quality ($\gamma = 0.4$), this method can also converge but with more iterations steps.

3.3.2 Evaluation of Experiment

Theorem 3.2 proves Algorithm 2 can effectively estimate the parameters after several iterations. In a practical situation, without a high quality turntable, it is infeasible to align the accelerometer in the expected orientation with the desired level of accuracy. Thus, an ideal experiment cannot be perfectly implemented in real life. To assess the result of calibration, G-efficiency [62] is often adopted to evaluate the performance of the calibration. For a specific run of experiment $\boldsymbol{\xi}^*$, its G-efficiency is defined as:

$$G_{eff} = \frac{p}{\underset{\boldsymbol{x}}{Max}\, d\left(\boldsymbol{x}, \boldsymbol{\xi}^*\right)}, \tag{3.31}$$

where p is the number of unknown parameters and $d(\boldsymbol{x}, \boldsymbol{\xi}^*)$ is defined as in (3.5) for the specific experiment $\boldsymbol{\xi}^*$. For in field calibration, it is very difficult to obtain the optimum result due to the lack of a high quality turntable, but it will be more likely to

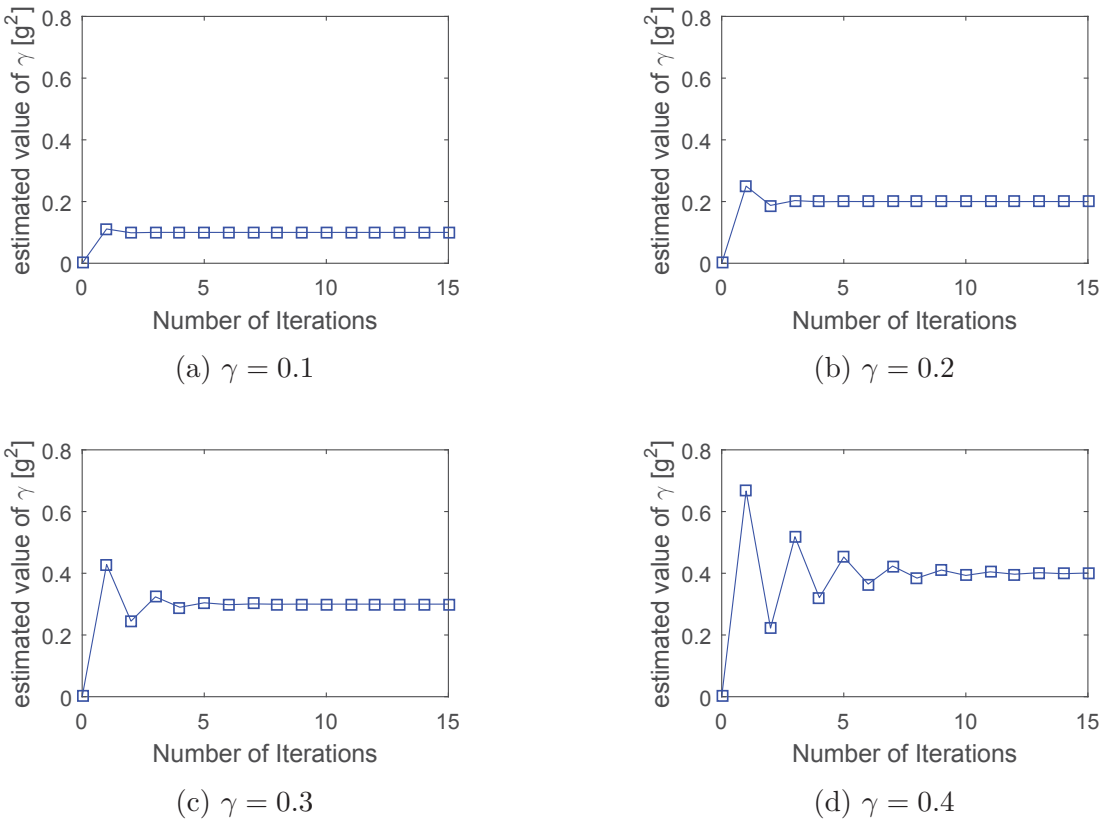

(a) $\gamma = 0.1$ (b) $\gamma = 0.2$

(c) $\gamma = 0.3$ (d) $\gamma = 0.4$

Fig. 3.2 Iteration times for accurately estimating $\hat{\boldsymbol{\gamma}}$ with a different initial γ.

obtain better results if the instruction of the 6-observation experimental scheme (3.6) has been followed.

3.4 Simulations and Experiments

3.4.1 Simulations

In order to evaluate the proposed calibration method, we firstly study this calibration method by simulation under different conditions, such as different noise levels, orientation misalignment, and poor manufacturing quality. For each run of simulation, a set of parameters were generated under certain conditions. Considering the parameters generated as true value, a set of measurements were obtained from 6 orientations following the experimental scheme described in Fig. 3.1. Then, the proposed calibration method

was implemented to estimate the unknown parameters based on the measurements of 6 orientations, and the estimation results were calculated and recorded.

First, let us examine the performance of this calibration method under normal conditions. For the MEMS accelerometer, the typical errors of scale factors and offsets are within $\pm 10\%$ and $\pm 0.1g$ respectively. These can cause significant difference in angle measurement during orientation in the worst-case scenario [11]. To obtain reliable results from simulation, the parameters were generated randomly under the following conditions: the errors of scale factors follow a uniform distribution $U(-10\%, 10\%)$; the offsets follow $U(-0.1g, 0.1g)$. In a practical situation, the users are usually unable to collect measurements from the exact locations of the experimental scheme. Under this assumption, the misalignments of the initial 6 orientations are biased with $U(0\%, 10\%)$.

Then, the proposed calibration method was implemented based on the generated measurements following the above requirements. For the iterative procedure, it was repeated 3 times. According to the datasheets of some recently developed MEMS accelerometers, the noise of output is around $100 \sim 400ug/\sqrt{Hz}$. With a maximum $100Hz$ output frequency, the range of noise density in g is around $1mg \sim 4mg$. Therefore, during the simulation, the noise, under normal distribution with a zero mean, was set in two variances: $1mg$ and $5mg$. The process is as follows. After 30 sets of parameters were generated, for each set of parameters, 500 times simulation were performed. For each simulation, we generated measurements from 6-orientation according to the experimental scheme and these orientations follow the requirement above. Then Algorithm 2 was applied to calculate the scale factors and offsets. After that, we randomly generated 500 sets of measurements for testing.

In total, we have $15,000$ simulations for the proposed calibration method. Since we know the true value of the scale factor and the offset, we compare the estimated parameters with the real parameters. Fig. 3.3 shows the box plot of the error between estimated parameters and the true value of the parameters. Fig. 3.3 indicates that the estimated parameters are unbiased, and the median value of the estimation error for the scale factors and offsets are 0. For most of the simulations, the errors of estimated parameters under $1mg$ and $5mg$ noise level are between $\pm 2 \times 10^{-3}$ and $\pm 1 \times 10^{-2}$ respectively. Beside this, we also calculated the error of the estimated response for

each axis, and the results are shown in Fig. 3.4. The two sub-figures of Fig. 3.4 show that the errors of the estimated responses for each axis are between $\pm 4 \times 10^{-3} g$ and $\pm 2 \times 10^{-2} g$ for different noise levels.

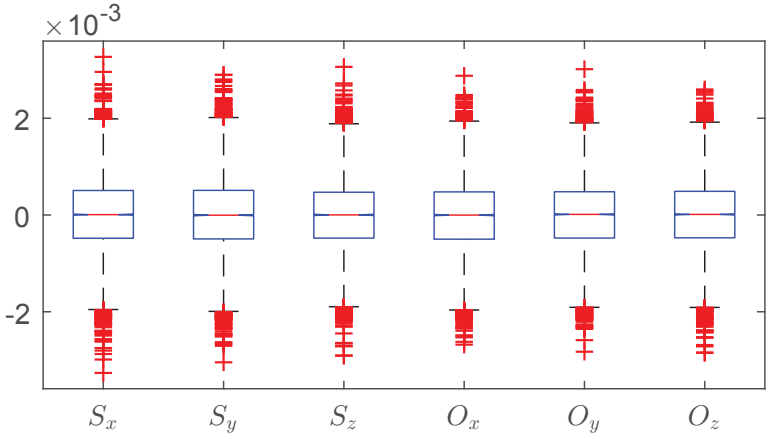

(a) 1mg noise level

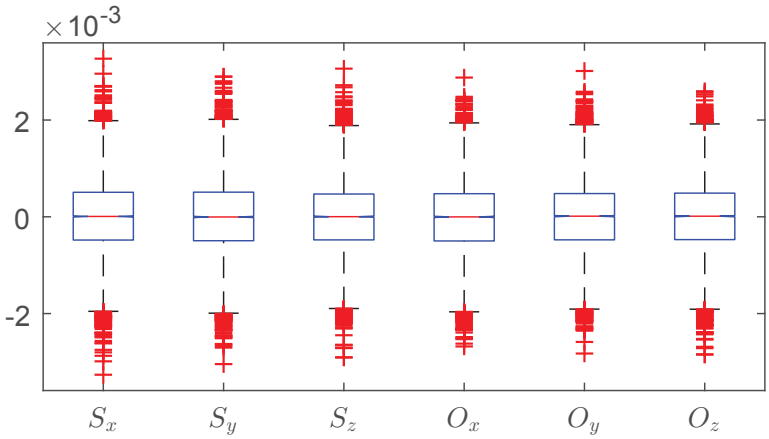

(b) 5mg noise level

Fig. 3.3 Error of the estimated scale factors and offsets [g] compared to the true value.

To show the convergence rate of the proposed calibration method, we randomly select a set of results from the previous simulation, which is listed in Table. 3.1. It indicates that the proposed calibration method can converge within 3 times of iterations.

The simulation results also indicate the proposed experimental scheme and the parameter estimation method is robust for low quality TAs. Let us assume that the outgoing quality is worse than the typical situation. The errors of scale factors follow

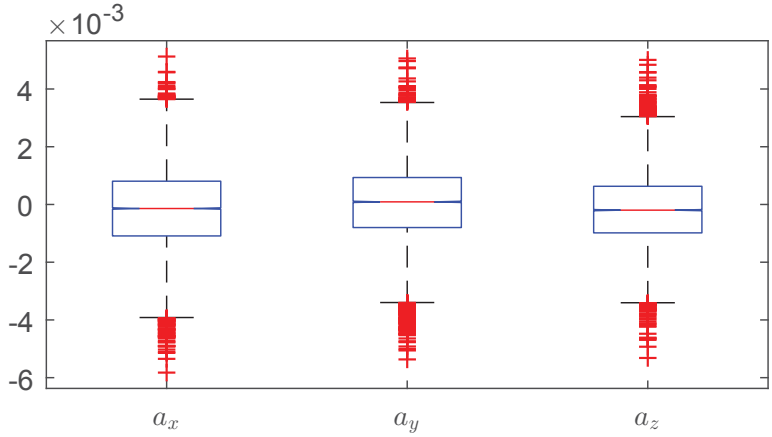

(a) 1mg noise level

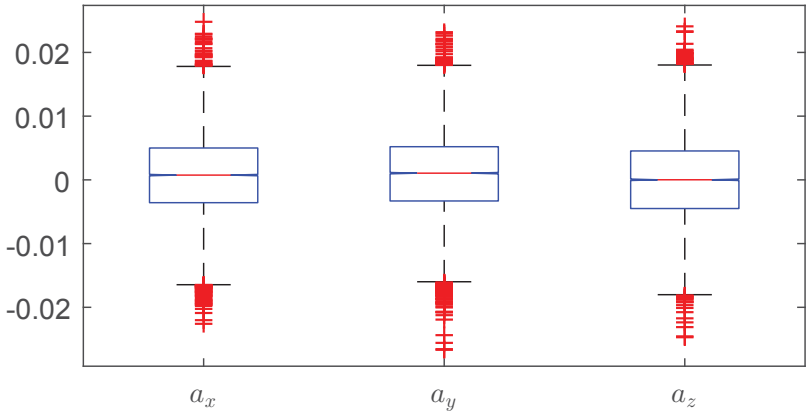

(b) 5mg noise level

Fig. 3.4 Error of the estimated acceleration [g] of each axis compared to the true value.

uniform distribution $U(-15\% \sim -10\%, 10\% \sim 15\%)$; the offsets follow $U(-10\% \sim -5\%, 5\% \sim 10\%)$. The misalignments of the initial 6 orientations are biased with $U(0\%, 10\%)$. The rest assumptions are the same as the previous simulation. The results are shown in Fig. 3.5 and Fig. 3.6, which indicate that this calibration method is also suitable for the calibration of TA with low outgoing quality. The error ranges of the estimated parameters and responses are similar to those of the normal condition, but with more outliers. All outliers are within $\pm 3 \times 10^{-3}$ and $\pm 2 \times 10^{-2}$ under $1mg$ and $5mg$ noise levels respectively. Meanwhile, for the errors of the estimated responses, the maximum value of the outliers slightly increased to $\pm 7 \times 10^{-3} g$ and $\pm 3 \times 10^{-2} g$.

Table 3.1 Calibration under normal conditions with 0mg, 1mg and 5mg noise levels

Number of iterations	$S_x[1]$	$S_y[1]$	$S_z[1]$	$O_x[g]$	$O_y[g]$	$O_z[g]$
Calibration results for 0mg noise						
True value	0.9690	1.0559	0.9489	-0.0335	-0.0509	-0.0808
1	0.9738	1.0612	0.9536	-0.0335	-0.0509	-0.0808
2	0.9689	1.0559	0.9488	-0.0335	-0.0509	-0.0808
3	0.9690	1.0559	0.9489	-0.0335	-0.0509	-0.0808
Calibration results for 1mg noise						
True value	0.9663	1.0528	1.0531	0.0437	0.0544	0.0180
1	0.9689	1.0547	1.0560	0.0436	0.0545	0.0173
2	0.9667	1.0523	1.0536	0.0437	0.0545	0.0173
3	0.9667	1.0523	1.0536	0.0437	0.0545	0.0173
Calibration results for 5mg noise						
True value	1.0771	0.9260	1.0605	0.0208	-0.0841	-0.0453
1	1.0801	0.9321	1.0632	0.0156	-0.0850	-0.0442
2	1.0753	0.9280	1.0586	0.0156	-0.0850	-0.0442
3	1.0754	0.9280	1.0586	0.0156	-0.0850	-0.0442

Furthermore, it can be seen that the estimation accuracy is also related to the noise level, i.e., a better TA with less noise often obtains more accurate results after calibration.

Finally, simulations for the proposed method and the classical method are performed for comparison purposes. The errors of scale factors follow a uniform distribution $U(-10\%, 10\%)$ and the offsets follow $U(-0.1g, 0.1g)$. The initial observation misalignment is set as $U(0\%, 10\%)$. We set up two noise levels (variances as $1mg$ and $5mg$ respectively) for testing. We generated 6-observations for calibration and 500 extra observations for testing. The error of each observation for each axis is shown in Fig. 3.7, which shows that the proposed calibration method can achieve higher accuracy compared to the classical 6-position method in different noise levels.

3.4.2 Experiments

Two popular commercial grade MEMS TAs, ADXL335 and ADXL345 from the Analog Device, were calibrated by the proposed method. The two accelerometers are three-axis; each axis is almost ideal vertical with the other two. The ADXL335 is an analog accelerometer, while the ADXL345 is a digital accelerometer. The convergence-

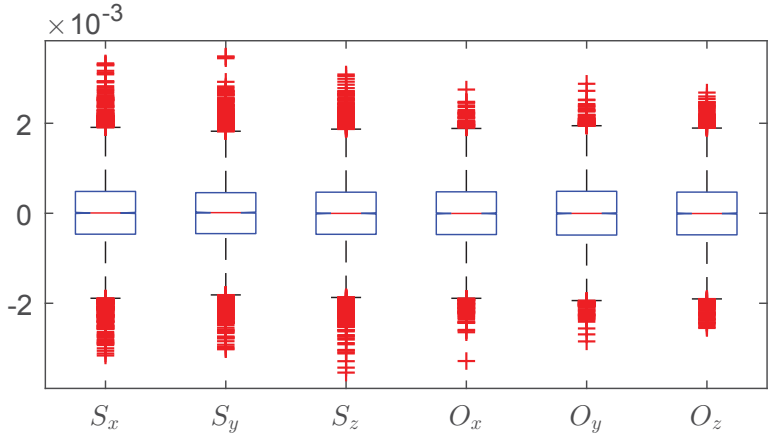

(a) 1mg noise level

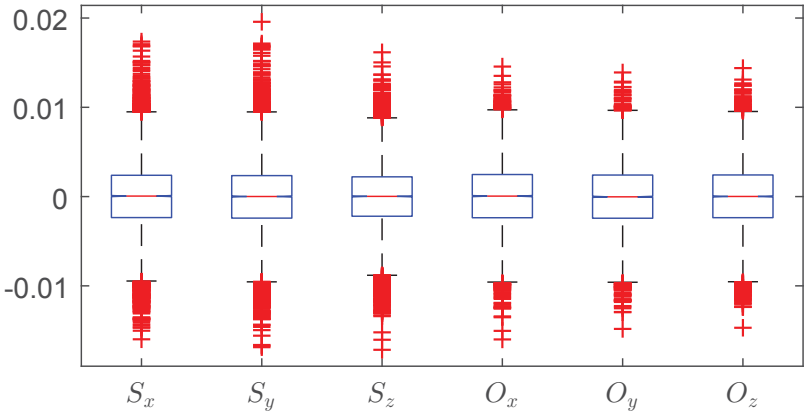

(b) 5mg noise level

Fig. 3.5 Error of the estimated scale factors and offsets [g] compared to the true value with poor outgoing quality.

guaranteed iteration LSE method, Algorithm 2, has been implemented in a micro-controller (TI MSP430) for the *online* estimation of the parameters.

Based on the experimental scheme, the accelerometer was directed to six different orientations as presented in Fig. 3.1. Then, we applied Algorithm 2 to calculate scale factors and offsets. In order to satisfy the convergence condition of Algorithm 2, the outputs from these accelerometers were converted to gravity with unit g based on standard factory parameters (i.e., sensitivity). To evaluate the accuracy of the estimated scale factor and offset, we mounted the accelerometer on a turntable with two degree of freedom and recorded the output from 100 different orientations. These

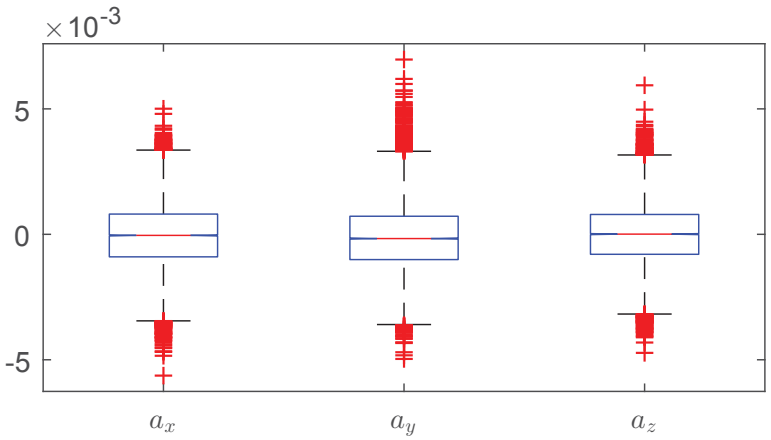

(a) 1mg noise level

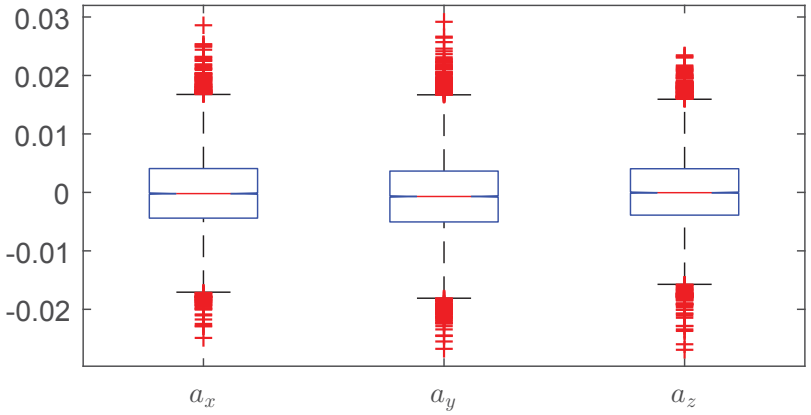

(b) 5mg noise level

Fig. 3.6 Error of the estimated acceleration [g] of each axis compared to the true value with poor outgoing quality.

100 orientations were considered as reference orientations, and the errors between the estimated orientations and reference orientations were calculated. The device is shown is Fig. 3.8. The turntable has 2 optical rotary stages with $5'$ resolution and $0.03mm$ reading accuracy.

We started with analog accelrometer (ADXL335) first. For the evaluation board of ADXL335, the output bandwidth is 50Hz and the measurement range is $\pm 3g$. We collected the output from ADXL335 by using a DAQ device (myRIO, NI). The unit of output was converted to g based on factory sensitivity ($330mV/g$) after removing zero g bias ($1.55V$). The accelerometer was then positioned as shown in Fig. 3.1 on

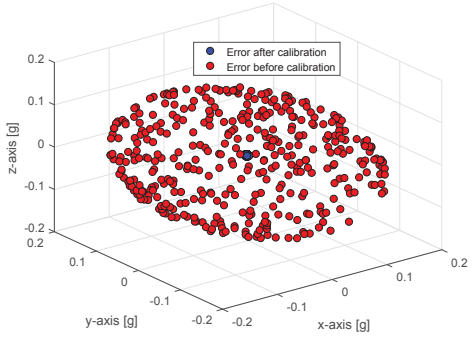

(a) 1mg noise level

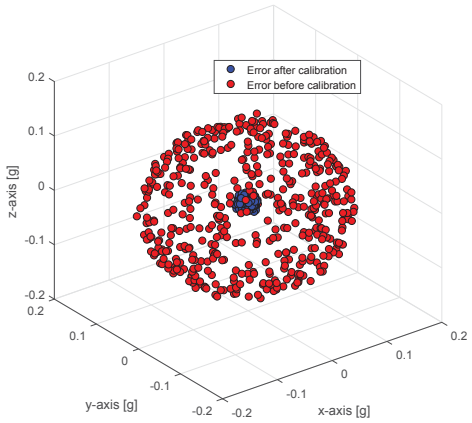

(b) 5mg noise level

Fig. 3.7 Error distribution of $\hat{a}_x$, $\hat{a}_y$ and $\hat{a}_z$ with a different noise level for the proposed method and and the classical approach.

a horizontal surface, which can be determined visually by the eye, since this method does not require precise orientation. Finally, after mounting the accelerometer on the turntable, we collected the outputs of 100 orientations and calculated the error. For each orientation, we rotated pitch ($\bar{p}$) for 36° first, followed by 10 yaw ($\bar{y}$) rotations from 0° to 360° with 36° intervals. Eventually, we had 100 observations in total. The true value of the 100 observations can be expressed as:

$$\begin{bmatrix} a_x \\ a_y \\ a_z \end{bmatrix}^T = \begin{bmatrix} a_{x,0} \\ a_{y,0} \\ a_{z,0} \end{bmatrix}^T \begin{bmatrix} c(\bar{p}) & 0 & s(\bar{p}) \\ 0 & 1 & 0 \\ -s(\bar{p}) & 0 & c(\bar{p}) \end{bmatrix} \begin{bmatrix} c(\bar{y}) & s(\bar{y}) & 0 \\ s(\bar{y}) & c(\bar{y}) & 0 \\ 0 & 0 & 1 \end{bmatrix}, \tag{3.32}$$

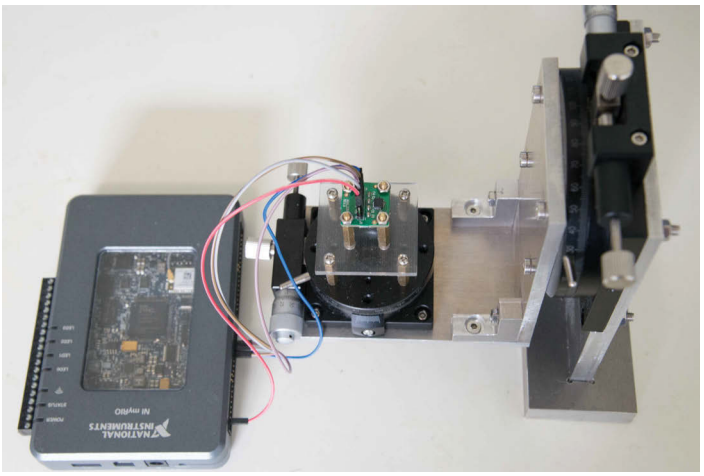

Fig. 3.8 Experiment device.

where $[a_{x,0}, a_{y,0}, a_{z,0}]^T$ is the initial value $[0, 0, 1]^T$, c and s represents $Cosine$ and $Sine$ respectively. The estimated $[\hat{a}_x, \hat{a}_y, \hat{a}_z]^T$ was compared with reference to $[a_x, a_y, a_z]^T$.

We also applied the proposed calibration method for a digital accelerometer ADXL345. During experiments, its output frequency was set to $100Hz$. The output range was selected as $\pm 2g$ with 10 bit resolution, which results in $256LSB/g$. The DAQ (myRIO) was applied for data acquisition and the I^2C communication protocol was chosen for data transfer. The other aspects of the experiment, including experimental scheme and parameter validation, were the same as ADXL335.

The results of experiments are analysed and then they are recorded in Table 3.2. The errors between the reference value $[a_x, a_y, a_z]^T$ and estimated value $[\hat{a}_x, \hat{a}_y, \hat{a}_z]^T$ were calculated for 100 testing orientations. Since we do not know the actual value of the scale factors and offsets, we compared and analysed the errors between the reference orientations and the estimated orientations. Due to the orientation inaccuracy of the turntable, the estimation of the vector sum ($\hat{a}_{vs}$) should be more accurate than that of the individual acceleration on each axis. It is also anticipated that the proposed experimental scheme from (3.6) optimises the variance of $\hat{a}_{vs}$.

The mean and standard deviation of errors are reported in Table 3.2. It shows that the standard deviation for overall acceleration is $0.0130g$ and $0.0076g$ for ADXL335 and ADXL345 respectively. It is the case that the estimation of $\hat{a}_{vs}$ achieved a higher level of accuracy compared to that from single axis.

Fig. 3.9 shows the convergence of the estimated parameters during each iteration, which indicates that convergence can be achieved after three iterative steps for the two accelerometers.

Table 3.2 Estimation error for overall acceleration and acceleration components on each axis

	Estimation error for ADXL335	
	Mean Error	Standard deviation
$\epsilon_{\hat{a}_x}(g)$	-0.0058	0.0184
$\epsilon_{\hat{a}_y}(g)$	-0.0048	0.0157
$\epsilon_{\hat{a}_z}(g)$	-0.0043	0.0153
$\epsilon_{\hat{a}_{vs}}(g)$	0.0002	0.0130
	Estimation error for ADXL345	
	Mean Error	Standard deviation
$\epsilon_{\hat{a}_x}(g)$	-0.0045	0.0293
$\epsilon_{\hat{a}_y}(g)$	-0.0042	0.0230
$\epsilon_{\hat{a}_z}(g)$	-0.0038	0.0080
$\epsilon_{\hat{a}_{vs}}(g)$	0.0010	0.0076

Overall, the desired results were achieved, which demonstrates the efficiency of the proposed experimental scheme and the parameter estimation method.

In real life, the experiments can hardly achieve the optimum situation. Therefore, G-efficiency has been proposed to evaluate the performance of experiments. However, for our special case, we have no idea about the true range of measurements before calibration. In fact, the range is an unknown ellipsoid rather than a sphere. Therefore, only approximate G-efficiency can be provided, which the measurements of calibration have been projected onto the surface of a unit sphere based on estimated parameters ($\hat{\boldsymbol{S}}$, $\hat{\boldsymbol{O}}$).

Based on Eq.3.31 and the estimated locations from measurements, the approximate G-efficiency for both experiments are:

- For ADXL 335, the approximate G-efficiency is 97.78%.
- For ADXL 345, the approximate G-efficiency is 94.19%.

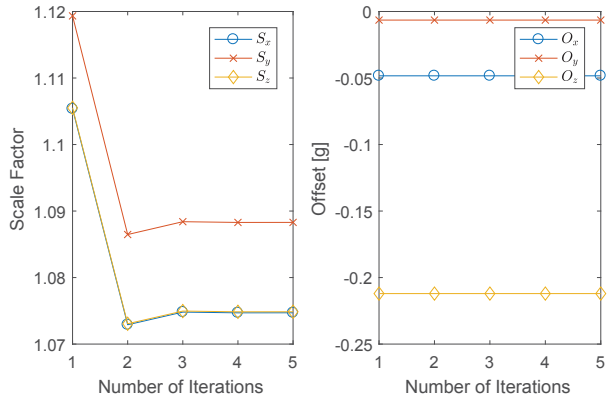

(a) 1mg noise level

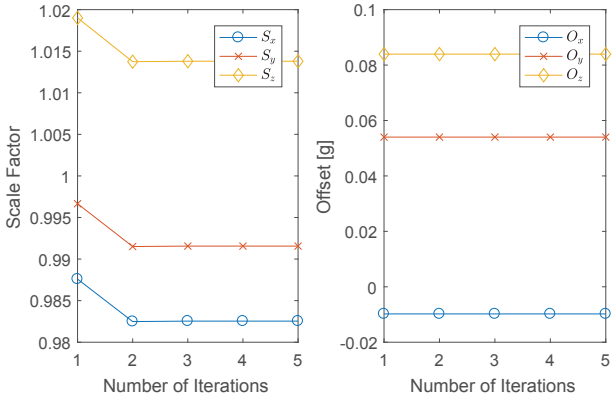

(b) 5mg noise level

Fig. 3.9 Calibration results for the two types of accelerometers.

3.5 Summary

In this chapter, a six-orientation G-optimal experimental scheme was proposed for a specific model of three factors. An auto-calibration method was presented based on this experimental scheme. To apply this experimental scheme, the auto-calibration model for tri-axial accelerometer was linearised and a convergence-guaranteed iterative algorithm was proposed to solve unknown parameters. To verify the presented method, both the simulation and the experiment were carried out.

Based on the simulation results, it can be concluded that the proposed calibration method can achieve accurate estimation in three iterations in most cases, and the

estimated response has a small mean error and standard deviation for different initial conditions.

Experiments were performed for the proposed calibration method by using two different types of MEMS accelerometers. As the true scale factors and offsets were unknown, the errors of the estimated responses were calculated and analysed. The experimental results clearly indicate that the proposed calibration approach can accurately estimate the vector sum of the three axes in the spherical design region. One of the advantages of the proposed approach is that the variance of the estimated response has been considered and minimised under G-optimality condition before the experiment. This experimental scheme is also efficient in the sense that it is less time consuming and it is cost saving.

Chapter 4

A Fast-Converge Real-Time Auto-Calibration Method for Tri-Axial Accelerometer

4.1 Introduction

Nowadays, several papers, including [11, 13, 19, 27] developed a new auto-calibration method for MEMS TAs, which does not need the extra sophisticated laboratory equipment for precise orientation information. Furthermore, based on auto-calibration, [20–22] consummated the auto-calibration by considering the quality of individual calibration, in which the selection of experimental observations is carefully investigated based on the design of experiment (DoE). Although the offline calibration can achieve desirable results, the output of MEMS TAs still suffer from drifting caused by the change of environment, such as ambient temperature, altitude, etc [23, 24]. In real life situation, if the MEMS TAs are intended to be used in multiple environments or with drastic environmental changes, the users need to frequently re-calibrate their MEMS TAs to amend the variation of parameters if they want to obtain the accurate output. Therefore, the online calibration is necessary to further improve the accuracy of measurement in real-time.

So far, to the author's best knowledge, most existing studies, including [13, 19, 28, 54, 64, 89], focused on offline TA calibration. Only limited papers [12, 25, 26, 90], are devoted to online calibration, which are mainly based on traditional calibration methods that constructed by employing different type of Kalman filters.

This chapter adopted a linearisation method based on the commonly used 6-parameter MEMS TAs model [11, 22]. After that, a modified damped recursive least square (MDRLS) estimation method is explored to estimate the unknown parameters. Noticeably, this method can converge to true value rapidly even when the parameters are varying. Furthermore, the damped term can effectively reduce the unwanted fluctuation of parameter estimation. In addition, this method can be implemented in an embedded Micro Control Unit (MCU) as the memory required to record the intermediate results is in fixed size. Comparing to the online calibration method in paper [26], the proposed method is based on auto-calibration, which does not require turntable to provide high-precision orientation. Unlike [25], the proposed method in this chapter can online estimate scale factors and offsets while the method from paper [25] can only estimate offset terms in real time. Furthermore, comparing to the UKF based calibration method [12, 60], the proposed method can achieve faster convergence speed and remain the same level of accuracy and no more extra prior statistical information is needed. The results from simulation and experiment are reported, which demonstrate the effectiveness of the proposed online calibration method.

The major contribution of this chapter can be summarised as follows. First, a linearisation method of 6-parameter TAs has been explored for online calibration. Second, a modified DRLS has been proposed to estimate the unknown parameters in real-time while keeps the estimation unbiased. Thirdly, the convergence speed and estimation effectiveness of the proposed method have been discussed based on both simulation and experiment. In the end, the convergence conditions of the proposed method has been analysed and discussed based on Monte Carlo simulation (see Note 4.1).

This chapter is organised as follows. In Section 4.2, the linearisation method for 6-parameter model is introduced for online calibration. In Section 4.3, the online

estimation method is proposed based on the linearised model. In Section 4.4, both the simulation and experiment are presented. Section 4.5 summarises the chapter.

4.2 Linearisation of the 6-Parameter Auto-Calibration Model for Online Calibration

In this study, we select the widely used 6-parameter model for MEMS accelerometer [11], which consists of three orthogonal scale factors $\boldsymbol{S} = diag\{[s_x, s_y, s_z]\}$ and three offsets $\boldsymbol{o} = \begin{bmatrix} o_x & o_y & o_z \end{bmatrix}^T$. According to [22, 28], for most of the commercial grade MEMS accelerometers, the accuracy of estimation based on the 6-parameter and 9-parameter models is almost identical.

For the selected 6-parameter model, let us define $\boldsymbol{v} = \begin{bmatrix} v_x & v_y & v_z \end{bmatrix}^T$ as the measured acceleration from accelerometer. With the scale factor $\boldsymbol{S}$ and offset $\boldsymbol{o}$, the mathematical model between the local acceleration $\boldsymbol{a} = \begin{bmatrix} a_x & a_y & a_z \end{bmatrix}^T$ and the measured acceleration $\boldsymbol{v}$ can be expressed as $\boldsymbol{a} = \boldsymbol{S}(\boldsymbol{v} + \boldsymbol{o})$, i.e.,

$$\begin{bmatrix} a_x \\ a_y \\ a_z \end{bmatrix} = \begin{bmatrix} s_x & 0 & 0 \\ 0 & s_y & 0 \\ 0 & 0 & s_z \end{bmatrix} \left(\begin{bmatrix} v_x \\ v_y \\ v_z \end{bmatrix} + \begin{bmatrix} o_x \\ o_y \\ o_z \end{bmatrix} \right). \tag{4.1}$$

The basic idea of auto-calibration is that the vector summation of the measured acceleration should be equal to local gravity ($1g$) in static state, i.e.,

$$g^2 = a_x^2 + a_y^2 + a_z^2 + \epsilon, \tag{4.2}$$

where ϵ represents the error.

Based on Eq.(4.2), with a total number of N measurement, the auto-calibration method is then trying to optimise the following cost function:

$$\begin{aligned} \min_{\boldsymbol{S},\boldsymbol{o}} \quad J(\boldsymbol{S},\boldsymbol{o}) &= \sum_{k=1}^{N} \left(a_x[k]^2 + a_y[k]^2 + a_z[k]^2 - g^2 \right) \\ &= \sum_{k=1}^{N} \left\{ \sum_{i=x,y,z} \left[s_i(v_i[k] + o_i) \right]^2 - g^2 \right\}, \end{aligned} \tag{4.3}$$

where $a_i[k]$ and $v_i[k]$ are the true accelerations and the output for the tth measurement respectively. For the online calibration, several optimisation methods were proposed to solve this problem based on unscented Kalman filter (UKF) [26] or other filtering algorithms [25]. Although the existing methods are able to estimate the unknown parameters with satisfied performance, the procedures are often complex and the discussion of its convergence conditions is often missing. It is not ideal to implement those calibration methods on a commonly used embedded MCU as the nonlinear online estimation method is generally complex.

According to [28], the error term ϵ in Eq.(4.2) is the summation of normal distribution and chi-square distribution. Comparing to normal distribution component, the chi-squared distribution part is neglectable [28]. The overall error can be considered as a normal distribution noise with zero mean.

To achieve an effective online auto-calibration, by neglecting some ignorable parameters, a linearisation method is proposed in this study to further decrease computational complexity.

After substituting Eq.(4.1) into Eq.(4.2), the auto-calibration for the kth measurement is given as follows:

$$\begin{aligned} g^2 = &\sum_{i=x,y,z} s_i^2 v_i^2[k] + 2 \sum_{i=x,y,z} s_i^2 o_i v_i[k] \\ &+ \sum_{i=x,y,z} s_i^2 o_i^2 + \epsilon, \end{aligned} \tag{4.4}$$

which is nonlinear with respect to the parameters $\boldsymbol{S}$ and $\boldsymbol{o}$. To linearise it, let us see the first and second terms in Eq.(4.4), which are contributed by scale factors, offsets and measurements. While the third term is only consisted of scale factors and offsets.

To analyse the effect of the third term in Eq.(4.4), we take some conventional values of scale factor error and offset from some recently developed MEMS accelerometers. According to their datasheets, normally, scale factor error and offset of each axis will be less than 10% and 0.1g respectively. Let us take MPU 9250 as an example. From data sheet, the typical maximum offsets of o_x, o_y, o_z are 80mg, 80mg, and 150mg respectively. With a large scale factor error (10%), the largest value of $\sum s_i^2 o_i^2$ is $0.0427g^2$ which is less than 5% comparing to overall value ($1g^2$). In this case, we can neglect the third term in Eq.(4.4) first. Later on, an online recursive compensation method will be applied to remove this bias. To linearise Eq.(4.4), we define a new set of parameters as follows [22]:

$$\boldsymbol{\beta} = \begin{bmatrix} 2s_x^2 o_x \\ 2s_y^2 o_y \\ 2s_z^2 o_z \\ s_x^2 \\ s_y^2 \\ s_z^2 \end{bmatrix} = \begin{bmatrix} \beta_1 \\ \beta_2 \\ \beta_3 \\ \beta_4 \\ \beta_5 \\ \beta_6 \end{bmatrix}. \tag{4.5}$$

As the proposed algorithm can only obtain $\boldsymbol{\beta}$ and the scale factor s_i ($i \in \{x, y, z\}$) is the square root of β_j ($j \in \{4, 5, 6\}$) respectively, it is necessary to determine the polarity of scale factor s_i before apply this calibration method, which can be easily determined by using a simple polarity test based on the direction of the gravity.

Since most of existing nonlinear method requires statistical property of noise, which is hard to identify in real life situation. We proposed another approach for the estimation of Eq.(4.3) based on the linearised model Eq.(4.4). A column vector $\boldsymbol{\gamma}_N \in R^{N\times 1}$ is defined where all its elements are identical:

$$\gamma_i = \gamma = (s_x^2 o_x^2 + s_y^2 o_y^2 + s_z^2 o_z^2). \tag{4.6}$$

Based on (4.4), (4.5) and (4.6), the matrix form for the linearised Eq.(4.4) with N measurements can be expressed as:

$$\boldsymbol{y}_N = \boldsymbol{X}_N \boldsymbol{\beta} + \boldsymbol{\gamma}_N + \boldsymbol{\epsilon}_N, \tag{4.7}$$

where the subscripts of $\boldsymbol{X}_N$, $\boldsymbol{y}_N$, $\boldsymbol{\gamma}_N$ and $\boldsymbol{\epsilon}_N$ represent the number of measurement. $\boldsymbol{X}_N$ is the matrix of measured acceleration, whose kth row can be expressed as

$$\boldsymbol{x}[k] = \begin{bmatrix} v_1[k] & v_2[k] & v_3[k] & v_1^2[k] & v_2^2[k] & v_2^3[k] \end{bmatrix}, \tag{4.8}$$

where $v_{x,y,z}(k)$ is replace by $v_{1,2,3}(k)$ for simplification. $\boldsymbol{y}_N \in R^{N\times 1}$ is defined as:

$$\boldsymbol{y}_N = \begin{bmatrix} g & g & \cdots & g \end{bmatrix}^T. \tag{4.9}$$

Eq.(4.7) can be rewritten as:

$$\boldsymbol{y}_N - \hat{\boldsymbol{\gamma}}_N \triangleq \boldsymbol{\delta}_N = \boldsymbol{X}_N\boldsymbol{\beta} + \epsilon_N. \tag{4.10}$$

Eq.(4.10) can be considered as a linear function of unknown parameters $\boldsymbol{\beta}$, and $\boldsymbol{\beta}$ can be solved recursively online. To further remove the bias caused by linearisation, $\hat{\gamma}$ can be updated recursively based on Eq.(4.5) and Eq.(4.6).

4.3 Modified Damped Recursive Least Square Estimation

Eq.(4.10) can be solved by using batch least square method. For a real-time parameter estimation, the recursive least square estimation (RLS) is often the most direct method. However, considering that the parameter variation of the typical tri-axial accelerometers in the market is often quite slow, we select the damped recursive least square (DRLS) as an initial algorithm.

Now, at time-step t, we define

$$\hat{\delta}[t] = y[t] - \hat{\gamma}[t] = g - \hat{\gamma}[t],$$

where $\hat{\gamma}[t]$ is the estimated bias at time-step t, which is based on the estimated $\hat{\boldsymbol{S}}[t-1]$ and $\hat{\boldsymbol{o}}[t-1]$ at time-step $(t-1)$:

$$\begin{aligned}\hat{\gamma}[t] =& s_x^2[t-1]o_x^2[t-1] + s_y^2[t-1]o_y^2[t-1] \\ &+ s_z^2[t-1]o_z^2[t-1].\end{aligned} \tag{4.11}$$

The purpose of the introduction of the estimated $\hat{\delta}[t]$ is to remove bias due to linearisation procedure. As the parameters of acclerometers are relatively stable due to its physical characteristics, a damped term can help to stabilise the estimation and minimise the variation caused by noise. Thus, a cost function of Eq.(4.10) is constructed as follows:

$$J(\hat{\boldsymbol{\beta}}) = (\sum_{k=1}^{t} \lambda^{t-k} e[k]^2) + \mu||\hat{\boldsymbol{\beta}}[t] - \hat{\boldsymbol{\beta}}[t-1]||_2^2, \tag{4.12}$$

where μ is a positive scale constant, $e[k]$ is the residual error of the kth observation,

$$e[k] = \hat{\delta}[k] - \boldsymbol{x}[k]\hat{\beta}[k], \tag{4.13}$$

and $\boldsymbol{x}[k]$ is the kth row of measurement matrix as defined in Eq.(4.8).

For the tth estimation, minimizing the cost function from (4.12) results in the recursive equations as [91]:

$$\begin{aligned}\hat{\boldsymbol{\beta}}[t] =& \hat{\boldsymbol{\beta}}[t-1] + \mu\lambda \boldsymbol{P}[t](\hat{\boldsymbol{\beta}}[t-1] - \hat{\boldsymbol{\beta}}[t-2]) \\ &+ \boldsymbol{P}[t]\boldsymbol{x}^T[t](\hat{\delta}[t] - \boldsymbol{x}[t]\hat{\boldsymbol{\beta}}[t-1]),\end{aligned} \tag{4.14}$$

$$\boldsymbol{P}[t] = (\mu(1-\lambda)\boldsymbol{I} + \lambda \boldsymbol{P}^{-1}[t-1] + \boldsymbol{x}[t]\boldsymbol{x}^T[t])^{-1}, \tag{4.15}$$

$$\hat{\delta}[t] = y[t] - \hat{\gamma}[t] = g - \hat{\gamma}[t], \tag{4.16}$$

where the inverse of matrix cost more time to process with MCU. Therefore, the recursive form of Eq.(4.15) can be derived as:

$$\boldsymbol{P}[t] = \frac{1}{\lambda}\left[\boldsymbol{P}'[t] - \frac{\boldsymbol{P}'[t]\boldsymbol{x}[t]\boldsymbol{x}^T[t]\boldsymbol{P}'[t]}{\lambda + \boldsymbol{x}^T[t]\boldsymbol{P}'[t]\boldsymbol{x}[t]}\right], \tag{4.17}$$

$$\boldsymbol{P}'[t] = \boldsymbol{P}[t-1] - \sum_{j=1}^{6} \frac{\boldsymbol{P}'_{j-1}[t-1]\boldsymbol{r}_j\boldsymbol{r}_j^T\boldsymbol{P}'_{j-1}[t-1]\mu'}{1 + \boldsymbol{r}_j^T\boldsymbol{P}'_{j-1}[t-1]\boldsymbol{r}_j\mu'}, \tag{4.18}$$

$$\boldsymbol{P}'_j[t-1] = \boldsymbol{P}'_{j-1}[t-1] - \frac{\boldsymbol{P}'_{j-1}[t-1]\boldsymbol{r}_j\boldsymbol{r}_j^T\boldsymbol{P}'_{j-1}[t-1]\mu'}{1 + \boldsymbol{r}_j^T\boldsymbol{P}'_{j-1}[t-1]\boldsymbol{r}_j\mu'}, \tag{4.19}$$

$$\boldsymbol{P}'_0[t-1] = P[t-1], \tag{4.20}$$

where $\boldsymbol{r}_j$ is the jth column of identity matrix $\boldsymbol{I}_6$ in this case, such as:

$$\boldsymbol{r}_2^T = \begin{bmatrix} 0 & 1 & 0 & 0 & 0 & 0 \end{bmatrix}, \tag{4.21}$$

and

$$\mu' = (1-\lambda)\mu/\lambda. \tag{4.22}$$

Then, the ith estimated original scale factor $\hat{\boldsymbol{S}}[t]$ and offset $\hat{\boldsymbol{o}}[t]$ can be calculated respectively. The calibrated result $\hat{\boldsymbol{a}}[t]$ is expressed as:

$$\hat{\boldsymbol{a}}[t] = \hat{\boldsymbol{S}}[t](\boldsymbol{v}[t] + \hat{\boldsymbol{o}}[t]). \tag{4.23}$$

After that, the residual term $\hat{\gamma}[t+1]$ will be updated based on Eq.(4.5) and Eq.(4.11) for the next estimation with new inputs.

The overall procedure of this calibration method is shown in Algorithm 3 below:

Algorithm 3 Modified damped recursive least square (MDRLS) for 6-parameter model of TA

Initial: λ, μ, $\boldsymbol{P}[0]$, $\hat{\boldsymbol{\beta}}[-1]$, $\hat{\boldsymbol{\beta}}[0]$, $\hat{\gamma}[1]$,$\boldsymbol{r_j}(j = 1, 2 \cdots, 6)$.
$\mu' = (1 - \lambda)\mu/\lambda$.
for $t = 1, 2, \cdots, m$ **do**
    $\hat{\delta}[t] = y[t] - \hat{\gamma}[t]$.
    Construct $\boldsymbol{x}[t]$ based on measurement $\boldsymbol{v}[t]$ and Eq.(4.8).
    Update $\boldsymbol{P}[t]$, $\boldsymbol{P}[t-1]$, r_j, μ', and λ based on Eq.(4.17)-Eq.(4.22).
    Solve estimated $\hat{\boldsymbol{\beta}}[t]$ based on Eq.(4.14) and measurement $\boldsymbol{v}[t]$.
    Solve estimated $\hat{s}_{x,y,z}[t]$ and $\hat{o}_{x,y,z}[t]$ based on Eq.(4.5).
    Update estimated $\hat{\gamma}[t+1]$ based on Eq.(4.5) and Eq.(4.11).
    Estimate $\hat{\boldsymbol{a}}[t]$ based on Eq.(4.23).
end for
Output: $\hat{\boldsymbol{a}}[t]$, $\hat{\boldsymbol{S}}[t]$ and $\hat{\boldsymbol{o}}[t]$.

4.4 Simulation and Experimental Validations

4.4.1 Simulations

For the MEMS tri-axial accelerometer, it is usually unable to obtain the true scale factors and offsets in real life situation. Hence, it is difficult to ideally evaluate the performance of the proposed online calibration accurately by experiments alone. Meanwhile, it is also difficult to evaluate some characteristics of the proposed method by limited number of real life experiments. Therefore, it is necessary to evaluate the proposed online calibration method by simulation first. To do so, we start with simulations of the proposed calibration method under different settings, including different initial condition and noise levels.

Firstly, for the MEMS accelerometer, the performance of the proposed online calibration method is evaluated under normal condition that the errors of scale factors and offsets are within $\pm 10\%$ and $\pm 0.1g$, respectively. For these normal tri-axial accelerometer without calibration, these errors can cause significant difference in angle

measurement in the worst case [28]. Furthermore, based on the datasheet of the most newly developed MEMS TAs, the noise density is around $100 \sim 400\ ug/\sqrt{Hz}$ [21]. With $100Hz$ output, the range of noise is around $1mg \sim 4mg$. Therefore, it is reasonable to set two noise levels ($1mg$ and $5mg$) for the simulation.

For the first part of simulation, a tri-axial accelerometer, whose errors of scale factors ($\boldsymbol{S}$) and offsets ($\boldsymbol{o}$) follow uniform distributions $U(-10\%, +10\%)$ and $U(-0.1g, 0.1g)$, was generated randomly at the beginning of each run. Then, 500 true accelerations ($\boldsymbol{a}$) on the surface of a sphere with $1g$ radium were randomly generated. These 500 ideal accelerations were converted to measurements ($\boldsymbol{v}$) based on the generated model ($\boldsymbol{S}$ and $\boldsymbol{o}$) with noise embedded. With these 500 measurements, the proposed algorithm was applied to estimate the scale factors and offsets online based on the following initial conditions: $\boldsymbol{S}[0] = \boldsymbol{S}[-1] = \boldsymbol{I}_3$, $\boldsymbol{o}[0] = \boldsymbol{0}_{3\times1}$, $\boldsymbol{P}(0) = 0.1 \cdot \boldsymbol{I}_6$, $\mu = 0.2$, $\lambda = 0.98$

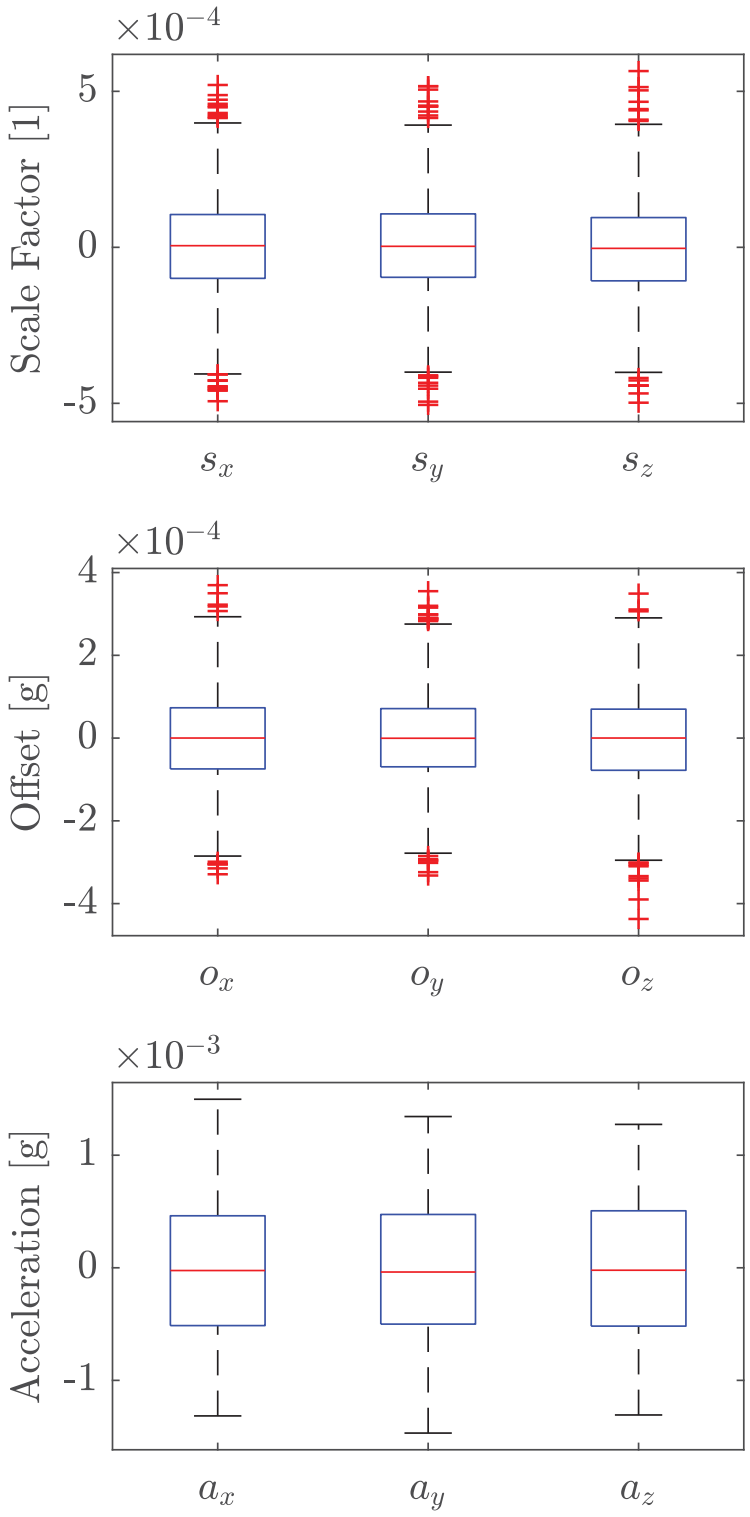

Fig. 4.1 Errors between estimations and true values of simulation 1 with $1mg$ noise level

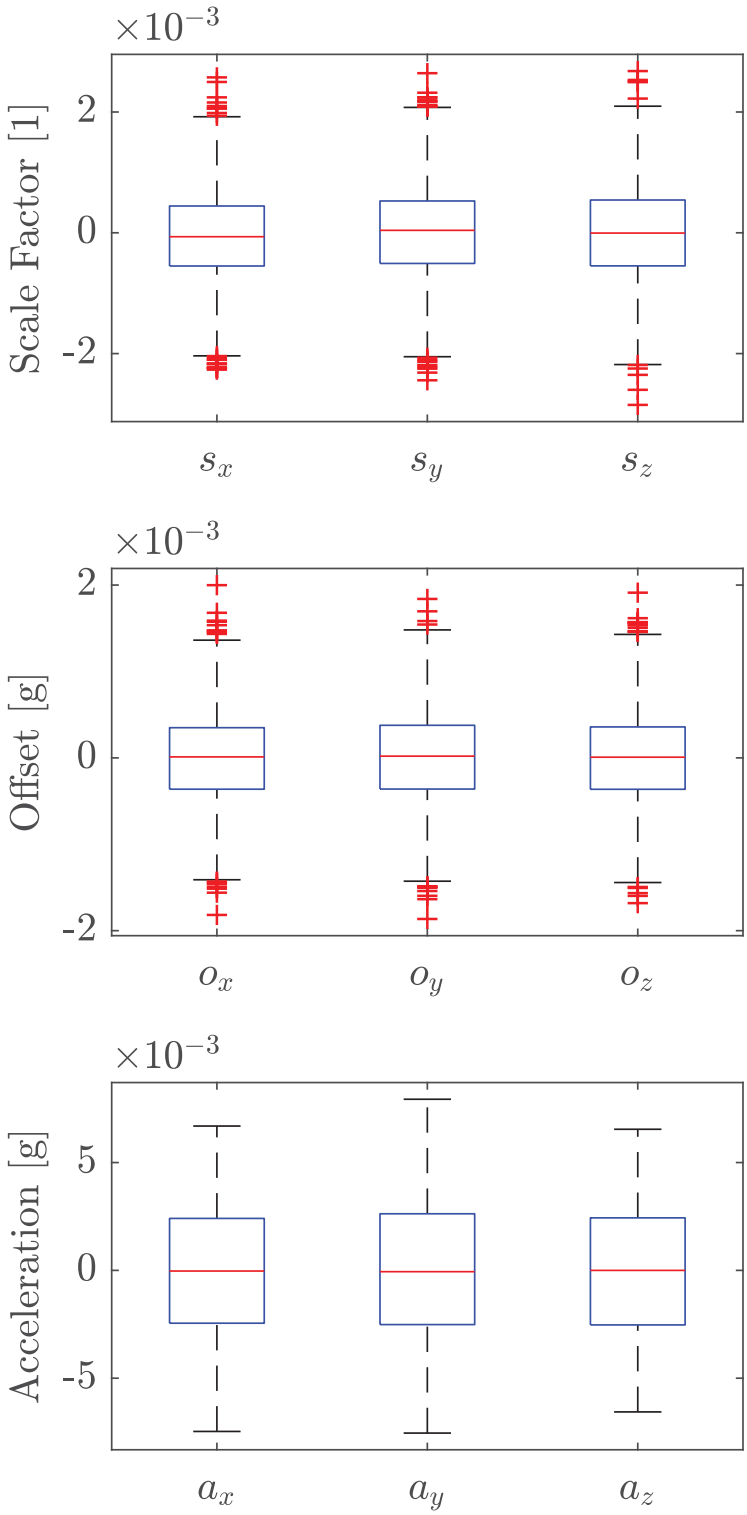

Fig. 4.2 Errors between estimations and true values of simulation 1 with $5mg$ noise level

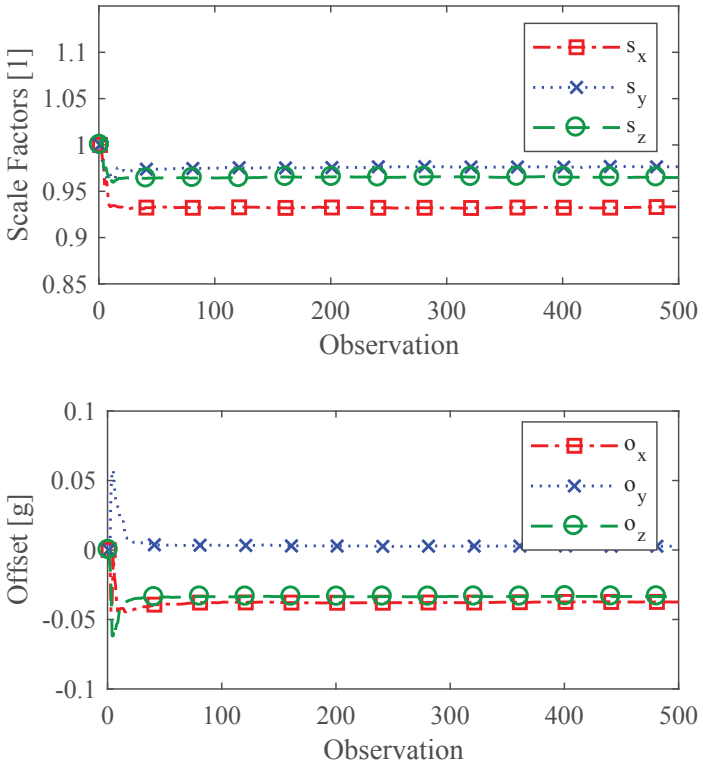

Fig. 4.3 A randomly chosen results of simulation 1 with $1mg$ noise level

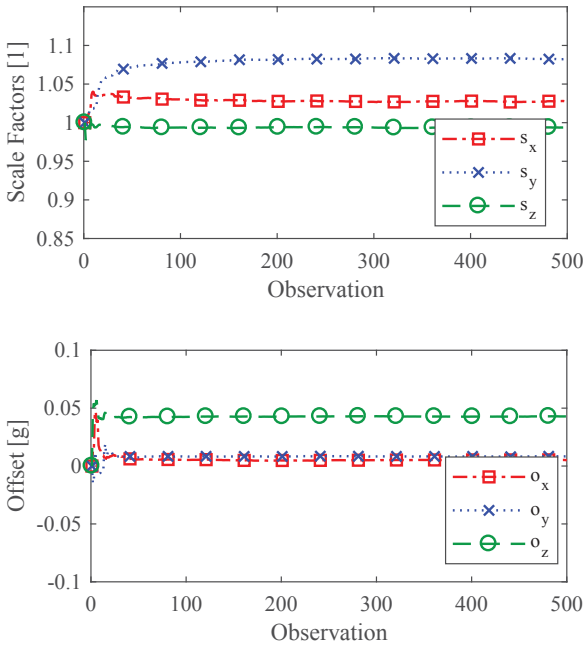

Fig. 4.4 A randomly chosen results of simulation 1 with $5mg$ noise level

In total, we executed 2000 runs of simulation and computed the error between the last estimation after 500 measurement and true parameters. The box-plot of the 2000 errors are shown in Fig. 4.1 and Fig. 4.2. These box-plot figures show that the estimated parameters are unbiased as the median values of scale factors and offsets are zero. For the simulations, the errors of estimated scale factors under $1mg$ and $5mg$ noise levels are mainly within $\pm 5 \times 10^{-4}$ and $\pm 3 \times 10^{-3}$, respectively. Meanwhile, the estimated offsets are mainly within $\pm 4 \times 10^{-4}$ and $\pm 2 \times 10^{-3}$. Furthermore, the errors of the estimated responses were calculated for each axis; it is shown that the estimated errors are within $\pm 1.5 \times 10^{-3} g$ and $\pm 7 \times 10^{-3} g$, which are only slightly larger than the noise level. It thus indicates that the proposed method can provide accurate estimation with small variance without bias. We randomly selected two simulation results which are shown in Fig. 4.3 and Fig. 4.4. These results demonstrate that the proposed algorithm can converge rapidly while the estimated parameters can remain stable during online estimation procedure.

The second set of simulation are designed to examine the performance of the proposed calibration method when the parameters are varying. At first, the model of TA and 500 measurements were generated based on the same assumptions of previous simulation. Then, for each stage, the scale factors and offsets were randomly increased/decreased 5% with another set of 300 measurements based on new parameters, which were repeated 3 times in total. This simulation is aimed to show that the propose method can track the variation of parameters rapidly. This simulation was also executed for 2000 times with two noise levels ($1mg$ and $5mg$). The error of the estimated parameters and responses are recorded for the last measurement of each stage.

A randomly chosen experiment is shown in Fig. 4.7 and Fig. 4.8 for $1mg$ and $5mg$ noise levels, respectively. As the figures shown, the proposed calibration method can converge within 150 measurements and the estimation procedure is stable and smooth. The overall results are reported in Fig. 4.5 and Fig. 4.6. These box-plots are similar to the first simulation which indicates that the proposed method can track the parameters accurately without bias. Furthermore, the overall estimation errors are still within $\pm 1.5 \times 10^{-3} g$ and $\pm 8 \times 10^{-3} g$ for $1mg$ and $5mg$ noise levels. Thus, all

simulation results show that the proposed method can achieve high accuracy without bias.

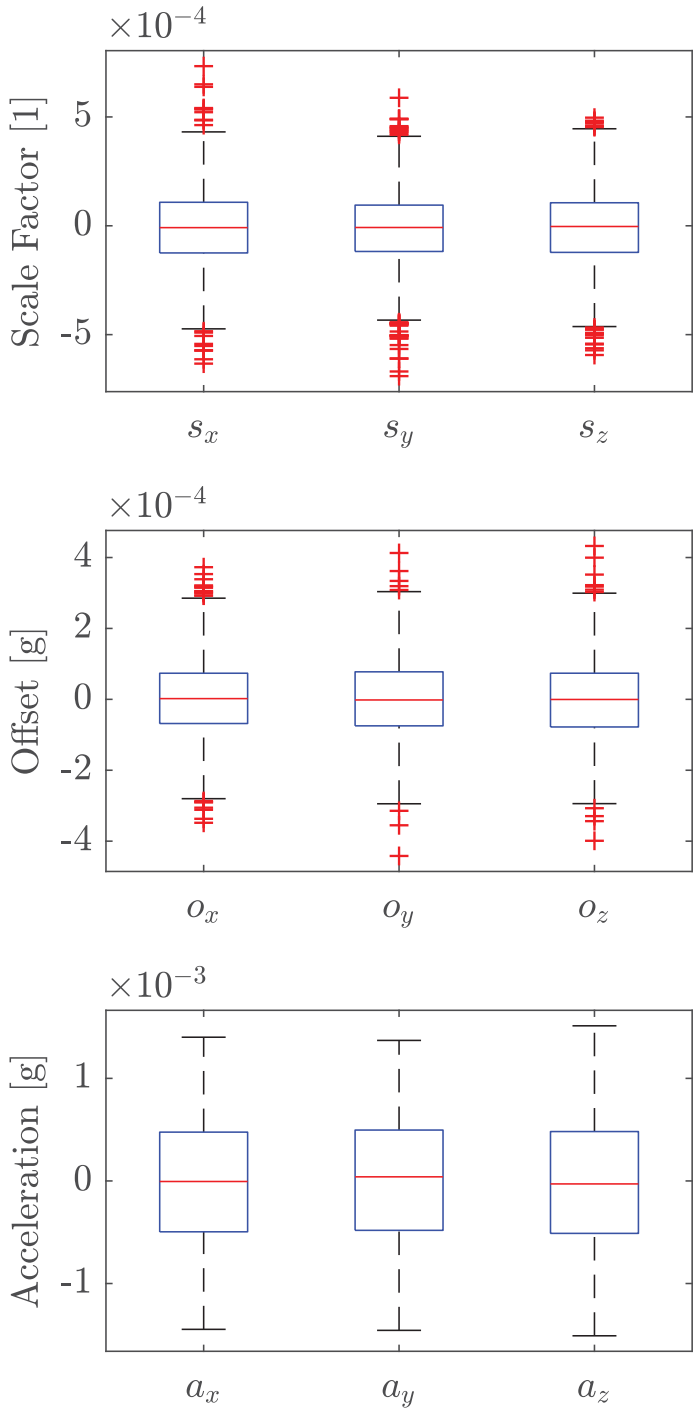

Fig. 4.5 Errors between estimations and true values of simulation 2 with $1mg$ noise level under parameter variations

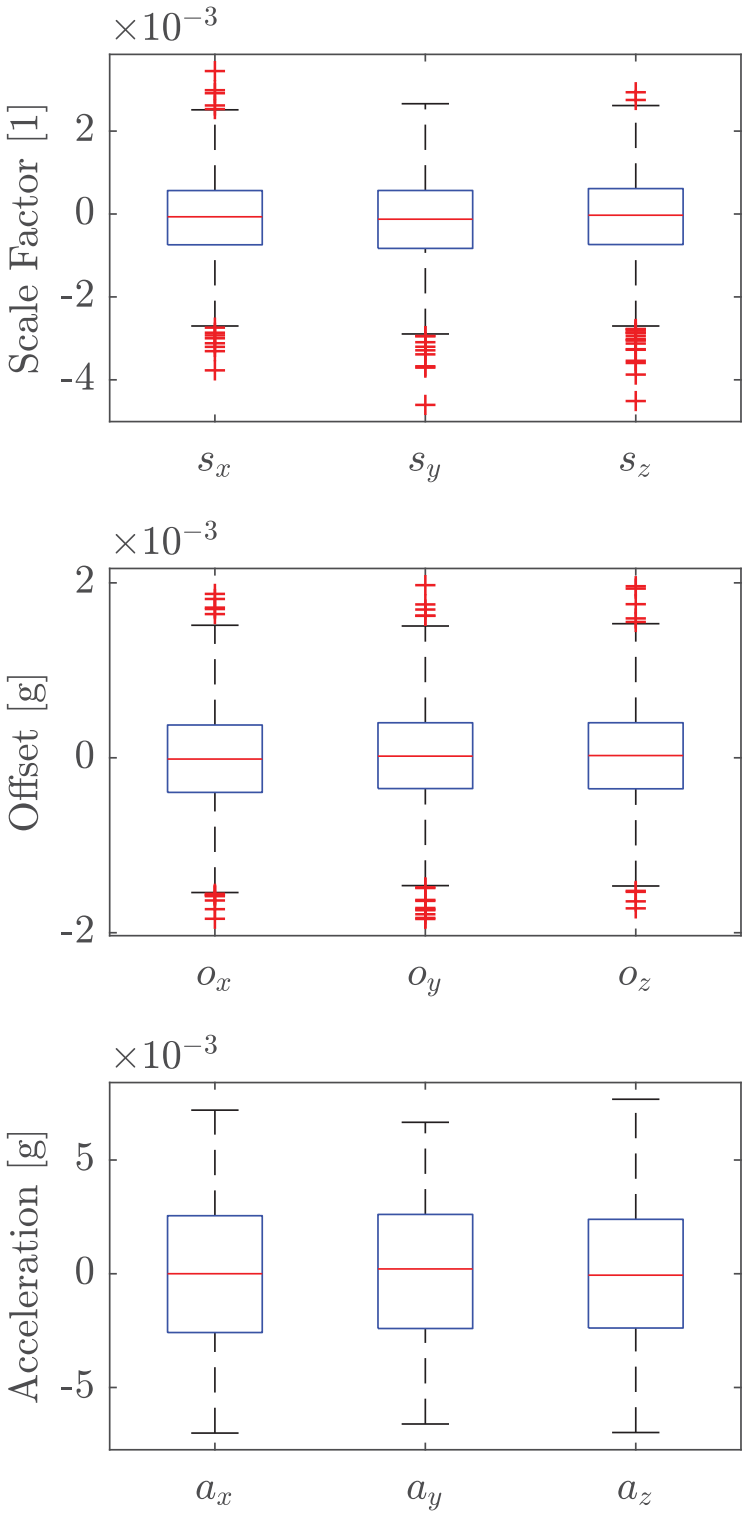

Fig. 4.6 Errors between estimations and true values of simulation 2 with $5mg$ noise level under parameter variations

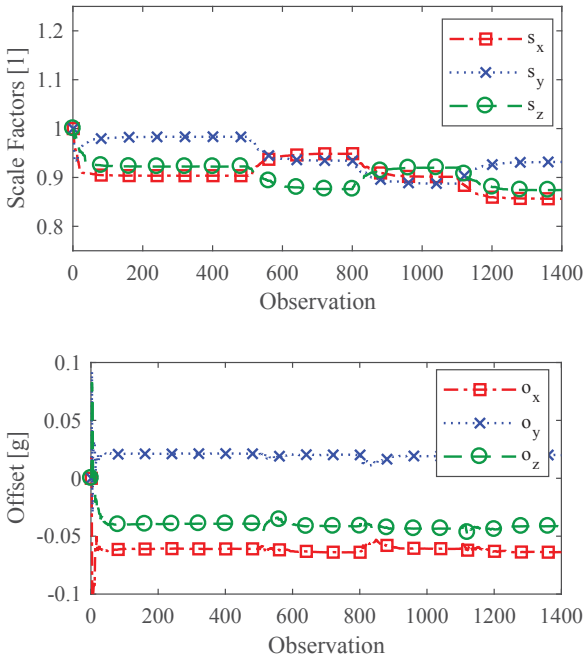

Fig. 4.7 A randomly chosen results of simulation 2 with $1mg$ noise level under parameter variations

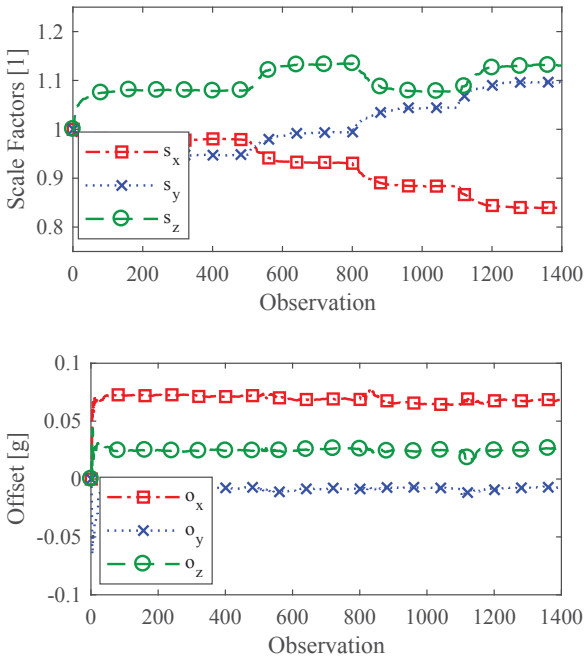

Fig. 4.8 A randomly chosen results of simulation 2 with $5mg$ noise level under parameter variations

Note 4.1 *The range of convergence of proposed algorithm is obtained by Monte Carlo method. For scale factors and offsets within* $0.7 \sim 1.3$ *and* $-0.25g \sim 0.25g$ *respectively, which are two times bigger than the normal commercial MEMS TAs,* $200,000$ *simulations have been implemented and all estimations were converged to true value. However, it is deserved to note that if the off-line auto-calibration algorithm proposed in [22] is pre-performed prior to this new proposed online MDRLS approach, a wider convergence range can be achieved [22].*

4.4.2 Experiments

To experimentally evaluate the proposed online calibration method, a health monitoring device with a MCU ($TI\ MSP430$), IMU ($MPU9150$) and *Bluetooth* was developed and used. The experiment was implemented in Centre for Health Technologies, University of Technology Sydney. For the IMU, according to the datasheet, it includes a MEMS tri-axial digital accelerometer with 16 *bit* analog to digital converter (ADC) and the output data rate can reach $1000\,Hz$. The device is shown in Fig. 4.9

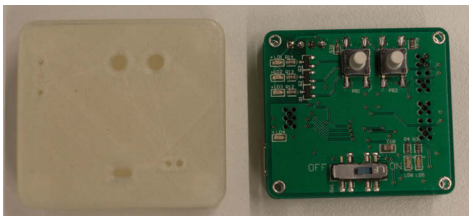

Fig. 4.9 The health monitoring device used in this experiment

Based on the proposed Algorithm 3, first of all, the accelerometer was randomly placed in 100 different orientations. Then, for these measurements ($\boldsymbol{v}_{lsb}$), the unit of outputs was converted from lsb to g,

$$\boldsymbol{v} = \boldsymbol{v}_{lsb}/c_{ratio}, \tag{4.24}$$

where c_{ratio} is the ratio of conversion which is $16384\,lsb/g$ in this experiment. Then, based on the measurement $\boldsymbol{v}$, the proposed algorithm was applied to calculate the scale factors and offsets. During experiment, the sampling frequency was set to $100\,Hz$. The output range was selected as $\pm 2g$. To evaluate the accuracy of the estimation,

we collected another 40 sets of data after the initial 100 orientations and estimated the acceleration based on the estimated parameters. The overall error and standard deviation of these 40 sets of data based on the online estimated parameters are record in Table. 4.1

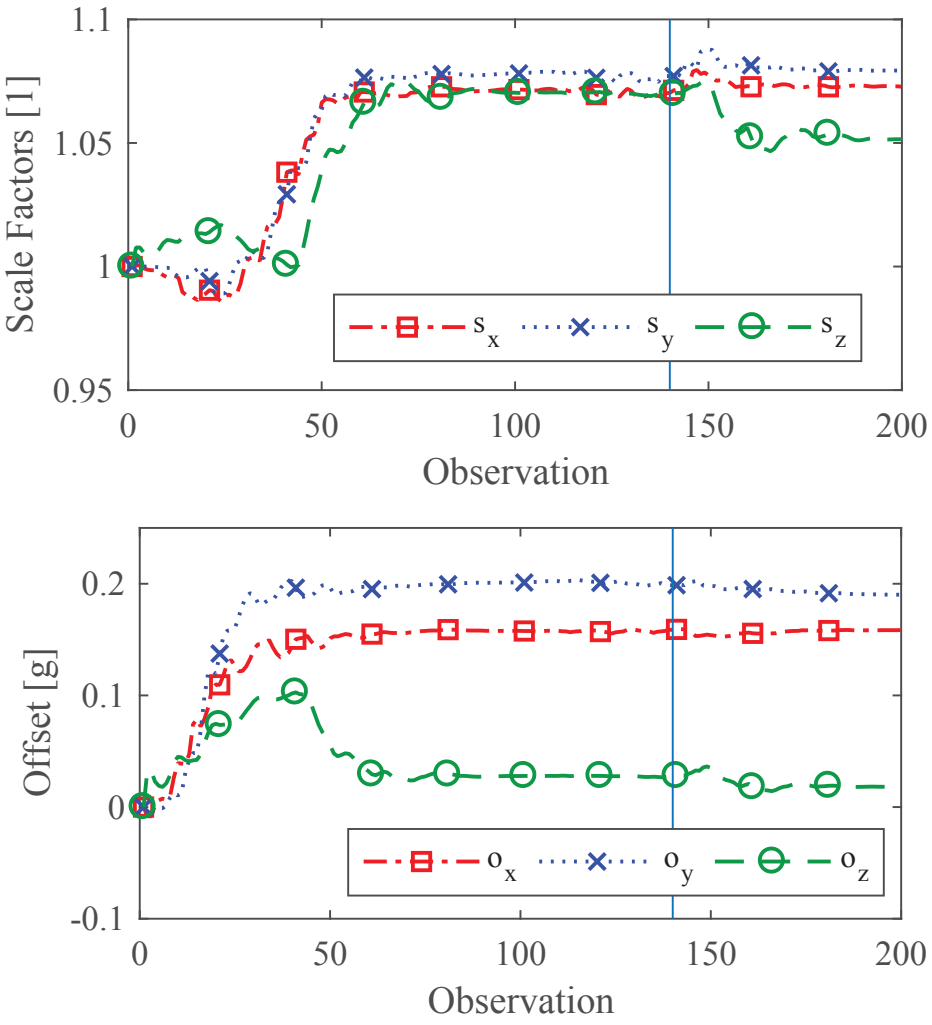

Fig. 4.10 Calibration results of real experiment based on proposed online auto-calibration method

Table 4.1 Estimation error of overall acceleration

	Mean Error $[g]$	Standard Deviation $[g]$
Before Calibration	0.0627	0.1561
Proposed Method	0.0003	0.0055
UKF based Method	-0.0086	0.0139

To evaluate the tracking performance of parameter variation during the change of temperate, the IMU module was warmed under a lamp for 20 *mins* to stimulate the change of temperature. Then, another 60 sets of data were collected for the second part of online estimation experiment. The error of estimation and standard deviation are recorded in Table. 4.2. The errors based on online calibration of these 60 measurements are named as 'Online Calibration'; the errors based on the scale factors and offsets before warmed up by lamp are named as 'Offline Calibration'. Furthermore, a prevailing auto-calibration method based on the UKF [12] is selected as comparison. To achieve online calibration with relatively fast converge and stable estimation, the forgetting factors of UKF has been tuned and 0.98 was selected. The results indicate that the proposed online calibration can increase accuracy significantly comparing to offline calibration method when the external temperature is varying. Moreover, the proposed online auto-calibration method is outperformed UKF based method in terms of mean error and standard deviation for this experiment. The estimations results of scale factors and offsets for all 200 estimations of the experiment are shown in Fig. 4.10.

Table 4.2 Estimation error based on online calibration and offline calibration

	Mean Error $[g]$	Standard Deviation $[g]$
Offline Method	0.0168	0.0091
Proposed Method	0.0001	0.0061
UKF based Method	-0.0022	0.0063

Last but not least, the accelerometer was mounted on a turntable (two degree of freedom with $5'$ resolution and $0.03mm$ reading accuracy). In this experiment, the turntable was rotated to 10 different orientations. The readings from turntable of these 10 orientations were considered as the reference orientations, and the errors between the estimations and the reference orientations value were calculated. For the first five orientations, we set pitch (θ) as 0°, 30°, 45°, 60° and 90° while the yaw and roll remaining the same. Then, we repeated this for roll (ψ) while pitch and yaw remaining the same. Eq.(4.25) shows the relationship between the reference orientation and initial

orientation:

$$\begin{bmatrix} a_x \\ a_y \\ a_z \end{bmatrix}^T = \begin{bmatrix} a_{x,0} \\ a_{y,0} \\ a_{z,0} \end{bmatrix}^T \boldsymbol{R}_y \boldsymbol{R}_z, \tag{4.25}$$

where $[a_{x,0}, a_{y,0}, a_{z,0}]^T$ is the value of initial orientation which is $[0, 0, 1]^T$, rotation matrices $\boldsymbol{R}_y(\theta)$ and $\boldsymbol{R}_z(\psi)$ are expressed as:

$$\boldsymbol{R}_y = \begin{bmatrix} c(\theta) & 0 & s(\theta) \\ 0 & 1 & 0 \\ -s(\theta) & 0 & c(\theta) \end{bmatrix}, \quad \boldsymbol{R}_z = \begin{bmatrix} 1 & 0 & 0 \\ 0 & c(\psi) & -s(\psi) \\ 0 & s(\psi) & c(\psi) \end{bmatrix}, \tag{4.26}$$

where s and c represent *Sine* and *Cosine* respectively. For this part of experiments, the estimations ($[\hat{a}_x, \hat{a}_y, \hat{a}_z]^T$) were compared with reference orientations ($[a_x, a_y, a_z]^T$).

The results of experiments were analysed and listed in Table 4.3. The errors between the reference orientations $[a_x, a_y, a_z]^T$ and the estimations $[\hat{a}_x, \hat{a}_y, \hat{a}_z]^T$ were calculated for these 10 testing orientations. Since we do not know the actual value of the scale factors and offsets, we compared and analysed the errors between the reference orientations and the estimations. Due to the orientation inaccuracy of the turntable, the estimation of the vector sum ($\hat{a}_{vs}$) should be more accurate than that of the individual acceleration on each axis. It is also anticipated that the proposed algorithm minimises the variance of $\hat{a}_{vs}$.

Table 4.3 Estimation error of overall acceleration and acceleration components on each axis

	Before Calibration	
	Mean Error $[g]$	Standard Deviation $[g]$
$\epsilon_{\hat{a}_x}$	-0.1889	0.0219
$\epsilon_{\hat{a}_y}$	-0.1665	0.0260
$\epsilon_{\hat{a}_z}$	-0.0501	0.0186
$\epsilon_{\hat{a}_{vs}}$	0.0522	0.2422
	Proposed Method	
	Mean Error $[g]$	Standard Deviation $[g]$
$\epsilon_{\hat{a}_x}$	-0.0102	0.0075
$\epsilon_{\hat{a}_y}$	0.0012	0.0059
$\epsilon_{\hat{a}_z}$	-0.0019	0.0071
$\epsilon_{\hat{a}_{vs}}$	0.0002	0.0032
	UKF Based Method	
	Mean Error $[g]$	Standard Deviation $[g]$
$\epsilon_{\hat{a}_x}$	-0.0116	0.0058
$\epsilon_{\hat{a}_y}$	0.0051	0.0046
$\epsilon_{\hat{a}_z}$	-0.0025	0.0071
$\epsilon_{\hat{a}_{vs}}$	0.0062	0.0061

Overall, the achieved results demonstrate the efficiency of the proposed parameter estimation method.

4.5 Summary

In this chapter, a linearisation method for the 6-parameter TA model has been introduced for online auto-calibration. To solve the unknown parameters, based on the linearised model in real-time, a modified damped recursive least square estimation method was constructed. The proposed online calibration method can accurately estimate the unknown parameters within 150 measurements and remain stable. Partic-

ularly, the proposed online calibration method can track scale factors and offsets when parameters are varying due to temperature variation, etc.

To verify the presented method, both simulation and experiment were performed. Based on the results of simulation, it can be concluded that the proposed calibration method can achieve desired accuracy within 150 iterations in most cases, and the estimated response is unbiased with small standard deviation related to noise level. Furthermore, the results from simulation indicated that the proposed method can track the varying parameters rapidly.

A self-designed IMU module was used to implement the experiment of the proposed online calibration method. The scale factors and offsets cannot be compared between true values and estimations as the true values were unknown, therefore, only the errors between estimated orientations and references orientations were calculated and analysed. The experimental results also showed that the proposed online calibration approach could accurately estimate the vector sum of the three axes.

Overall, both simulations and experiments demonstrated the proposed online calibration method is very efficient for parameter tracking and will be very useful for the calibration of the portable device with varying working environments.

Chapter 5

Online Auto-Calibration of Tri-Axial Accelerometer with Time-Variant Model Structures

5.1 Introduction

Recently, several papers [11, 13, 19, 27] proposed a new idea for the calibration of tri-axial accelerometer, referred to as auto-calibration, which is suitable for implementation without sophisticated laboratory equipment. Furthermore, [20–22] consummated the auto-calibration by considering the quality of individual calibration, in which the selection of experimental observations is well discussed based on Design of Experiment (DoE). However, the output of MEMS accelerometer still suffers from drifting caused by ambient temperature [23, 24]. If the accelerometer is intended to be used in multiple environments with sharp temperature variations, the user may need to frequently re-calibrate their accelerometers to overcome the variation of calibrated parameters. Therefore, an online calibration is desired to improve the measurement accuracy. To the author's best knowledge, most studies, including [13, 19, 28, 54, 55] focus on offline TA calibration. Only, a few papers [12, 25, 26] are devoted to online calibration, but the methods proposed are mainly based on classical calibration methods that constructed by employing Kalman filter technique.

For the online calibration in the previous studies, most researchers selected predefined 6- or 9-parameter models [12, 25, 26, 92]. However, only paper [28] theoretically explained the advantage of selecting 6- and 9-parameter model based on Akaike information criterion (AIC) from the offline auto-calibration prospective. For 6-parameter model, the misalignment term is not considered, but it likely exists for some tri-axial accelerometers. Moreover, as the structure of model changes during external variation of the environment, some parameters may become zero, conventional parameter estimation methods still estimate these parameters and the estimations are caused by noise. In order to improve the accuracy of estimated parameters, the parameters which are zero should be identified and removed. An online parameter estimation algorithm which can automatically determine the model structure is expected.

This chapter firstly introduces a new linearisation method based on the most commonly used 9-parameter auto-calibration model [11, 21]. After that, a sparse recursive least square (SPARLS) estimation method [40] is utilised to solve the unknown parameters. Particularly, we demonstrate that this method is effective while the model parameters are varying. Furthermore, based on the characteristic of $\mathcal{L}_1$-norm penalised expectation-maximum (EM) algorithm, this method can automatically determine the model complexity in an optimal manner. In addition, this method has successfully been implemented in an embedded Micro Control Unit (MCU) for online testing. Both simulation and experimental results are provided which show the effectiveness of the proposed approach.

The major contributions of the chapter can be summarised as follows. Firstly, it is the first time that the SPARLS algorithm is applied to solve a special nonlinear parameter estimation problem for the auto-calibration of TA, which is non-convex in nature. Secondly, the proposed approach is able to accurately estimate the significant TA parameters in real-time while penalising the insufficient parameters converging to zero. Thirdly, the convergence condition of the iterative approach has been identified and investigated based on vast numerical simulations. Finally, the effectiveness of the approach has been demonstrated by both simulation and real-time experiment.

This chapter is organised as follows. In section 5.2, the linearisation method for 9-parameter model is introduced. In section 5.3, the online estimation method is

presented based on the linearised model. In section 5.4, both the simulation and experiment are presented. Section 5.5 summarises the chapter.

5.2 Linearisation of Tri-axial Accelerometer 9-Parameter Model

For the auto-calibration of tri-axial accelerometer, 6-, 9- and 12-parameter models are widely selected by researchers. In [28], the authors demonstrate that for most MEMS accelerometers, 6- and 9-parameter models are accurate enough. For this reason, as the proposed method can automatically adjust the number of unknown parameters, the 9-parameter model is selected. Let us define $\boldsymbol{V} = [v_x, v_y, v_z]^T$ as the measurement from accelerometer of each axis and $\boldsymbol{A} = [a_x, a_y, a_z]^T$ as the true local acceleration. The relationship between the measurement $\boldsymbol{V}$ and the true value $\boldsymbol{A}$ can be expressed as:

$$\begin{aligned} \boldsymbol{A} &= \boldsymbol{S} \cdot \boldsymbol{T} \cdot (\boldsymbol{V} + \boldsymbol{O}) + \boldsymbol{\varsigma} \\ &= \boldsymbol{K} \cdot (\boldsymbol{V} + \boldsymbol{O}) + \boldsymbol{\varsigma}, \end{aligned} \tag{5.1}$$

where $\boldsymbol{O} = [o_x, o_y, o_z]^T$ represents the offset vector, $\boldsymbol{\varsigma}$ is a zero mean white noise vector, and $\boldsymbol{S}$ represents the scale factor matrix:

$$\boldsymbol{S} = \begin{bmatrix} S_x & 0 & 0 \\ 0 & S_y & 0 \\ 0 & 0 & S_z \end{bmatrix}, \tag{5.2}$$

where S_x, S_y and S_z denote sensitivity factor for each axis. $\boldsymbol{T}$ is described as:

$$\boldsymbol{T} = \begin{bmatrix} 1 & 0 & 0 \\ \phi_{xy} & 1 & 0 \\ \phi_{xz} & \phi_{yz} & 1 \end{bmatrix}, \tag{5.3}$$

where ϕ_{xy}, ϕ_{xz} and ϕ_{yz} denote error in the alignment of the three single axis sensors of a complete three-axis accelerometer. $\boldsymbol{K}$ is the dot product of $\boldsymbol{S}$ and $\boldsymbol{T}$:

$$\boldsymbol{K} = \begin{bmatrix} S_x & 0 & 0 \\ S_x\phi_{xy} & S_y & 0 \\ S_z\phi_{xz} & S_z\phi_{yz} & S_z \end{bmatrix} \triangleq \begin{bmatrix} k_{xx} & 0 & 0 \\ k_{xy} & k_{yy} & 0 \\ k_{xz} & k_{yz} & k_{zz} \end{bmatrix}. \tag{5.4}$$

The matrix $\boldsymbol{K}$ can be considered as the completed scale factor matrix, where diagonal elements (k_{xx}, k_{yy}, k_{zz}) and off-diagonal (k_{xy}, k_{xz}, k_{yz}) are sensitivity scale factors and misalignment elements respectively.

Based on this model, classical method [93] can solve unknown scale factors and offsets from $\boldsymbol{K}$ and $\boldsymbol{O}$ directly, but it normally requires high precision equipment which is hardly accessed by most users. Thus, auto-calibration is developed and widely used for TA calibration. The idea of auto-calibration method is that the measurements of tri-axial accelerometer should be equal to local gravity in static state, i.e.,

$$g = \sqrt{a_x^2 + a_y^2 + a_z^2}. \tag{5.5}$$

Based on (5.5), the error $\tilde{\epsilon}_i$ for the i-th measurement can be expressed as follows [11],

$$\tilde{\epsilon}_i = a_{x,i}^2 + a_{y,i}^2 + a_{z,i}^2 - g^2 \quad i = 1, 2, \cdots, n, \tag{5.6}$$

where n is the number of total measurements.

Then, with Eq.(5.1) and Eq.(5.6), if we assume that $\boldsymbol{\beta}$ is the vector of the unknown parameters, the cost function can be often defined as:

$$J(\boldsymbol{\beta}) = \sum_{i=1}^{n} \left(|| f_{\boldsymbol{\beta}}(\boldsymbol{V}_i) - g^2 || \right), \tag{5.7}$$

where $\boldsymbol{V}_i = [v_{x,i}, v_{y,i}, v_{z,i}]^T$ $(i = 1, 2, \cdots, n)$ is the i-th measurement, and $f_{\boldsymbol{\beta}}(\boldsymbol{V}_i)$ is a scalar function of $\boldsymbol{V}_i$. The parameter estimation can then be formulated as a nonlinear non-convex optimisation problem:

$$\hat{\boldsymbol{\beta}} = \arg\min_{\boldsymbol{\beta}} J(\boldsymbol{\beta}). \tag{5.8}$$

In real life situation, to minimise the effect of environmental temperature, daily drift and so on, some online calibration methods are proposed. Several optimisation methods [26],[25],[12] are selected to solve this problem based on unscented Kalman filter (UKF) [26],[12] or extended Kalman filter [25]. However, most of these methods are not based on auto-calibration; precise orientation information is still required. Although existing off-line methods are able to identify the unknown parameters, it will be inconvenient for users to re-calibrate frequently.

To achieve online calibration by inertial measurement unit (IMU), we propose a method to linearise the cost function to decrease computational complexity. According to [28], $\tilde{\epsilon}_i$ in Eq.(5.6) is the summation of zero mean Gaussian distribution and Chi-square distribution. Comparing to the Gaussian distribution component, the Chi-squared distribution part is negligible [28]. Hence, the error $\tilde{\epsilon}_i$ can be approximated as normal distribution with zero mean. Based on Eq.(5.1) and Eq.(5.5), the squared form of auto-calibration method of the i-th measurement is given by:

$$\begin{aligned} g^2 = \; & \left[k_{xx}\left(v_{x,i}+o_x\right)\right]^2 + \left[k_{xy}\left(v_{x,i}+o_x\right)+k_{yy}\left(v_{y,i}+o_y\right)\right]^2 \\ & + \left[k_{xz}\left(v_{x,i}+o_x\right)+k_{yz}\left(v_{y,i}+o_y\right)+k_{zz}\left(v_{z,i}+o_z\right)\right]^2 + \epsilon_i, \end{aligned} \tag{5.9}$$

where ϵ_i is a zero mean white noise. Apparently, Eq.(5.9) is nonlinear for unknown parameters $k_{xx}, k_{yy},\ k_{zz}, k_{xy}, k_{xz},\ k_{yz}, o_x, o_y, o_z$. Recently, the MEMS packing and soldering technologies have been improved rapidly, leading to the reduction of the value of the undesired parameters to a very low level. The square or product terms of the off-diagonal elements of $\boldsymbol{K}$ and offset $\boldsymbol{O}$ are close to zero ($k_{ij} < 0.01$ and $O_i < 0.1$). To linearise Eq.(5.9), we can neglect some terms which have small impact during estimation. Let us expand Eq.(5.9), so that several terms contain at least the square of $k_{xy}, k_{xz}, k_{yz},\ o_x, o_y, o_z$ or their products. Furthermore, even for those terms with measurements $(v_{x,i}, v_{y,i}, v_{z,i})$, the maximum value of measurements is $1g$ during calibration. To simplify the online estimation procedure, let us replace the sum of these terms as ψ_i for the i-th measurement, and we will estimate ψ_i iteratively during online estimating procedure. Eq.(5.9) can then be rewritten as:

$$\begin{aligned} g^2 - \psi_i =& k_{xx}^2 v_{x,i}^2 + 2k_{xx}^2 v_{x,i} o_x + 2k_{xy} k_{yy} v_{x,i} v_{y,i} + k_{yy}^2 v_{y,i}^2 + 2k_{yy}^2 v_{y,i} o_y \\ &+ k_{zz}^2 v_{z,i}^2 + 2k_{zz}^2 v_{z,i} o_z + 2k_{xz} k_{zz} v_{x,i} v_{z,i} + 2k_{yz} k_{zz} v_{y,i} v_{z,i} + \epsilon_i, \end{aligned} \tag{5.10}$$

where the residual ψ_i is assumed as a constant during each iteration, expressed as:

$$\begin{aligned} \psi_i =& \left(k_{xy}(v_{x,i} + o_x)\right)^2 + \left(k_{xz}(v_{x,i} + o_x) + k_{yz}(v_{y,i} + o_y)\right)^2 + k_{xx}^2 o_x^2 + k_{yy}^2 o_y^2 + k_{zz}^2 o_z^2 \\ &+ 2k_{xy} k_{yy}(v_{x,i} o_y + v_{y,i} o_x + o_x o_y) + 2k_{xz} k_{zz}(v_{x,i} o_z + v_{z,i} o_x + o_x o_z) \\ &+ 2k_{yz} k_{zz}(v_{y,i} o_z + v_{z,i} o_y + o_y o_z). \end{aligned} \tag{5.11}$$

After re-arranging the original parameters, a new set of parameters can be defined as:

$$\begin{cases} \beta_1 = 2k_{xx}^2 o_x \\ \beta_2 = 2k_{yy}^2 o_y \\ \beta_3 = 2k_{zz}^2 o_z \\ \beta_4 = 2k_{xy} k_{yy} \\ \beta_5 = 2k_{xz} k_{zz} \\ \beta_6 = 2k_{yz} k_{zz} \\ \beta_7 = k_{xx}^2 \\ \beta_8 = k_{yy}^2 \\ \beta_9 = k_{zz}^2 \end{cases} \tag{5.12}$$

Thus, Eq.(5.10) can be rewritten as:

$$\begin{aligned} g^2 - \psi_i =& \beta_1 v_{x,i} + \beta_2 v_{y,i} + \beta_3 v_{z,i} + \beta_4 v_{x,i} v_{y,i} + \beta_5 v_{x,i} v_{z,i} + \beta_6 v_{y,i} v_{z,i} + \beta_7 v_{x,i}^2 \\ &+ \beta_8 v_{y,i}^2 + \beta_9 v_{z,i}^2 + \epsilon_i. \end{aligned} \tag{5.13}$$

Assuming that we have n sets of measurement data, Eq.(5.13) can be rearranged into a matrix form as:

$$\begin{aligned} g^2\mathbb{1}_n - \boldsymbol{\psi}_n &= \boldsymbol{X}_n\boldsymbol{\beta}_n + \boldsymbol{\epsilon}_n \\ \boldsymbol{y}_n &= \boldsymbol{X}_n\boldsymbol{\beta}_n + \boldsymbol{\epsilon}_n, \end{aligned} \tag{5.14}$$

where the i-th rows of $g^2\mathbb{1}_n$, $\boldsymbol{\psi}_n$, $\boldsymbol{X}_n$ are g, ψ_i and $[v_{x,i}, v_{y,i}, v_{z,i}, v_{x,i}v_{y,i}, v_{x,i}v_{z,i}, v_{y,i}v_{z,i}, v_{x,i}^2, v_{y,i}^2, v_{z,i}^2]$, $i \in \{1, 2, \cdots, n\}$ respectively. Vector $\boldsymbol{\beta}_n = [\beta_{1,n}, \beta_{2,n}, \beta_{3,n}, \beta_{4,n}, \beta_{5,n}, \beta_{6,n}, \beta_{7,n}, \beta_{8,n}, \beta_{9,n}]^T$.

Therefore, for the i-th measurement, the instantaneous error can be expressed as:

$$\begin{aligned} e_i &= y_i - \hat{y}_i \\ &= y_i - \boldsymbol{x}_i\hat{\boldsymbol{\beta}}_n, \end{aligned} \tag{5.15}$$

where $\hat{\boldsymbol{\beta}}_n$ is the estimated unknown parameters of n times measurements. Hence, we have the following optimisation problem:

$$\hat{\boldsymbol{\beta}}_n = \arg\min_{\boldsymbol{\beta}_n} \quad f_{\boldsymbol{\beta}}(e_1, e_2, \cdots, e_n). \tag{5.16}$$

With a non-negative forgetting factor λ, which is a non-negative constant scalar, the alternative cost function of Eq.(5.16) can be adjusted as:

$$J(\boldsymbol{\beta}_n) = \sum_{i=1}^{n} \lambda^{n-i}|e_i|^2, \tag{5.17}$$

which is a well-known cost function that can be solved directly by Recursive Least Squares(RLS) method. To convert Eq.(5.17) into matrix form, let us define:

$$\boldsymbol{D}_n = diag(\lambda^{n-1}, \lambda^{n-2}, \cdots, 1), \tag{5.18}$$

$$\boldsymbol{y}_n = [y_1, y_2, \cdots, y_n]^T, \tag{5.19}$$

and

$$\boldsymbol{X}_n = \begin{pmatrix} \boldsymbol{x}_1^T \\ \boldsymbol{x}_2^T \\ \vdots \\ \boldsymbol{x}_n^T \end{pmatrix}, \tag{5.20}$$

where $\boldsymbol{x}_i^T$ (the i-th row of $\boldsymbol{X}_n$) is $[v_{x,i}, v_{y,i}, v_{z,i}, v_{x,i}v_{y,i}, v_{x,i}v_{z,i}, v_{y,i}v_{z,i}, v_{x,i}^2, v_{y,i}^2, v_{z,i}^2]$. Therefore, the RLS cost function can be written in the following form:

$$J(\boldsymbol{\beta}_n) = ||\boldsymbol{D}_n^{1/2}\boldsymbol{y}_n - \boldsymbol{D}_n^{1/2}\boldsymbol{X}_n\hat{\boldsymbol{\beta}}_n||_2^2, \tag{5.21}$$

where the i-th diagonal element $d_{ii,n}^{1/2}$ of $\boldsymbol{D}_n^{1/2}$ is the squared root of the i-th diagonal element $d_{ii,n}$ of $\boldsymbol{D}_n$, as:

$$d_{ii,n}^{1/2} = \sqrt{d_{ii,n}}. \tag{5.22}$$

Although Recursive Least Square (RLS) method can be applied to solve the unknown parameter based on cost function (5.21), it can not consider the physical characteristic of MEMS accelerometer. As we know, for the matrix $\boldsymbol{K}$ in (5.4), the misalignment error may be quite small due to the improvement of MEMS technologies. Therefore, instead of applying Akaike information Criterion (AIC) [28] to determine the true model of a specific accelerometer, we can adopt a spares recursive least square (SPARLS) [40] method to solve the unknown parameter. In practice, this method can play a role in reducing the number of undesired parameters. With a sparse RLS, the model can automatically be selected and updated in a real-time manner. Based on Eq.(5.21), the cost function of linearised auto-calibration model with $\mathcal{L}_1$ regulariser can be described as follows:

$$\min_{\hat{\boldsymbol{\beta}}_n} \frac{1}{2\sigma^2}||\boldsymbol{D}_n^{1/2}\boldsymbol{y}_n - \boldsymbol{D}_n^{1/2}\boldsymbol{X}_n\hat{\boldsymbol{\beta}}_n||_2^2 + \gamma||\hat{\boldsymbol{\beta}}_n||_1, \tag{5.23}$$

where σ is the standard deviation of noise, γ represents a trade off between estimation error and sparsity of the parameter, and the term $\gamma||\hat{\boldsymbol{\beta}}_n||_1$ can be considered as $\mathcal{L}_1$ regularisation. Typically, for $\mathcal{L}_1$ regularisation, the penalty term can reduce the overfitting which can lead to the shrinkage of unknown parameters [65].

5.3 Online Calibration Method for Linearised 9-Parameter Model

After obtaining a linearise auto-calibration model of TA and the corresponding cost function with $\mathcal{L}_1$-norm regularisation (5.23), the parameter estimation problem can be solved by various optimisation methods. Then, we can solve the original parameter $\boldsymbol{K}$ and $\boldsymbol{O}$ of TA model (5.1) based on (5.4) and (5.12). Here, we adopt a recursive sparse method from [40], which can remove insignificant parameters and significantly reduce the computational complexity. With some modifications, this method can estimate the removal term $\boldsymbol{\psi}_n$ recursively, which results in the reduction of the bias and thereby achieving an accurate estimation accuracy.

To apply this method, let us recall the linearised TA model (5.14) with n observations:

$$\boldsymbol{y}_n = \boldsymbol{X}_n \boldsymbol{\beta}_n + \boldsymbol{\xi}_n, \tag{5.24}$$

where for online estimation, the error term can be adjusted to $\boldsymbol{\xi}_n \sim \mathcal{N}(\boldsymbol{0}, \sigma^2 \boldsymbol{D}_n^{-1})$.

For Eq.(5.24), to solve $\hat{\boldsymbol{\beta}}_n$ without undeserved parameters, penalised log-likelihood estimation $\log p(\boldsymbol{y}_n|\boldsymbol{\beta}_n) - pen(\boldsymbol{\beta}_n)$ can be applied where pen represents penalty. However, for penalised log-likelihood estimation, in general, it is hard to be maximised directly [68]. Therefore, a penalised expectation-maximum (EM) algorithm is adopt to maximise the penalised complete log-likelihood. To estimated $\boldsymbol{\beta}_n$ with penalised expectation-maximum problem, we decompose $\boldsymbol{\xi}_n$ as:

$$\boldsymbol{\xi}_n = \alpha \boldsymbol{X}_n \boldsymbol{\tau}_n + \boldsymbol{D}_n^{-1/2} \boldsymbol{\delta}_n, \tag{5.25}$$

where α is a positive parameter. $\boldsymbol{\tau}_n$ and $\boldsymbol{\delta}_n$ are independent noise such that:

$$\begin{aligned} &\boldsymbol{\tau}_n \sim \mathcal{N}(\boldsymbol{0}, \boldsymbol{I}), \\ &\boldsymbol{\delta}_n \sim \mathcal{N}(\boldsymbol{0}, \sigma^2 \boldsymbol{I} - \alpha^2 \boldsymbol{D}_n^{1/2} \boldsymbol{X}_n \boldsymbol{X}_n^T \boldsymbol{D}_n^{1/2}). \end{aligned} \tag{5.26}$$

To guarantee that $\boldsymbol{\delta}_n$ has a positive semi-definite covariance matrix, we need to make sure that $\alpha^2 \leq \sigma^2/\lambda_1$, where λ_1 is the largest eigenvalue of $\boldsymbol{D}_n^{1/2} \boldsymbol{X}_n \boldsymbol{X}_n^T \boldsymbol{D}_n^{1/2}$.

Then, based on (5.25) and (5.26), Eq.(5.24) can be rearranged as:

$$\begin{cases} \boldsymbol{v}_n &= \boldsymbol{\beta}_n + \alpha\boldsymbol{\tau}_n \\ \boldsymbol{y}_n &= \boldsymbol{X}_n\boldsymbol{v}_n + \boldsymbol{D}_n^{-1/2}\boldsymbol{\delta}_n \end{cases} \tag{5.27}$$

where $\boldsymbol{v}_n$ is the hidden variable for penalised EM algorithm.

It is easy to verify that the variance of $\boldsymbol{y}_n$ from Eq.(5.27) is:

$$\begin{aligned} \mathrm{Var}[\boldsymbol{y}_n] &= \alpha^2\boldsymbol{X}_n\boldsymbol{X}_n^T + \boldsymbol{D}_n^{-1/2}\left(\sigma^2\boldsymbol{I} - \alpha^2\boldsymbol{D}_n^{1/2}\boldsymbol{X}_n\boldsymbol{X}_n^T\boldsymbol{D}_n^{1/2}\right)\boldsymbol{D}_n^{-1/2} \\ &= \sigma^2\boldsymbol{D}_n^{-1}, \end{aligned} \tag{5.28}$$

where it is the same for the variance of $\boldsymbol{y}_n$ from Eq.(5.24).

Thereby, the *complete penalised log-likelihood* of penalised expectation maximum algorithm can be expressed as $\log p(\boldsymbol{y}_n, \boldsymbol{v}_n|\boldsymbol{\beta}_n) - pen(\boldsymbol{\beta}_n)$ which can be achieved in two steps. For the expectation step, the condition expectation is calculated. For the maximisation step, the parameters are computed to maximise condition expectation [68]. The specific penalised recursive EM method, which can be applied for solving our particular problem, can be encapsulated in the following two steps:

- E-step: Calculate the conditional expectation $\log p(\boldsymbol{y}_n|\boldsymbol{\beta}_n)$ for Eq.(5.23), defined as Q-function $Q(\boldsymbol{\beta}_n, \hat{\boldsymbol{\beta}}_n^{(l)})$ in the l-th iteration:

$$Q(\boldsymbol{\beta}_n, \hat{\boldsymbol{\beta}}_n^{(l)}) = E\left[\log p(\boldsymbol{y}_n, \boldsymbol{v}_n|\boldsymbol{\beta}_n)|\boldsymbol{y}_n, \hat{\boldsymbol{\beta}}_n^{(l)}\right], \tag{5.29}$$

- M-step: Updates the estimated $\hat{\boldsymbol{\beta}}_n^{(l+1)}$ based on:

$$\hat{\boldsymbol{\beta}}_n^{(l+1)} = \arg\max_{\beta_n}\left(Q(\boldsymbol{\beta}_n, \hat{\boldsymbol{\beta}}_n^{(l)}) - pen(\hat{\boldsymbol{\beta}}_n^{(l)})\right). \tag{5.30}$$

Considering the second equation of Eq.(5.27), when $\boldsymbol{v}_n$ is known, $\boldsymbol{y}_n$ can be directly estimated without necessarily known $\boldsymbol{\beta}_n$, i.e., in this case, $\boldsymbol{y}_n$ is independent of $\boldsymbol{\beta}_n$. Therefore, the complete likelihood $p(\boldsymbol{y}_n, \boldsymbol{v}_n|\boldsymbol{\beta}_n)$ can be simplified as:

$$\begin{aligned} p(\boldsymbol{y}_n, \boldsymbol{v}_n|\boldsymbol{\beta}_n) &= p(\boldsymbol{y}_n|\boldsymbol{v}_n, \boldsymbol{\beta}_n)p(\boldsymbol{v}_n|\boldsymbol{\beta}_n) \\ &= p(\boldsymbol{y}_n|\boldsymbol{v}_n)p(\boldsymbol{v}_n|\boldsymbol{\beta}_n). \end{aligned} \tag{5.31}$$

Then, if we define that $\Sigma_y = \sigma^2 \boldsymbol{D}_n^{-1} - \alpha^2 \boldsymbol{X}_n \boldsymbol{X}_n^T$, the complete log-likelihood $\log p(\boldsymbol{y}_n, \boldsymbol{v}_n | \boldsymbol{\beta}_n)$ can be computed as:

$$\begin{aligned}
\log p(\boldsymbol{y}_n, \boldsymbol{v}_n | \boldsymbol{\beta}_n) &= \log p\left((\boldsymbol{y}_n | \boldsymbol{v}_n) p(\boldsymbol{v}_n | \boldsymbol{\beta}_n)\right) \\
&= \log \left\{ \frac{1}{2\pi^{n/2} ||\Sigma_y||^{1/2}} \exp\left(-\frac{(\boldsymbol{y}_n - \boldsymbol{X}_n \boldsymbol{v}_n)^T \Sigma_y^{-1} (\boldsymbol{y}_n - \boldsymbol{X}_n \boldsymbol{v}_n)}{2} \right) \right. \\
&\left. \cdot \frac{1}{2\pi^{n/2} ||\alpha^2 \boldsymbol{I}||^{1/2}} \exp\left(-\frac{||\boldsymbol{v}_n - \boldsymbol{\beta}_n||^2}{2\alpha^2} \right) \right\} \\
&= \log \left\{ L_1 \cdot \frac{1}{2\pi^{n/2} ||\alpha^2 \boldsymbol{I}||^{1/2}} \exp\left(-\frac{||\boldsymbol{v}_n - \boldsymbol{\beta}_n||^2}{2\alpha^2} \right) \right\} \\
&= \log L_2 - \frac{||\boldsymbol{v}_n - \boldsymbol{\beta}_n||^2}{2\alpha^2},
\end{aligned} \tag{5.32}$$

where L_1 and L_2 are independent of $\boldsymbol{\beta}_n$. Based on Eq.(5.29), the Q-function can be expressed as:

$$Q(\boldsymbol{\beta}_n, \hat{\boldsymbol{\beta}}_n^{(l)}) = \log L_2 - \frac{||\boldsymbol{v}_n - \hat{\boldsymbol{\beta}}_n^{(l)}||^2}{2\alpha^2}. \tag{5.33}$$

After the expectation step, to maximise the Q-function with penalty, the value of hidden variable $\boldsymbol{v}_n$ needs to be calculated first. Since $p(\boldsymbol{v}_n | \boldsymbol{y}_n, \hat{\boldsymbol{\beta}}_n^{(l)}) \propto p(\boldsymbol{y}_n | \boldsymbol{v}_n) p(\boldsymbol{v}_n | \hat{\boldsymbol{\beta}}_n^{(l)})$ from Eq.(5.31), with Eq.(5.26) and Eq.(5.27), we have:

$$\begin{aligned}
p(\boldsymbol{y}_n | \boldsymbol{v}_n) &= \mathcal{N}(\boldsymbol{X}_n \boldsymbol{v}_n | \sigma^2 \boldsymbol{D}_n^{-1} - \alpha^2 \boldsymbol{X}_n \boldsymbol{X}_n^T) \\
p(\boldsymbol{v}_n | \hat{\boldsymbol{\beta}}_n^{(l)}) &= \mathcal{N}(\hat{\boldsymbol{\beta}}_n^{(l)} | \alpha^2 \boldsymbol{I}).
\end{aligned} \tag{5.34}$$

Then, with $p(\boldsymbol{v}_n | \boldsymbol{y}_n, \hat{\boldsymbol{\beta}}_n^{(l)}) \propto p(\boldsymbol{y}_n | \boldsymbol{v}_n) p(\boldsymbol{v}_n | \hat{\boldsymbol{\beta}}_n^{(l)})$ and Eq.(5.34), the estimate value of the hidden variable $\hat{\boldsymbol{v}}_n^{(l)}$ can be computed as (details in [94], chapter 2):

$$\begin{aligned}
\hat{\boldsymbol{v}}_n^{(l)} &= \alpha^2 \boldsymbol{X}_n^T (\alpha^2 \boldsymbol{X}_n \boldsymbol{X}_n^T + \sigma^2 \boldsymbol{D}_n^{-1} - \alpha^2 \boldsymbol{X}_n \boldsymbol{X}_n^T)^{-1} (\boldsymbol{y}_n - \boldsymbol{X}_n \hat{\boldsymbol{\beta}}_n^{(l)}) + \hat{\boldsymbol{\beta}}_n^{(l)} \\
&= \frac{\alpha^2}{\sigma^2} \boldsymbol{X}_n^T \boldsymbol{D}_n (\boldsymbol{y}_n - \boldsymbol{X}_n \hat{\boldsymbol{\beta}}_n^{(l)}) + \hat{\boldsymbol{\beta}}_n^{(l)} \\
&= \frac{\alpha^2}{\sigma^2} \boldsymbol{X}_n^T \boldsymbol{D}_n \boldsymbol{y}_n + (\boldsymbol{I} - \frac{\alpha^2}{\sigma^2} \boldsymbol{X}_n^T \boldsymbol{D}_n \boldsymbol{X}_n) \hat{\boldsymbol{\beta}}_n^{(l)}.
\end{aligned} \tag{5.35}$$

Eventually, with Eq.(5.33), the penalised maximum likelihood Eq.(5.30) can be rewritten as:

$$\begin{aligned}\hat{\boldsymbol{\beta}}_n^{(l+1)} &= \arg\max_{\beta_n}\left(Q(\boldsymbol{\beta}_n, \hat{\boldsymbol{\beta}}_n^{(l)}) - pen(\hat{\boldsymbol{\beta}}_n^{(l)})\right) \\ &= \arg\max_{\beta_n}\left(-\frac{||\boldsymbol{v}_n - \hat{\boldsymbol{\beta}}_n^{(l)}||^2}{2\alpha^2} - pen(\hat{\boldsymbol{\beta}}_n^{(l)})\right) \\ &= \arg\max_{\beta_n}\left(-||\boldsymbol{v}_n - \hat{\boldsymbol{\beta}}_n^{(l)}||^2 - 2\alpha^2 pen(\hat{\boldsymbol{\beta}}_n^{(l)})\right).\end{aligned} \tag{5.36}$$

To solve Eq.(5.36), with $\mathcal{L}_1$ regularisation, the penalty term $pen(\hat{\boldsymbol{\beta}}_n^{(l)})$ can be rewritten as:

$$pen(\hat{\boldsymbol{\beta}}_n^{(l)}) = \gamma||\boldsymbol{\beta}_n^{(l)}||_1 = \gamma\sum_i |\beta_{i,n}^{(l)}|, \quad i = 1, 2, 3\cdots M. \tag{5.37}$$

where M is the number of unknown parameters and $\hat{\beta}_{i,n}^{(l)}$ is the i-th element of $\hat{\boldsymbol{\beta}}_n^{(l)}$.

Therefore, $\hat{\boldsymbol{\beta}}_n^{(l+1)}$ can be obtained by applying a soft-threshold function. For the $(l+1)$-th iteration, the i-th element $\hat{\beta}_{i,n}^{(l+1)}$ of $\hat{\boldsymbol{\beta}}_n^{(l+1)}$ can be computed by [68]:

$$\hat{\beta}_{i,n}^{(l+1)} = sgn(\hat{v}_{i,n}^{(l)})\left(|\hat{v}_{i,n}^{(l)}| - \gamma\alpha^2\right), \tag{5.38}$$

where $\hat{v}_{i,n}^{(l)}$ is the i-th element of $\hat{\boldsymbol{v}}_n^{(l)}$.

To further increase the accuracy of the estimation, the residual term ψ_{n+1} from Eq.(5.10) is updated based on the estimated $\hat{\beta}_{i,n}^{(t)}$ after a total of t times of iteration. For the n-th input, the estimated original parameter matrix $\hat{\boldsymbol{K}}_n$ of Eq.(5.4) can be

solved based on Eq.(5.12):

$$\begin{cases} \hat{k}_{xx,n} &= \sqrt{\hat{\beta}_{7,n}^{(t)}} \\ \hat{k}_{yy,n} &= \sqrt{\hat{\beta}_{8,n}^{(t)}} \\ \hat{k}_{zz,n} &= \sqrt{\hat{\beta}_{9,n}^{(t)}} \\ \hat{k}_{xy,n} &= \hat{\beta}_{4,n}^{(t)}/2\sqrt{\hat{\beta}_{8,n}^{(t)}} \\ \hat{k}_{xz,n} &= \hat{\beta}_{5,n}^{(t)}/2\sqrt{\hat{\beta}_{9,n}^{(t)}} \\ \hat{k}_{yz,n} &= \hat{\beta}_{6,n}^{(t)}/2\sqrt{\hat{\beta}_{9,n}^{(t)}} \\ \hat{o}_{x,n} &= \hat{\beta}_{1,n}^{(t)}/2\hat{\beta}_{7,n}^{(t)} \\ \hat{o}_{y,n} &= \hat{\beta}_{2,n}^{(t)}/2\hat{\beta}_{8,n}^{(t)} \\ \hat{o}_{z,n} &= \hat{\beta}_{3,n}^{(t)}/2\hat{\beta}_{9,n}^{(t)} \end{cases} \tag{5.39}$$

Then, the estimated residual $\hat{\psi}_{n+1}$ of Eq.(5.10) can be estimated based on Eq.(5.11). For online implementation, assuming that after t-th iteration within EM algorithm, a new set of data x_{n+1} is inputted into the system, and the following updation can be applied to Eq.(5.35) for the initial estimation of $\boldsymbol{v}_{n+1}^{(0)}$:

$$\boldsymbol{v}_{n+1}^{(0)} = \lambda\frac{\alpha^2}{\sigma^2}\boldsymbol{X}_n^T\boldsymbol{D}_n\boldsymbol{y}_n + \frac{\alpha^2}{\sigma^2}y_{n+1}\boldsymbol{x}_{n+1} + (\boldsymbol{I} - \lambda\frac{\alpha^2}{\sigma^2}\boldsymbol{X}_n^T\boldsymbol{D}_n\boldsymbol{X}_n - \frac{\alpha^2}{\sigma^2}\boldsymbol{x}_{n+1}\boldsymbol{x}_{n+1}^T)\hat{\boldsymbol{\beta}}_n^{(t)}, \tag{5.40}$$

where y_n can be replaced by $g^2 - \hat{\psi}_n$. This procedure can reduce the bias caused by linearisation of original TA models of auto-calibration. Therefore, we have:

$$\begin{aligned} \boldsymbol{v}_{n+1}^{(0)} = \lambda\frac{\alpha^2}{\sigma^2}\boldsymbol{X}_n^T\boldsymbol{D}_n(g^2\mathbb{1}_n - \hat{\boldsymbol{\psi}}_n) + \frac{\alpha^2}{\sigma^2}(g^2 - \hat{\psi}_{n+1})\boldsymbol{x}_{n+1} \\ + (\boldsymbol{I} - \lambda\frac{\alpha^2}{\sigma^2}\boldsymbol{X}_n^T\boldsymbol{D}_n\boldsymbol{X}_n - \frac{\alpha^2}{\sigma^2}\boldsymbol{x}_{n+1}\boldsymbol{x}_{n+1}^T)\hat{\boldsymbol{\beta}}_n^{(t)}. \end{aligned} \tag{5.41}$$

To simplify Eq.(5.41), let us define:

$$\boldsymbol{H}_n = \frac{\alpha^2}{\sigma^2}\boldsymbol{X}_n^T\boldsymbol{D}_n(g^2\mathbb{1}_n - \hat{\boldsymbol{\psi}}_n), \tag{5.42}$$

and

$$\boldsymbol{R}_n = \boldsymbol{I} - \frac{\alpha^2}{\sigma^2}\boldsymbol{X}_n^T\boldsymbol{D}_n\boldsymbol{X}_n. \tag{5.43}$$

Eq.(5.40) can then be simplified as:

$$\boldsymbol{v}_{n+1}^{(0)} = \lambda \boldsymbol{H}_n + \frac{\alpha^2}{\sigma^2}(g^2 - \hat{\psi}_{n+1})\boldsymbol{x}_{n+1} + (\lambda \boldsymbol{R}_n - \frac{\alpha^2}{\sigma^2}\boldsymbol{x}_{n+1}\boldsymbol{x}_{n+1}^T + (1-\lambda)\boldsymbol{I})\hat{\boldsymbol{\beta}}_n^{(t)}. \quad (5.44)$$

Then, let us recall Eq.(5.35) and Eq.(5.38), the relationship between $\hat{\boldsymbol{v}}_n^{(l)}$ and $\hat{\boldsymbol{v}}_n^{(l-1)}$ is:

$$\begin{aligned} \hat{\boldsymbol{v}}_n^{(l)} &= \frac{\alpha^2}{\sigma^2}\boldsymbol{X}_n^T\boldsymbol{D}_n(g^2\mathbb{1}_n - \hat{\boldsymbol{\psi}}_n) + (\boldsymbol{I} - \frac{\alpha^2}{\sigma^2}\boldsymbol{X}_n^T\boldsymbol{D}_n\boldsymbol{X}_n)\hat{\boldsymbol{\beta}}_n^{(l)} \\ &= \boldsymbol{H}_n + \boldsymbol{R}_n sgn(\hat{\boldsymbol{v}}_n^{(l-1)})\left(|\hat{\boldsymbol{v}}_n^{(l-1)}| - \gamma\alpha^2\right), \end{aligned} \quad (5.45)$$

where the i-th element of $sgn(\hat{\boldsymbol{v}}_n^{(l-1)})\left(|\hat{\boldsymbol{v}}_n^{(l-1)}| - \gamma\alpha^2\right)$ can be computed by:

$$sgn(\hat{v}_{i,n}^{(l)})\left(|\hat{v}_{i,n}^{(l)}| - \gamma\alpha^2\right) = \begin{cases} \hat{v}_{i,n}^{(l)} - \gamma\alpha^2 & i \in \mathcal{U}_+^{(l)} \\ \hat{v}_{i,n}^{(l)} + \gamma\alpha^2 & i \in \mathcal{U}_-^{(l)} \\ 0 & i \notin \mathcal{U}_+^{(l)} \cup \mathcal{U}_-^{(l)} \end{cases} \quad (5.46)$$

where $\mathcal{U}_+^{(l)}$ and $\mathcal{U}_-^{(l)}$ are defined as:

$$\begin{cases} \mathcal{U}_+^{(l)} &= \{i : \hat{v}_{i,n}^{(l)} > \gamma\alpha^2\} \\ \mathcal{U}_-^{(l)} &= \{i : \hat{v}_{i,n}^{(l)} < -\gamma\alpha^2\} \end{cases} \quad (5.47)$$

In summation, let us assume we need t times of iteration during EM algorithm. Then, the complete algorithm for the online TA calibration can be summarised by Algorithm 4 and Algorithm 5.

Algorithm 4 SPARLS

Initial: $\boldsymbol{R}_1 = \boldsymbol{I} - \frac{\alpha^2}{\sigma^2}\boldsymbol{x}_1\boldsymbol{x}_1^T$, $\boldsymbol{H}_1 = \frac{\alpha^2}{\sigma^2}\boldsymbol{x}_1 y_1$, $\psi_1 = 0$ and t.
for any $\boldsymbol{x}_n$ **do**,
    $\boldsymbol{R}_n = \lambda\boldsymbol{R}_{n-1} - \frac{\alpha^2}{\sigma^2}\boldsymbol{x}_n\boldsymbol{x}_n^T + (1-\lambda)\boldsymbol{I}$.
    $\boldsymbol{H}_n = \lambda\boldsymbol{H}_{n-1} + \frac{\alpha^2}{\sigma^2}(g^2 - \hat{\psi}_n)\boldsymbol{x}_n$.
    Run EM ($\boldsymbol{R}_n$, $\boldsymbol{H}_n$, $\hat{\boldsymbol{\beta}}_{n-1}$, $\mathcal{U}_+^{(l)}$, $\mathcal{U}_-^{(l)}$, t, TA's measurement ($v_{x,n}$, $v_{y,n}$, $v_{z,n}$)).
    Update $\hat{\boldsymbol{\beta}}_n, \hat{\psi}_{n+1}$.
end for
Output: $\hat{\boldsymbol{\beta}}_n, \hat{\psi}_n$

Algorithm 5 EM Algorithm for the linearised TA model

Input: $\boldsymbol{R}_n$, $\boldsymbol{H}_n$, $\hat{\boldsymbol{\beta}}_n$, $\mathcal{U}_+^{(l)}$, $\mathcal{U}_-^{(l)}$, t, TA's measurement $(v_{x,n},\, v_{y,n},\, v_{z,n})$.

$\hat{\boldsymbol{v}}_n^{(0)} = \boldsymbol{R}_{\mathcal{U}_+^{(l)},n}\hat{\boldsymbol{\beta}}_{\mathcal{U}_+^{(l)},n} + \boldsymbol{R}_{\mathcal{U}_-^{(l)},n}\hat{\boldsymbol{\beta}}_{\mathcal{U}_-^{(l)},n} + \boldsymbol{H}_n$.

$\mathcal{U}_+^{(0)} = \{i : \hat{v}_{i,n}^{(0)} > \gamma\alpha^2\}$.

$\mathcal{U}_-^{(0)} = \{i : \hat{v}_{i,n}^{(0)} < -\gamma\alpha^2\}$.

for $l = 1, 2, 3, \cdots, t$, **do**

$$\begin{aligned}\hat{\boldsymbol{v}}_n^{(l)} = {} & \boldsymbol{R}_{\mathcal{U}_+^{(l-1)},n}\left(\hat{\boldsymbol{v}}_{\mathcal{U}_+^{(l-1)},n}^{(l-1)} - \gamma\alpha^2\mathbf{1}_{\mathcal{U}_+^{(l-1)},n}\right) \\ & + \boldsymbol{R}_{\mathcal{U}_-^{(l-1)},n}\left(\hat{\boldsymbol{v}}_{\mathcal{U}_-^{(l-1)},n}^{(l-1)} + \gamma\alpha^2\mathbf{1}_{\mathcal{U}_-^{(l-1)},n}\right) + \boldsymbol{H}_n.\end{aligned}$$

$\mathcal{U}_+^{(l)} = \{i : \hat{v}_{i,n}^{(l)} > \gamma\alpha^2\}$.

$\mathcal{U}_-^{(l)} = \{i : \hat{v}_{i,n}^{(l)} < -\gamma\alpha^2\}$.

end for

for $i = 1, 2, 3, \cdots, M$, **do**

$$\hat{\beta}_{i,n} = \begin{cases} \hat{v}_{i,n}^{(l)} - \gamma\alpha^2 & i \in \mathcal{U}_+^{(l)} \\ \hat{v}_{i,n}^{(l)} + \gamma\alpha^2 & i \in \mathcal{U}_-^{(l)} \\ 0 & i \notin \mathcal{U}_+^{(l)} \cup \mathcal{U}_-^{(l)} \end{cases}$$

end for

Estimate original parameter of $(\hat{\boldsymbol{K}})$ based on $\hat{\boldsymbol{\beta}}_n$:

$$\begin{cases} \hat{k}_{xx,n} &= \sqrt{\hat{\beta}_{7,n}} \\ \hat{k}_{yy,n} &= \sqrt{\hat{\beta}_{8,n}} \\ \hat{k}_{zz,n} &= \sqrt{\hat{\beta}_{9,n}} \\ \hat{k}_{xy,n} &= \hat{\beta}_{4,n}/2\sqrt{\hat{\beta}_{7,n}} \\ \hat{k}_{xz,n} &= \hat{\beta}_{5,n}/2\sqrt{\hat{\beta}_{8,n}} \\ \hat{k}_{yz,n} &= \hat{\beta}_{6,n}/2\sqrt{\hat{\beta}_{9,n}} \\ \hat{o}_{x,n} &= \hat{\beta}_{1,n}/2\hat{\beta}_{7,n} \\ \hat{o}_{y,n} &= \hat{\beta}_{2,n}/2\hat{\beta}_{8,n} \\ \hat{o}_{z,n} &= \hat{\beta}_{3,n}/2\hat{\beta}_{9,n} \end{cases} \tag{5.48}$$

12: Estimate $\hat{\psi}_n$ based estimated $\hat{\boldsymbol{K}}$:

$$\begin{aligned}\hat{\psi}_n = &\left(\hat{k}_{xy,z}(v_{x,n}+\hat{o}_{x,n})\right)^2 + \left(\hat{k}_{xz,n}(v_{x,n}+\hat{o}_{x,n}) + \hat{k}_{yz,n}(v_{y,n}+\hat{o}_{y,n})\right)^2 \\ &+ \hat{k}^2_{xx,n}\hat{o}^2_{x,n} + \hat{k}^2_{yy,n}\hat{o}^2_{y,n} + \hat{k}^2_{zz,n}\hat{o}^2_{z,n} \\ &+ 2\hat{k}_{xy,n}\hat{k}_{yy,n}(v_{x,n}\hat{o}_{y,n} + v_{y,n}\hat{o}_{x,n} + \hat{o}_{x,n}\hat{o}_{y,n}) \\ &+ 2\hat{k}_{xz,n}\hat{k}_{zz,n}(v_{x,n}\hat{o}_{z,n} + v_{z,n}\hat{o}_{x,n} + \hat{o}_{x,n}\hat{o}_{z,n}) \\ &+ 2\hat{k}_{yz,n}\hat{k}_{zz,n}(v_{y,n}\hat{o}_{z,n} + v_{z,n}\hat{o}_{y,n} + \hat{o}_{y,n}\hat{o}_{z,n}).\end{aligned} \tag{5.49}$$

13: Output: $\hat{\boldsymbol{\beta}}_n$, $\hat{\psi}_n$, $\mathcal{U}_+^{(t)}$, $\mathcal{U}_-^{(t)}$.

The region of convergence of the proposed algorithm will be numerically investigated by numerical simulation in Section 5.4.

5.4 Simulation and Experimental Results

5.4.1 Simulations

In real life, we can not access to the true scale factors, offsets and misalignments for individual TAs. Therefore, it is difficult to accurately validate the performance of proposed calibration method by experiments alone. Meanwhile, it is also difficult to verify whether the proposed calibration method can correctly identify the zero parameters by experiments because it depends on actual MEMS TAs. Hence, simulations are important to validate the proposed calibration method.

First, the true scale factors, offsets and misalignments were pre-defined. Then, by applying the proposed calibration method, scale factors, offsets and misalignments are estimated and compared to pre-defined true values. Several types of simulations were carried out to examine different aspects of the proposed method.

Let us examine the performance of the online calibration method under normal condition first. For MEMS accelerometer, generally, the typical errors of scale factors and offsets are within $\pm 10\%$ and $\pm 0.1g$ respectively. These can cause 20° difference in angle measurement during orientation in the worst-case scenario [11]. With current MEMS technology, it is confident to assume the misalignment between each axis is

within 5%. In order to obtain reliable results from simulation, the parameters were generated randomly under the following conditions: the errors of scale factors follow uniform distributions $U(-10\%, 10\%)$; the offsets follow $U(-0.1g, 0.1g)$ and misalignments follow $U(-5\%, 5\%)$. According to the datasheets of some recently developed MEMS TAs, the noise density of the measurements is around $100 \sim 5400ug/\sqrt{Hz}$ for most commercial grade low cost MEMS TAs. With a typical $100Hz$ output frequency, the range of noise level in g is around $1mg \sim 4mg$. Thus, in this simulation, we used two different noise levels, $1mg$ and $5mg$ standard deviation with zero mean subject to Gaussian distribution. For each noise level, 500 ideal points on sphere with $'1g'$ radium were generated randomly. Then, with the pre-defined model, these 500 generate points from $'1g'$ sphere were converted to observations that noise was added based on different noise levels. After that, the proposed calibration were applied for these 500 observations. We repeated this simulation 100 times for the two noise levels respectively. Additionally, we set the following initial values for each unknown parameter:

- Scale factors (k_{xx}, k_{yy}, k_{zz}) : 1
- Misalignments (k_{xy}, k_{xz}, k_{yz}) : 0
- Offsets (o_x,o_y,o_z) : 0

Since the proposed method is an online method, the first 100 observations are used to obtain stable estimation. Therefore, only the errors after the initial 100 observations are recorded in Table 5.1. Besides that, we randomly chose 1 out of the 100 simulations with $1mg$ and $5mg$ noise levels respectively. Fig. 5.1 and Fig. 5.2 show two cases for the proposed method, which is chosen randomly from the 100 simulations.

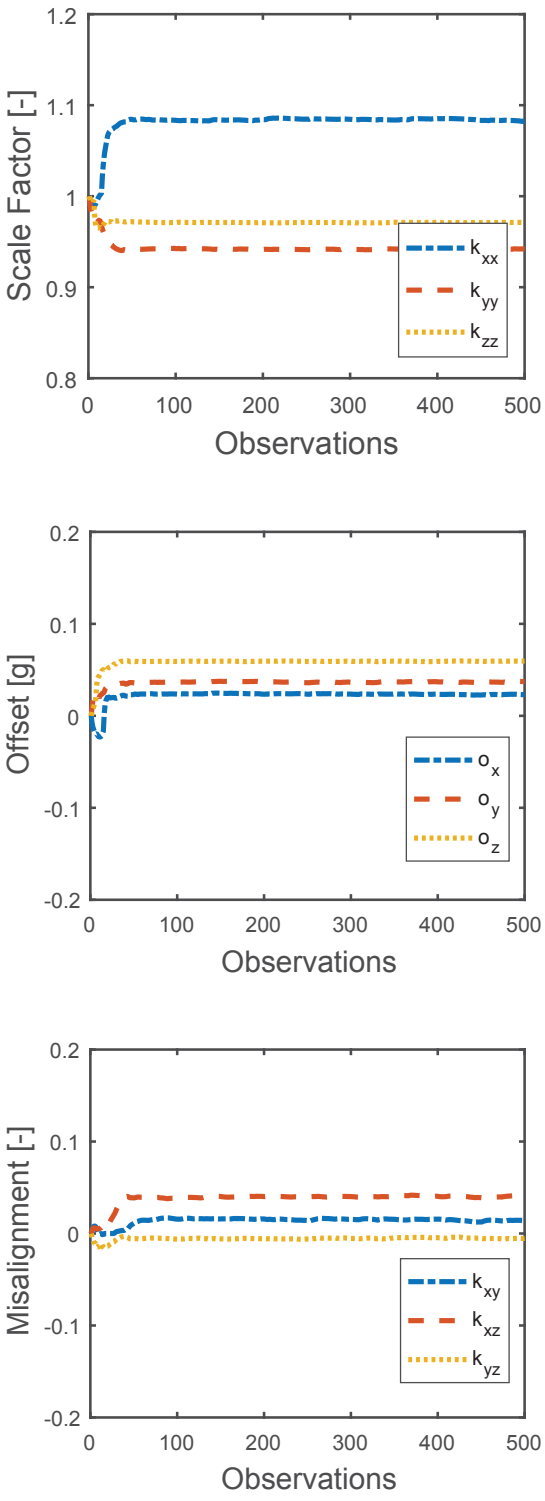

Fig. 5.1 Estimated parameters by proposed calibration during online estimation under $1mg$ noise level.

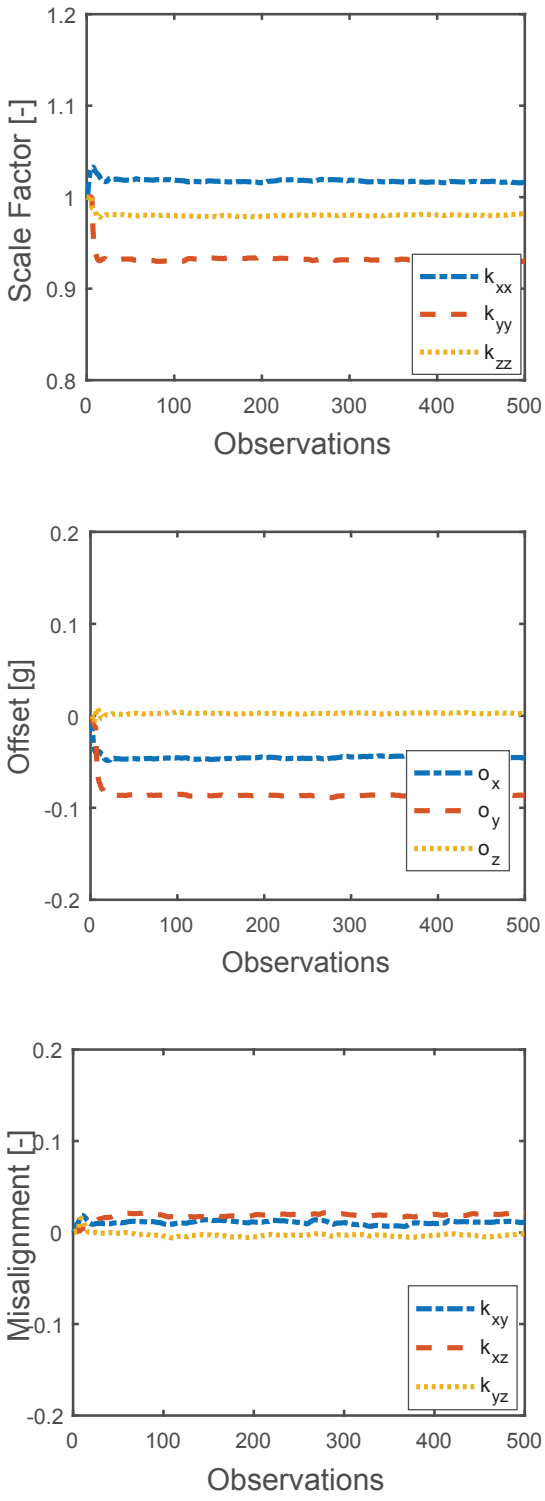

Fig. 5.2 Estimated parameters by proposed calibration during online estimation under $5mg$ noise level.

Table 5.1 Calibration results of 100 simulations under normal condition

Error distribution	Parameter	Calibration error for $1mg$ noise		Calibration error for $5mg$ noise	
		Mean Error $[g]$	SD $[g]$	Mean Error $[g]$	SD $[g]$
Scale Factor error U(-10%,10%)	k_{xx}	-2.44e-04	-7.73e-04	-2.19e-04	1.32e-03
	k_{yy}	-6.84e-04	-7.41e-04	-6.41e-04	1.26e-03
	k_{zz}	-3.32e-04	3.31e-04	-3.95e-04	1.81e-03
Offset error U(-10%,10%)	o_x	1.36e-04	2.30e-03	-1.30e-04	2.51e-03
	o_y	-1.46e-04	2.14e-03	-2.49e-04	2.37e-03
	o_z	-1.55e-04	2.17e-03	-1.41e-04	2.34e-03
Misalignment error U(-5%,5%)	k_{xy}	-1.55e-04	3.42e-03	-1.14e-04	3.92e-03
	k_{xz}	-1.34e-04	2.43e-03	-1.43e-04	2.76e-03
	k_{yz}	1.64e-04	2.44e-03	2.24e-05	2.65e-03

To verify whether the proposed calibration method can correctly identify the parameters which are zero, the misalignments were set to zero. Then, the errors of scale factors still follow a uniform distribution $U(-10\%, 10\%)$, the offsets follow $U(-0.1g, 0.1g)$ as previous. For each simulation, 200 observations were generated and tested for $1mg$ and $5mg$ noise level. A total of 100 times of simulations were carried out for this step. Fig. 5.3 and Fig. 5.5 show a typical run of simulation for this test. Eventually, all zero parameters were correctly identified within 100 steps of iteration.

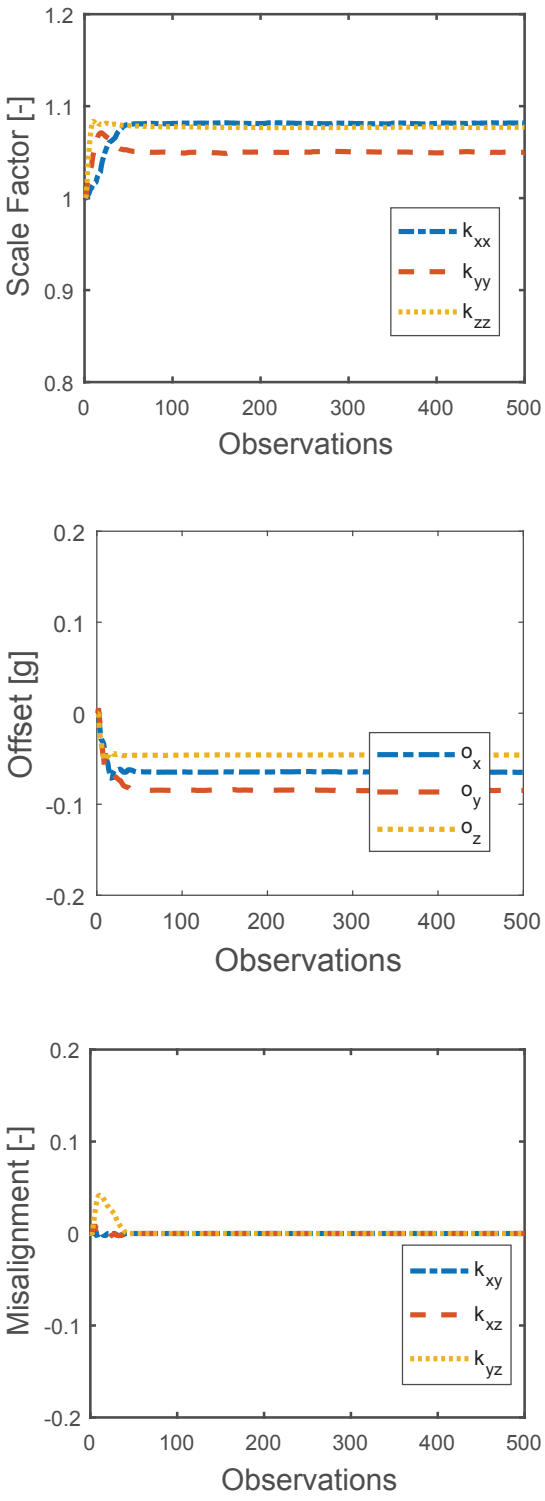

Fig. 5.3 Sparsity test of proposed calibration method under $1mg$ noise level.

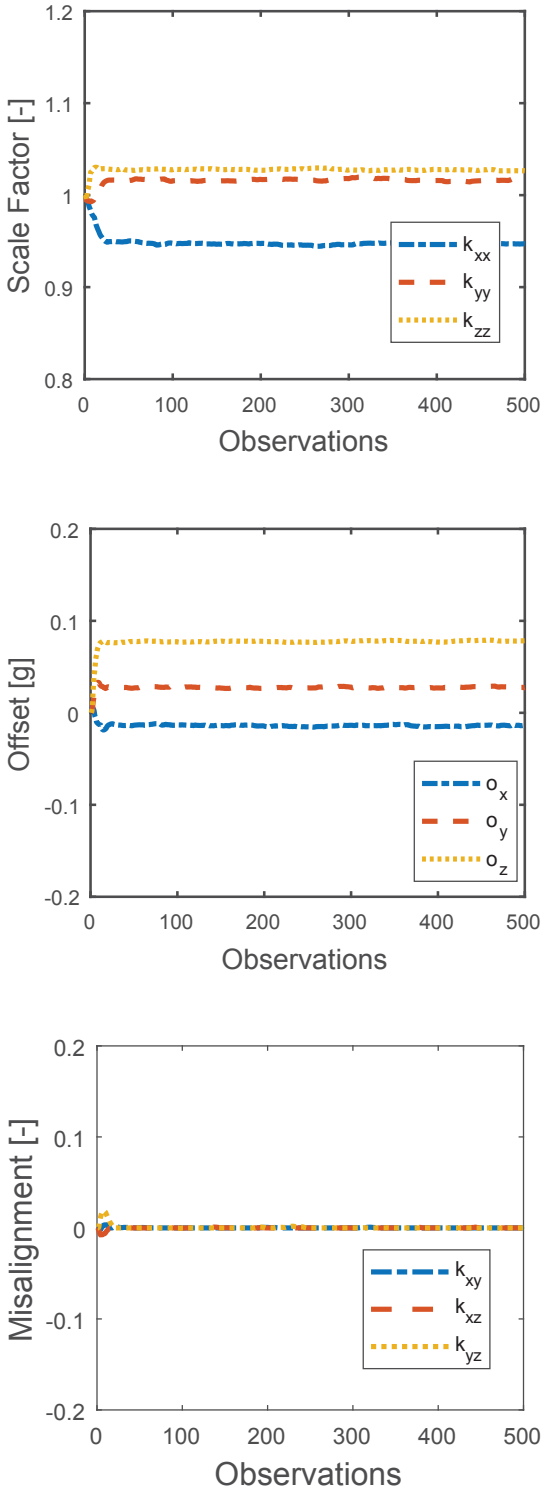

Fig. 5.4 Sparsity test of proposed calibration method under $5mg$ noise level.

The convergence of EM algorithm for linear model has been proved [40]. However, as the model of auto-calibration is nonlinear, the convergence of the proposed online EM-based algorithm should still be investigated. The convergence condition for the iterative approach might be similar with that for 6-parameter TA model as presented in [22]. However, comparing with the convergence analysis for 6-parameter model, the major difficulty here is due to the neglected term ψ_i. From Eq.(5.11), it can be observed that ψ_i is a function of input acceleration ($v_{x,i}$, $v_{y,i}$, and $v_{z,i}$), which are randomly changing during online calibration. This makes the rigorous proof of the convergence becomes difficult. In this section, we will use Monte Carlo simulation to numerically show that the convergence of the proposed algorithm is guaranteed if the initial estimation error of the TA parameters is within a certain range.

Let us reset the uncertainty range of the unknown parameters: errors of scale factors k_{xx}, k_{yy}, k_{zz} follow $U(-30\%, 30\%)$ (i.e., the scale factors are within the range $(-0.7, 1.3)$), offsets o_x, o_y, o_z are within the range $U(-0.25, 0.25)$ and misalignment k_{xy}, k_{xz}, k_{yz} are within the range $U(-0.1, 0.1)$. It should be noted that almost all MEMS TAs available in the current market are well below these error ranges. Now, for each set of simulation, we generated 500 random obversion on $1g$ sphere with $5mg$ noise density, and we executed $500,000$ sets of simulation. From the results of $500,000$ sets of simulations, it was seen that all estimated parameters were convergent. To show the rate of convergence, we chose two sets of simulation and showed the results in Fig. 5.4 and Fig. 5.5. Fig. 5.6 shows the initial 200 times of estimation of ψ. It indicates the estimated $\hat{\psi}$ can converge to the true value in a short period of time.

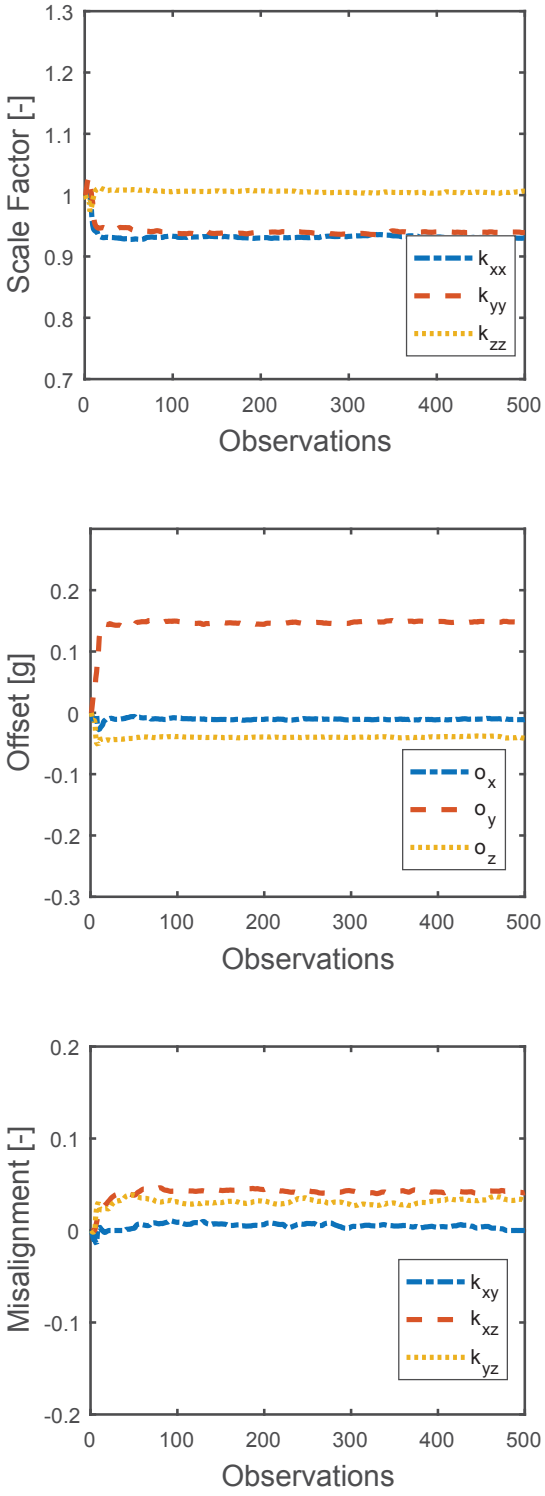

Fig. 5.5 Sparsity test of proposed calibration method under $5mg$ noise level.

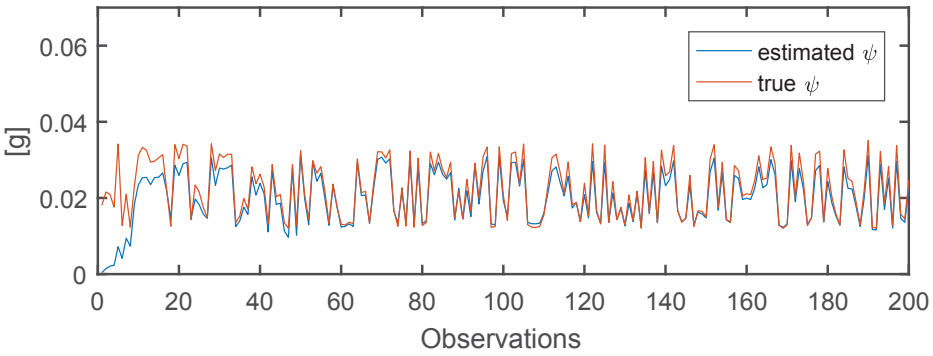

Fig. 5.6 Estimate $\hat{\psi}$ and true ψ

However, if we increase the variation ranges of the scale factors and offsets to $U(-40\%, 40\%)$ and $U(-30\%, 30\%)$ respectively, it can be observed that, in some cases, the estimation does not converge.

5.4.2 Experiments

To implement the proposed linearisation and calibration method, we developed a health monitoring device which contains SCM (TI F430), IMU (InvenSense MPU9150) and featured with Bluetooth module for wireless communication in Centre for Health Technologies, University of Technology Sydney. From the datasheet of MPU9150, the integrated accelerometer is a digital 3-axis accelerometer. Therefore, we can apply the 9-parameter model together with the proposed calibration algorithm for online calibration. The device of the experiments is shown in Fig. 5.7.

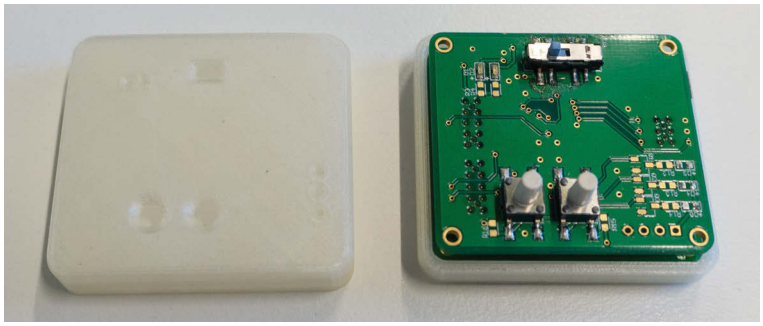

Fig. 5.7 A self-designed IMU module for the experiment

Based on Algorithm 4 and 5, firstly, the accelerometer was randomly placed in 100 different orientations. Then, we applied the proposed algorithms to calculate scale factors, offsets and misalignments. The outputs from the accelerometer were converted to acceleration with unit g based on standard factory parameters (i.e., sensitivity) first based on initial lsb/g. During experiments, the sampling frequency was set to $100Hz$. The output range was selected as $\pm 2g$ with 14 bit resolution, which results in 16384 lsb/g. The data was transferred through Bluetooth directly between computer and IMU module. To evaluate the accuracy of the estimation, we collected another 40 sets of data and estimated the acceleration based on estimation parameters. Furthermore, for the performance of parameter variation tracking during the change of temperate, the IMU module was illuminated by a lamp for 20mins. After that, we collect another 60 sets of data for online estimation. The results are shown in Fig. 5.8

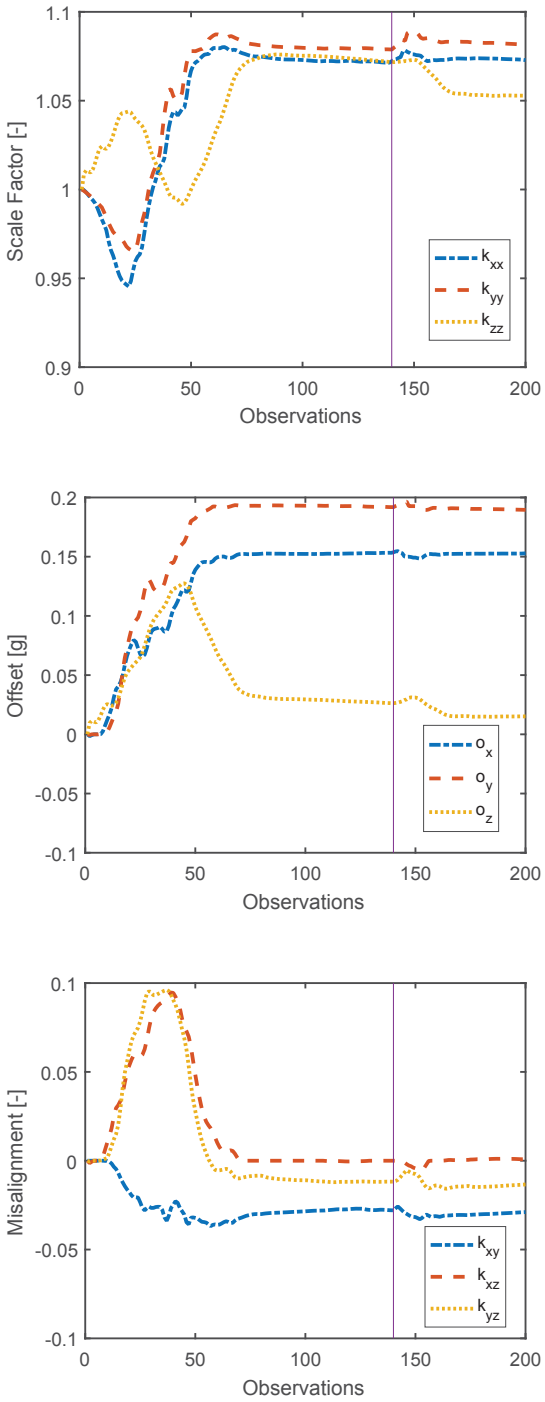

Fig. 5.8 Estimated parameters of 200 set of observations.

In Fig. 5.8, the unknown parameters were estimated within 80 observations. In addition, the variation of parameters of the accelerometer has been identified by the

proposed algorithm, indicating that the proposed online algorithm can track parameter variations during temperature changes. Furthermore, in Fig. 5.8-(c), the misalignment k_{xz} is within the threshold. Therefore, the model is simplified by assigning $\hat{k}_{xy}$ to zero. This indicates that the proposed algorithm can adapt to the model structure variation due to the changing of temperature. The errors between the vector sum of the estimated accelerations and the local acceleration $'1g'$ of observations 100 to 200 were recorded in Table 5.2, which shows that the accuracy of measurements is significantly increased after online calibration.

Table 5.2 Estimation error of the vector sum before and after calibration

	Error between estimation and local acceleration	
	mean error $[g]$	standard deviation $[g]$
Before calibration	0.0917	0.2645
After calibration	0.0003	0.0159

Additionally, to demonstrate the effectiveness of this online calibration method during parameter varying, the error of the vector sum based on different estimated parameters is analysed for the last 40 sets of observations. For group 1, the error of the vector sum was calculated based on a set of fixed estimated parameters from the $140th$ estimations. For group 2, the new estimator from the online calibration method was used to calculate the error of vector sum. The result is reported in Table 5.3, which indicates that the proposed online calibration method can significantly improve the measurement accuracy.

Table 5.3 Error between estimation and local acceleration based on different parameters

	Estimation error of vector sum	
	mean error $[g]$	standard deviation $[g]$
Group 1	0.0386	0.0142
Group 2	0.0001	0.0084

We also mounted the accelerometer on a turntable with two degree of freedom and recorded the output from 10 different orientations. These 10 orientations were considered as reference orientations, and the errors between the estimated orientations and reference orientations were calculated. The turntable has 2 optical rotary stages with $5'$ resolution and $0.03mm$ reading accuracy. For the first five orientations, we set

pitch ($\bar{p}$) as 0°, 30°, 45°, 60° and 90° while yaw and roll remained the same. Then, we repeated this for roll ($\tilde{p}$) while pitch and yaw remaining the same. Eq.(5.50) shows the relationship between reference orientation and initial value:

$$\begin{bmatrix} a_x \\ a_y \\ a_z \end{bmatrix}^T = \begin{bmatrix} a_{x,0} \\ a_{y,0} \\ a_{z,0} \end{bmatrix}^T \begin{bmatrix} c(\bar{p}) & 0 & s(\bar{p}) \\ 0 & 1 & 0 \\ -s(\bar{p}) & 0 & c(\bar{p}) \end{bmatrix} \begin{bmatrix} 1 & 0 & 0 \\ 0 & c(\tilde{p}) & -s(\tilde{p}) \\ 0 & s(\tilde{p}) & c(\tilde{p}) \end{bmatrix}, \tag{5.50}$$

where $[a_{x,0}, a_{y,0}, a_{z,0}]^T$ is the initial value $[0, 0, 1]^T$, c and s represent *Cosine* and *Sine* respectively. The estimated $[\hat{a}_x, \hat{a}_y, \hat{a}_z]^T$ was compared with $[a_x, a_y, a_z]^T$.

The results of experiments were analysed and listed in Table 5.4. The errors between the reference values $[a_x, a_y, a_z]^T$ and estimated values $[\hat{a}_x, \hat{a}_y, \hat{a}_z]^T$ were calculated for these 10 testing orientations. Since we do not know the actual value of the scale factors, offsets and misalignments, we compared and analysed the errors between the reference orientations and the estimated orientations. Due to the orientation inaccuracy of the turntable, the estimation of the vector sum ($\hat{a}_{vs}$) should be more accurate than that of the individual acceleration on each axis. It is also anticipated that the proposed algorithm optimises the variance of $\hat{a}_{vs}$.

Table 5.4 Estimation error of overall acceleration and acceleration components on each axis

	Estimation error	
	Mean Error [g]	Standard deviation [g]
$\epsilon_{\hat{a}_x}$	0.0163	0.0075
$\epsilon_{\hat{a}_y}$	-0.0080	0.0070
$\epsilon_{\hat{a}_z}$	-0.00002	0.0030
$\epsilon_{\hat{a}_{vs}}$	0.0011	0.0100

Overall, the achieved results demonstrate the efficiency of the proposed parameter estimation method.

5.5 Summary

In this chapter, a linearisation method for 9-parameter TA model has been presented for auto-calibration. To solve the unknown parameters from the linearised model online, a modified sparse least square estimation method was introduced. The online calibration method can automatically remove the insignificant parameters during online calibration. Furthermore, the proposed calibration method can track parameters when the parameters change due to daily drift and/or temperature variation.

It should be noted that this study is the very first research that focused on online calibration with automatic model selection for the auto-calibration of 9 parameters. Comparing to most previous researches, which were mainly based on off-line calibration, this method can achieve real-time online calibration of a 9-parameter auto-calibration model. Furthermore, in contrast with the UKF based online calibration method [12], the proposed calibration approach has embedded an $\mathcal{L}_1$ norm penalty term for the elimination of the insignificant parameters in order to improve the reliability of the calibration.

To verify the presented method, both simulation and experiment were carried out. Based on the simulation results, it can be concluded that the proposed calibration method can achieve accurate estimation within 50 iterations in most cases, and the estimated response has a small mean error and standard deviation. Furthermore, the results from simulation indicated that the proposed method can correctly identify the parameters which were zero.

Experiments were performed for the proposed calibration method with a self-designed IMU. As the true scale factors and displacements were unknown, the error between the estimated orientations and the reference orientations was calculated and analysed. The experimental results demonstrated that the proposed calibration approach could accurately estimate the vector sum of the three axes in the whole measurement region.

Chapter 6

Dynamic Modelling of Oxygen Uptake During Exercises

6.1 Introduction

Previous researches conducted on the oxygen uptake modelling can be divided into two categories: (i) static status modelling and (ii) dynamic status modelling. For the static status modelling, an early stage study in [95] proposes a linear static model to approximately estimate oxygen uptake for a given range of walking speed. Simple nonlinear static models are also discussed in [96–98] for the compensation of nonlinearities. On the other hand, the transient response of oxygen uptake has captured the interests of many researches. For example, the authors of [36, 37] have developed a first-order system to approximate the process based on step response. Later, the work in [34] has developed a nonlinear dynamic model for oxygen uptake modelling during treadmill exercise with pseudo random binary signal (PRBS) as the input. However, it is relatively difficult for the exercisers to follow the PRBS signal during the treadmill exercise generally.

In real life, the standard deviation of noise in VO_2 measurements is quite large due to the limitations of portable gas analyser. For the modelling of a process with large noise, as determining the order is difficult, a nonparametric model such as impulse response (IR) model is a good choice. However, conventional system identification

methods for impulse response estimation normally requires relatively complex input such as PRBS [35] to significantly stimulate the system. In previous studies, the response of oxygen uptake can only be roughly modelled as a first-order system due to the lack of suitable modelling techniques. Recently, a new kernel based estimation method has been developed for nonparametric model estimation [41, 78]. To avoid ill-conditioned solutions due to the existence of large noises, a regularised term is incorporated into the cost function [99], which can limit the one-step variation of the estimated parameters. This new kernel based method projects the parameters of IR into a reproducing kernel Hilbert space (RKHS) which can reduce high frequency components in IR model. Furthermore, by using this method, more accurate results can also be obtained enabling us to employ simple inputs such as step input.

In this chapter, in order to implement nonparametric modelling of VO_2 response to dynamic exercises, the kernel based estimation method has been adopted and modified. An $\mathcal{L}_1$ regularisation term has been added into the cost function to penalise the least significant term of IR which can result in reducing the order of the impulse response model. Particularly, we have demonstrated that this method is still valid when the input of the system is a single step response for this specific $VO_2 - Speed$ system. For this research, several popular kernels were tested, such as stable spline (SS) kernel, diagonal kernel (DI) and diagonal/correlated (DC) kernel. Furthermore, we showed through several simulation examples that SS and DC kernels can achieve higher accuracy compared to DI kernel for this problem. Eventually, the proposed method was experimentally validated by using the VO_2 data collected from twenty participants. The results were compared with the estimated model based on Akaike's Information Criterion (AIC) selected autoregressive with exogenous terms (ARX) model with predicted error method for parameter estimation.

The main contributions of this work can be summarised as follows. Firstly, a new nonparametric modelling approach has been developed based on the kernel-based impulse response estimation approach, which can efficiently reduce the order of the IR model by incroporating an $\mathcal{L}_1$ penalty term. Secondly, for the developed IR model identification, appropriate kernels selection has been investigated using extensive simulations, and the stable spline kernel (SS) was recommended as the best candidate. Thirdly, it was demonstrated by both experiment and simulation that the proposed

method is efficient for the modelling of IR of cardiorespiratory response to dynamic exercise, which often confronts a highly noisy measurement under the stimulation of a simple input signal. Finally, an averaged impulse response model has been established, which is able to quantitatively describe the oxygen update on-kinetics for treadmill exercise.

This chapter is organised as follows. In section 6.2, the nonparametric method for VO_2 modelling is proposed and kernel selection is also discussed. In section 6.3, the simulation is carried out for the validation of the proposed method. In section 6.4, the experimental results are presented. Section 6.5 summarises the chapter.

6.2 New Modelling Method for VO_2 During Exercise

In most of the previous studies, the step response of oxygen uptake during exercise (Fig.6.1) has been considered as an exponential function [74, 100]:

$$VO_2(t) = VO_2^0 + \beta[1 - e^{-\frac{(t-t_d)}{T_p}}], \tag{6.1}$$

where t_d is the time delay, β is the steady state gain of the system, T_p is the time constant and VO_2^0 is the baseline value of oxygen uptake. Based on Laplace transform, the transfer function in regarding with Eq.(6.1) can be derived as follows:

$$VO_2(s) = \frac{\beta e^{-t_d s}}{T_p s + 1}. \tag{6.2}$$

However, sometimes, a first order system with time delay cannot obtain the best results due to the pattern of measurements (breath by breath) and the individual variation of oxygen uptake. It is likely that the model of $VO_2 - speed$ of some individuals should be described by high order dynamic systems. However, to correctly identify a high order system, specific input such as pseudorandom binary sequence (PRBS) is necessary to well stimulate the system. As we know, during running exercise, even on treadmill, it is unpractical for users to follow an ideal PRBS signal as input. Therefore,

previously the VO_2 uptake during running exercise has been mainly considered as a first order system and modelled by a first order ARX model. However, having a step input, a first order transfer function and a high order transfer function which can be decomposed to serval first order transfer function, can lead to quite similar responses. Therefore, it is generally difficult to identify the correct order for the transfer function describing the input-output relation. Hence, to overcome this shortage, nonparametric methods are developed to provide better accuracy in this situation. In order to obtain more acceptable results, we exploited a newly developed nonparametric modelling method which make use of finite impulse response (FIR) to describe the system's characteristic.

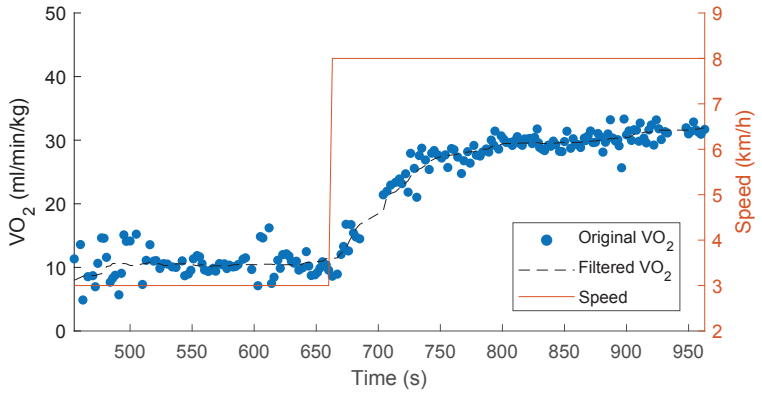

Fig. 6.1 Oxygen uptake during running on treadmill.

6.2.1 Kernel Based Estimation Method of Finite Impulse Response

In this section, a new kernel based nonparametric estimation method is exploited to model the oxygen uptake during running exercise. For this nonparametric estimation method, it is not required to predefine the order of the model in advance. Furthermore, it will be shown that the proposed method can provide stable and smooth estimation comparing to other estimation methods [78].

For nonparametric model, let us select t with sampling time T as the time index, the relationship between the running speed ($u(t)$) and oxygen uptake ($y(t)$) can be considered as a single input single output (SISO) dynamic system. Therefore, for the

impulse response of this SISO system, the discrete time output can be calculated as [80]:

$$y(t) = G_o(q)u(t) + \epsilon(t), \quad t = 1, 2, 3 \cdots, M \tag{6.3}$$

where q represents the shift operator, i.e. $qu(t) = u(t+1)$, $\epsilon(t)$ is the Gaussian white noise and $G_0(q)$ is expressed as:

$$G_o(q) = \sum_{k=1}^{\infty} g_k^0 q^{-k}, \quad k = 1, 2, 3 \cdots, \infty, \tag{6.4}$$

where g_k^0 represents the coefficient from the impulse response $G_o(q)$. For linear response, the impulse response decays exponentially for stable $G_0(q)$. Therefore, normally, the mth order finite impulse response is able to describe the system as:

$$G(q, \boldsymbol{\theta}) = \sum_{k=1}^{m} g_k q^{-k}, \quad \boldsymbol{\theta} = [g_1, g_2, \cdots, g_m]^T. \tag{6.5}$$

where $\boldsymbol{\theta} \in \mathbb{R}^m$ can be considered as unknown parameter. Hence, the model in Eq.(6.3) can be written as:

$$y(t) = \boldsymbol{\varphi}^T(t)\boldsymbol{\theta} + \epsilon(t), \tag{6.6}$$

where $\boldsymbol{\varphi}(t) \in \mathbb{R}^m$ contains the input information of the system:

$$\boldsymbol{\varphi}(t) = [u(t-1), u(t-2), \cdots, u(t-m)]^T. \tag{6.7}$$

Then, the FIR model can be expressed in matrix form as:

$$\boldsymbol{Y}_N = \boldsymbol{\phi}_N \boldsymbol{\theta} + \boldsymbol{\varepsilon}_N, \tag{6.8}$$

where $N = M - m$, and M is the number of data point that we collected. The ith row of $\boldsymbol{Y}_N \in \mathbb{R}^N$, $\boldsymbol{\epsilon}_N \in \mathbb{R}^N$ and $\boldsymbol{\phi}_N \in \mathbb{R}^{N \times m}$ are $y(m+1)$, $\epsilon(m+1)$ and $[u(m+i-1), u(m+i-2), \cdots, u(i)]$.

Apparently, the straightforward cost function of Eq.(6.8) can be expressed as:

$$\hat{\boldsymbol{\theta}} = \arg\min_{\boldsymbol{\theta} \in \mathbb{R}^m} ||\boldsymbol{Y}_N - \boldsymbol{\phi}_N \boldsymbol{\theta}||_2^2. \tag{6.9}$$

By minimising the cost function (6.9), $\hat{\boldsymbol{\theta}}$ can be solved by least square (LS) estimation or maximum likelihood (ML) estimation easily, it is not appropriate for modelling the oxygen uptake by impulse response, as the input is only a square signal, and the measurements are normally extremely noisy [34] and it is likely that $\boldsymbol{\phi}_N^T\boldsymbol{\phi}_N$ is ill-condition. Hence, to guarantee the validity of the obtained model and avoid any ill-conditioned solution, a regularisation term is crucial to reduce the variation of the estimated parameters in the objective function [99]. Then, the cost function can be considered as:

$$\hat{\boldsymbol{\theta}} = \arg\min_{\boldsymbol{\theta}\in\mathbb{R}^m} ||\boldsymbol{Y}_N - \boldsymbol{\phi}_N\boldsymbol{\theta}||_2^2 + \gamma\boldsymbol{\theta}^T\boldsymbol{W}\boldsymbol{\theta}, \tag{6.10}$$

where the first term implies the modelling error, γ is a positive coefficient controlling the trade off between the error term and the regularisation term. $\boldsymbol{W}$ is a weighting matrix, which can be used to prioritised between system parameters. For a normal regulariser $\boldsymbol{\theta}^T\boldsymbol{W}\boldsymbol{\theta}$, regularised least square estimation (ReLS) is a standard method to solve Eq.(6.10). This can be seen as an improved method out of Ridge regression or weighted Ridge regression [101] depending on the selection of matrix $\boldsymbol{W}$.

However, ReLS cannot achieve desired solution when the input stimulation is insignificant and the measurement has high noise level. In order to obtain a better FIR model of the oxygen uptake model, we introduce a newly developed kernel method [41, 78]. Let us recall Eq.(6.5), assuming that the FIR function $g \in R^m$, then the function g in regularisation term can be projected into a reproducing kernel Hilbert space (RKHS), i.e., $g \to g_{\mathcal{H}}$ ($R^m \times R^m \to R^{m\times m}(\mathcal{H})$). The advantage of this transform is the penalisation of the high frequency components in the function g [78]. Different from ReLS which only focuses on solving matrix with ill-condition, the regularisation term $g_{\mathcal{H}}$ can perform better for minimising the mean square error of finite impulse response $g(\cdot)$ [80]. If we use the kernel matrix $\boldsymbol{P}$ based on $g_{\mathcal{H}}$ to replace $\boldsymbol{W}$ in Eq.(6.10), the kernel based estimation method can be expressed as:

$$\hat{\boldsymbol{\theta}} = \arg\min_{\boldsymbol{\theta}\in\mathbb{R}^m} ||\boldsymbol{Y}_N - \boldsymbol{\phi}_N\boldsymbol{\theta}||_2^2 + \gamma\boldsymbol{\theta}^T\boldsymbol{P}^{-1}\boldsymbol{\theta}, \tag{6.11}$$

where $\boldsymbol{P}$ represents the kernel matrix whose details are given in the next section.

With the priori information in kernel matrix $\boldsymbol{P}^{-1}$, the estimated $\hat{\boldsymbol{\theta}}$ from Eq.(6.11) can provide better and smoother results comparing to ReLS or Ridge regression [78]. Furthermore, unlike support vector regression (SVR) [79], for this nonparametric method, the inputs and system parameters from the error term are not projected to a higher dimension as the estimated system parameters from SVR are normally hard to recover from projected space to original system parameters. Furthermore, during the VO_2 uptake modelling, this model tends to have relatively large time constant based on the previous research [34]. Hence, we expect that the last several parameters of the estimated FIR approach to zero. Therefore, we need to add an extra $\mathcal{L}_1$ regularisation as another regulariser to sparsify the transfer function identified, by which the overall cost function can be expressed as:

$$\hat{\boldsymbol{\theta}} = \arg\min_{\boldsymbol{\theta}\in\mathbb{R}^m} ||\boldsymbol{Y}_N - \boldsymbol{\phi}_N\boldsymbol{\theta}||_2^2 + \gamma\boldsymbol{\theta}^T\boldsymbol{P}^{-1}\boldsymbol{\theta} + \alpha||\boldsymbol{\theta}||_1. \tag{6.12}$$

where α is a positive coefficient to control the trade off between $\mathcal{L}_1$ regulariser and kernel regulariser $\gamma\boldsymbol{\theta}^T\boldsymbol{P}^{-1}\boldsymbol{\theta}$.

The above equation can be considered as a special case of elastic net [66], in which the $\mathcal{L}_2$ norm regularisation is weighted by kernel matrix $\boldsymbol{P}^{-1}$. Let us rearrange Eq.(6.12) and define two new parameters as:

$$\boldsymbol{\phi}_N^* = \frac{1}{\sqrt{1+\gamma}}\begin{bmatrix}\boldsymbol{\phi}_N \\ \sqrt{\gamma}\boldsymbol{R}\end{bmatrix}, \tag{6.13}$$

where $\boldsymbol{R}$ is the upper triangular matrix from Cholesky factorisation of kernel matrix $\boldsymbol{P}^{-1}$ ($\boldsymbol{P}$ is symmetric).
If denote, $\boldsymbol{Y}_N^* \in \mathbb{R}^{N+m}$ can be defined as:

$$\boldsymbol{Y}_N^* = \begin{bmatrix}\boldsymbol{Y}_N \\ \boldsymbol{0}\end{bmatrix}, \tag{6.14}$$

then, the cost function Eq.(6.12) can be written as:

$$\hat{\boldsymbol{\theta}}^* = \min_{\boldsymbol{\theta}^*\in\mathbb{R}^m} ||\boldsymbol{Y}_N^* - \boldsymbol{\phi}_N^*\boldsymbol{\theta}^*||_2^2 + \frac{\alpha}{\sqrt{1+\gamma}}||\boldsymbol{\theta}^*||_1, \tag{6.15}$$

where $\boldsymbol{\theta}^*$ is defined as:

$$\boldsymbol{\theta}^* = \sqrt{1+\gamma}\boldsymbol{\theta}. \tag{6.16}$$

Due to the limitation of the input signal, the input matrix $\boldsymbol{\phi}_N^T\boldsymbol{\phi}_N$ is not orthogonal. Therefore, the close form solution of LASSO [65] cannot be applied to solve Eq.(6.15) directly. Here, an interior-point method [102] is adopted for this $\mathcal{L}_1$ norm regularisation for $\hat{\boldsymbol{\theta}}^*$. At the end, $\hat{\boldsymbol{\theta}}^*$ can be restored to $\hat{\boldsymbol{\theta}}$ according to Eq.(6.16) as:

$$\hat{\boldsymbol{\theta}} = \frac{1}{\sqrt{1+\gamma}}\hat{\boldsymbol{\theta}}^*. \tag{6.17}$$

6.2.2 Kernel Selection

Several kernels have been applied or developed for the proposed nonparameteric kernel estimation method, such as polynomial kernel, radial basis function (RBF) kernel, stable spline (SS) kernel, diagonal/correlated (DC) kernel, diagonal (DI) kernel, etc. In the proposed nonparametric modelling method, the kernel matrix must be symmetric positive definite, due to the use of Cholesky matrix decomposition. For this research, SS kernel, DI kernel and DC kernel are selected. SS kernel, DC kernel and DI kernel are developed in [41, 80]. In addition, for a stable process, as its impulse response is treated as a function which decays exponentially with a certain rate, the SS, DC and DI kernels, which belong to amplitude modulated locally stationary (ALMS) kernel, can often achieve deserved results when identifying FIR model. These three kernels are defined as follows:

- DI kernel:

$$P(i,j) = \begin{cases} c\lambda^i, & i = j \\ 0 \end{cases}, \tag{6.18}$$

  where $c > 0$, $1 > \lambda > 0$.

- SS kernel:

$$P(i,j) = \begin{cases} c\dfrac{\lambda^{2i}}{2}\left(\lambda^i - \dfrac{\lambda^j}{3}\right), & i \geq j \\ c\dfrac{\lambda^{2j}}{2}\left(\lambda^j - \dfrac{\lambda^i}{3}\right), & j \geq i \end{cases}, \tag{6.19}$$

where $c > 0, \lambda > 0$.

- DC kernel:

$$P(i,j) = c\rho^{|i-j|}\lambda^{|i+j|/2}, \tag{6.20}$$

where $c > 0$, $1>\lambda>0$, $|\rho| \leq 1$ and $|\rho| \neq 0$.

More details about the kernels above can be found in [103].

6.3 Simulations

Mostly, the relationship between the oxygen uptake and the jogging speed was considered as a first order system. To the author's best knowledge, due to the individual differences of the body condition of human beings, it is likely that the transfer function model of the VO_2 for each person is different in terms of gain value and order. For some people, the relationship between oxygen uptake and the joggling speed may not be a first order transfer function. Furthermore, it is generally hard to correctly identify the extract order of system through a single step response, especially under large observation noise. The major difference between a first order system and a high order system in step response is in their slope and damping. Therefore, it is likely that a second or higher order system is identified as a first order system though single step response. Therefore, during this simulation section, both first order systems and second order systems will be considered.

First of all, the performance of the proposed calibration method is tested on the first order system. In this simulation, we consider a first order system as

$$Y(s) = \frac{k \cdot X(s)}{T_p \cdot s + 1}, \tag{6.21}$$

where time-constant T_p follows the uniform distribution $U(10, 20)$ and the gain k follows $U(10, 20)$. During the simulation, the input signal $X(s)$ is a step response which jumps from 0 to 1 at time $180s$ and keeps at 1 for $300s$. For comparison purposes, the estimations of both ARX model and impulse response model were tested. Assuming that the sampling $T_s = 1(s)$, the discrete time ARX model of the first order system in

transfer function (6.21) is assumed as:

$$y(k) = a_1 x(k-1) + b_1 y(k-1) + \epsilon_1, \quad k = 2, 3, \cdots, n \tag{6.22}$$

where n is the number of samples, ϵ_1 is the zero mean Gaussian noise with $3dB$ signal-to-noise ratio (SNR). For ARX model, we used classic prediction error method (PEM) to solve the unknown parameters a_1 and b_1. For the estimation of the impulse response model, the proposed method is applied with FIR $m = 120$. In paper [104], the authors gave some extra constraints for the parameters' of kernels: (i) $0.9 \leq \lambda < 1$ for SS kernel; (ii) $0.72 \leq \lambda < 1$, $-0.99 \leq \rho \leq 0.99$ for DC kernel; (iii) $0.7 \leq \lambda < 1$ for DI kernel. The settings of kernels are listed as follows:

- SS kernel: $c = 1$, $\lambda = 0.98$
- DC kernel: $c = 1$, $\lambda = 0.9$, $\rho = 0.8$
- DI kernel: $c = 1$, $\lambda = 0.9$
- regulariser: $\gamma = 4$, $\alpha = 10$

We repeated this simulation for 1000 times, and the goodness-of-fit NRMSE (normalised root mean square error) is defined as:

$$\text{Fit Ratio} = \left(1 - \frac{||\hat{\boldsymbol{Y}_N} - \boldsymbol{Y_N}||_2}{||\boldsymbol{Y_N} - \text{mean}(\boldsymbol{Y_N})||_2}\right). \tag{6.23}$$

The results of simulations are recorded in Table 6.1 and the box plot of the results is shown in Fig. 6.2. For the results from nonparametric method with SS kernel and PEM method, one way analysis of variance (ANOVA) is implemented for the significance test of fit ratio. The p value is less than 0.0001. Therefore, the goodness-of-fit of the kernel estimation method is significantly better than PEM when the noise of measurement is large. Furthermore, one simulation is randomly chosen out of the 1000 simulations and the results are shown in Fig. 6.3 as comparison between proposed method and classic method. For a clear view, only the estimated results from kernel method with SS kernel and PEM are shown. From the graph, it is evident that the proposed kernel method can fit better when the measurement is noisy.

Table 6.1 Comparison of first order system simulation in terms of goodness-of-fit

Method	Mean	Standard Deviation	Best
PEM	0.7525	0.0444	0.8475
Kernel (SS)	0.8705	0.0264	0.9170
Kernel (DC)	0.8738	0.0254	0.9141
Kernel (DI)	0.8678	0.0254	0.9114

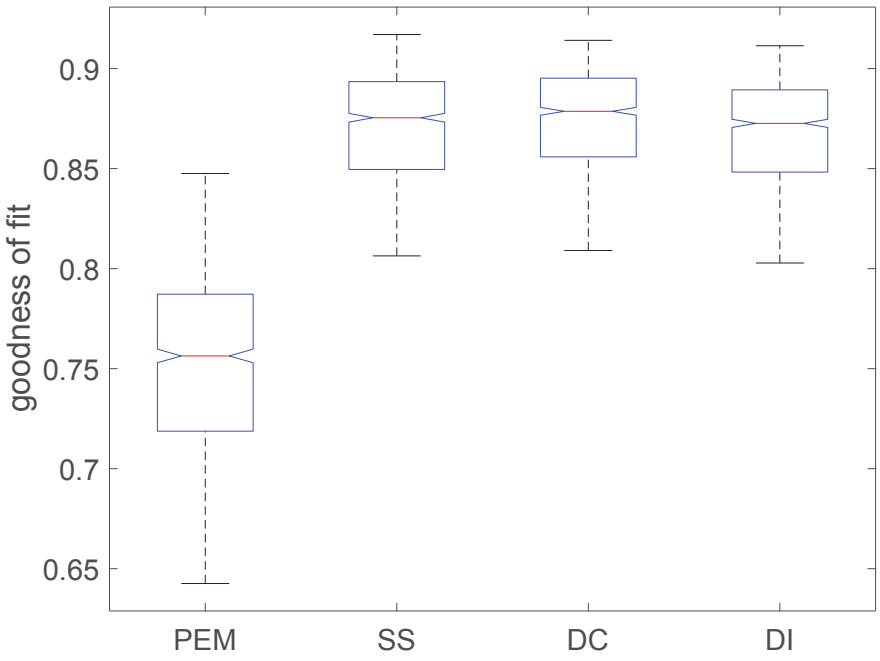

Fig. 6.2 Box plot of the goodness-of-fit of estimation from PEM and nonparametric method with SS, DC and DI kernel for first order model

Then, let us consider a second order system as:

$$Y(s) = \frac{k \cdot X(s)}{(\tau_1 \cdot s + 1)(\tau_2 \cdot s + 1)}, \tag{6.24}$$

where the variables τ_1 and τ_2 follow $U(10, 20)$ and $U(5, 10)$ respectively. The gain k follows $U(10, 20)$. In this simulation, the input signal X(s) is a step response which jump from 0 to 1 at time $180s$ and stay at 1 for $300s$. During the simulation, we used both first order and second order model in the ARX model. The second order ARX

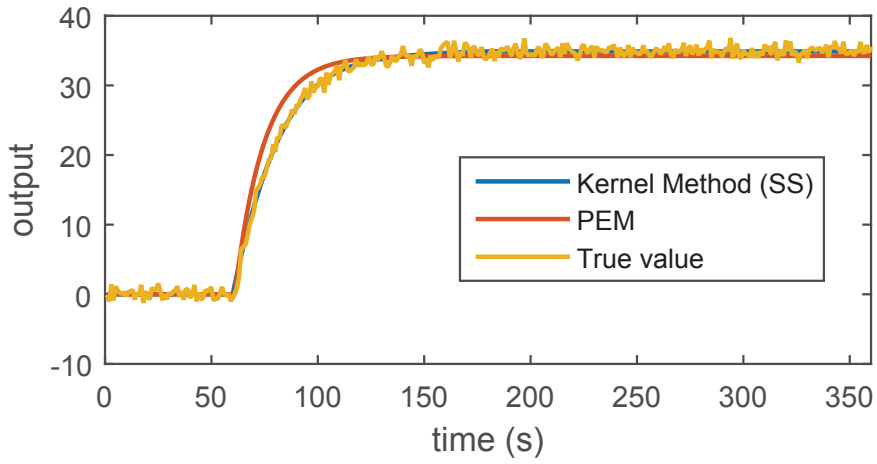

Fig. 6.3 Estimation of one simulation

model is expressed as:

$$\begin{aligned} y(k) =& a_1 x(k-1) + a_2 x(k-2) \\ &+ b_1 y(k-1) + b_2 y(k-2) + \epsilon_2, \quad k = 2, 3, \cdots, n, \end{aligned} \tag{6.25}$$

where ϵ_2 is also the zero mean Gaussian noise with $3dB$ SNR.

For impulse response estimation, SS, DI and DC kernels are selected in the simulation. For the FIR, we set $m = 120$, and the settings of the kernels are the same as the first order simulation. The simulations were repeated for 1000 times, and the results are reported in Table 6.2 and visualised in the box plot in Fig. 6.4.

Table 6.2 Comparison of second-order system simulation in terms of goodness-of-fit

Method	Mean	Standard Deviation	Best
PEM (first-order system)	0.7087	0.0554	0.8157
PEM (second-order system)	0.8133	0.0484	0.8955
SS Kernel	0.8694	0.0246	0.9075
DC Kernel	0.8758	0.0248	0.9184
DI Kernel	0.8615	0.0234	0.9073

Based on the results in Table 6.2, it is clearly seen that the kernel method outperforms previous methods. Another significant advantage is that the order of the model do not need to be determined separately. From the results given in Table 6.2, if the second-order system is identified as first-order system incorrectly, the differences

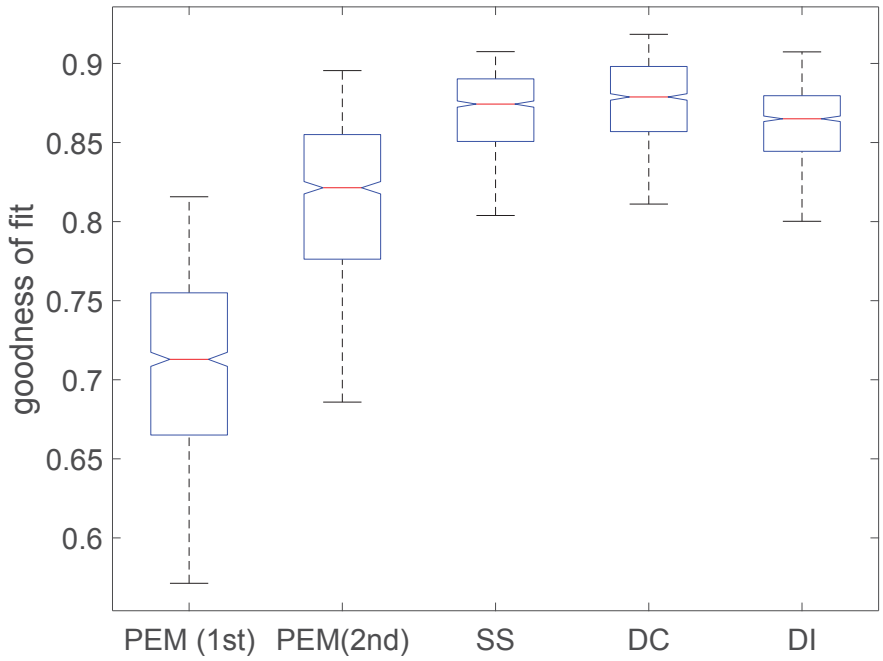

Fig. 6.4 Box plot of the goodness-of-fit of estimation from PEM and nonparametric method with SS, DC and DI kernel for second order model

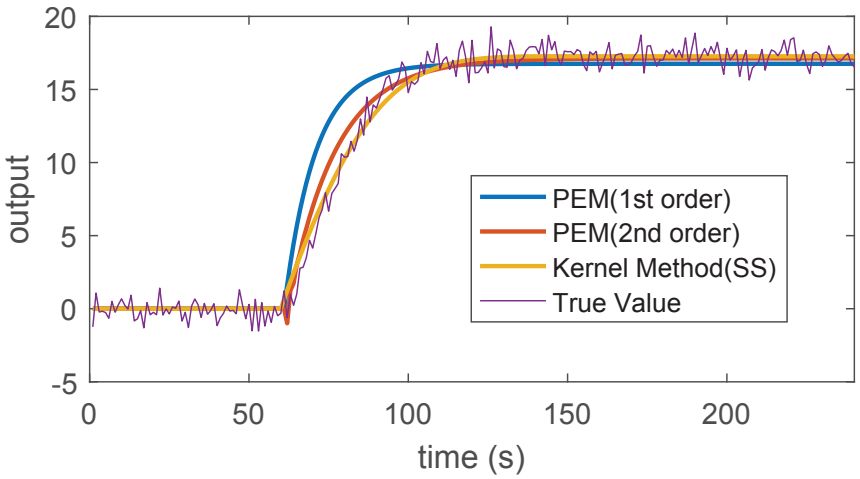

Fig. 6.5 Estimation of one simulation

between the achieved results are significant. Fig.6.5 shows one randomly chosen simulation. The figure shows that the estimated response from kernel method fits the best. Although SS kernel and DI kernel can achieve similar performance so far, paper [80] indicates that SS kernel can outperform DI kernel when the system has higher order. Therefore, we selected SS kernel to estimate the impulse response during our experiment section.

It is also necessary to verify that this method is better than ridge regression. Consider a second order system as:

$$Y(s) = \frac{15 \cdot X(s)}{(10 \cdot s + 1)(15 \cdot s + 1)}. \tag{6.26}$$

The SS kernel is selected for the proposed method with $c = 1$, $\lambda = 0.98$ and $m = 120$. For ridge regression, whose weighting matrix $\boldsymbol{W}$ in the regularisation term is a simple identify matrix, we also set $m = 120$ and both methods share the same weight of regulariser ($\gamma = 4$, $\alpha = 10$). First, Let us show that the estimated IR from kernel method and true IR in Fig. 6.6. As we can see from Fig. 6.6, the estimation output from SS kernel is very close to the true output without over-fitting. The comparison of results between kernel method and ridge regression is shown is Fig. 6.7. From Fig. 6.6 and Fig. 6.7, it can be seen that the IR model from ridge regression without the kernelised $\mathcal{L}_2$ norm penalty is inaccurate comparing to the kernel method. The results

from the kernel method is far better than the classic ridge regression. Specifically, the estimated IR from kernel method is very close to true IR.

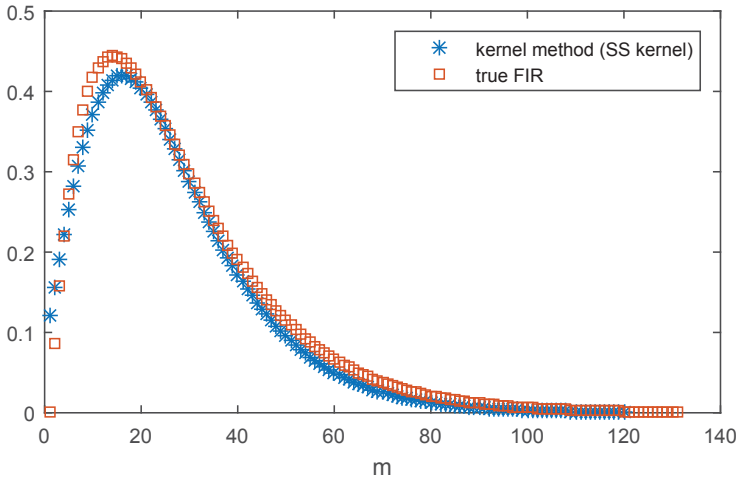

Fig. 6.6 Comparison among true IR and estimated IR based on SS kernel.

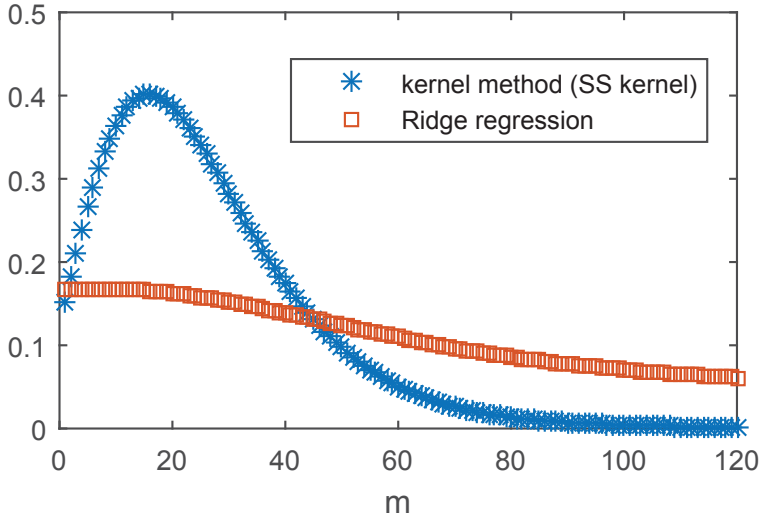

Fig. 6.7 IR from proposed kernel method and Ridge regression.

6.4 Experiments

In order to develop the impulse response model of the dynamic VO_2 responses to treadmill exercise, an experimental approach was employed in which twenty healthy

males subjects were asked to exercise. The physical characteristics of the participants are shown in Table 6.3.

Table 6.3 Age and BMI of participants

Subject	Age($year$)	Height(m)	Mass(kg)	BMI(kg/m^2)
Average	38.02	1.77	86.10	27.16
Standard Deviation	5.28	0.06	14.05	3.61

All data was acquired by a gas analyser $K4b^2$ (COSMED), which is a portable system for pulmonary gas exchange measurement with true breath-by-breath analysis. The UTS Human Research Ethics Committee (UTS HREC 2009000227) approved this study and an informed consent was obtained from every participant before the commencement of data collection[100].

Prior to the experiments, all participants were asked to observe the following requirements: the nutritional intake, physical activity and environment conditions. The participants were instructed to consume a standardised light meal at least two hours before the experiment. Meanwhile, they were asked not to engage in any other exercises for one day before experiment. The temperature and humidity of the laboratory were set at $20-25$℃ and around 50% relative humidity respectively.

During the experiment, all participants were seated for 5 min first, then stood next to the treadmill for another 2 min. Then, the participants were asked to start walking at 3 km/h for 4 min, followed by a run for 8 min at 8 km/h, and another walk for 8 min at 3 km/h. At the end, the participants rested for 5 min. One single experiment took 32 min in total. The protocol of this experiment is shown in Fig. 6.9. The participants only ran at a relatively low speed (8 km/h) to avoid anaerobic respiration. The typical experimental scenario with $K4b^2$ gas analyser and the automated treadmill system is shown in Fig. 6.8.

In this work, we only focused on the onset VO_2 response of treadmill exercise (i.e., from walking to running). Therefore, for the purposes of impulse response modelling, we only took the data from $t_1 = 420s$ to $t_2 = 1120s$ as shown in Fig. 6.9. Since the data of gas exchange recorded by $K4b^2$ is breath by breath based, the sampling time of

Fig. 6.8 The LabVIEW controlled treadmill system for experiments

$K4b^2$ is irregular, and the quality of the measurements is often relatively low because of the complexity of the gas exchange in cardiopulmonary system. This is also a reason why nonparametric modelling rather than structured modelling is selected in this study. Furthermore, only a $3rd$ median filter was applied to reduce the measurement noise with minimal influence of breath signals. An experiment was randomly chosen and the result of applying a $3rd$ median filter which is shown in Fig. 6.10. It is evident from Fig. 6.10 that the third order median filter can efficiently remove the noise, without losing many details from raw signals. As it is mentioned previously, the gas response of $K4b^2$ is breath by breath based, therefore, the sampling time of measurement is not constant. In order to deal with this issue, we used a classic interpolation method [105] to unify the sampling period to $1s$.

Overall, for the estimation of impulse response model, the sampling time was selected as $1s$, and the order of the model was selected as 300. The IR model can

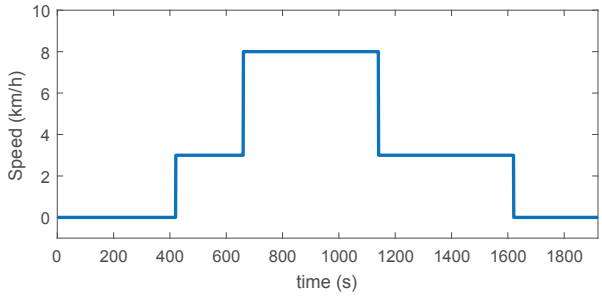

Fig. 6.9 Protocol of exercise for the experiment.

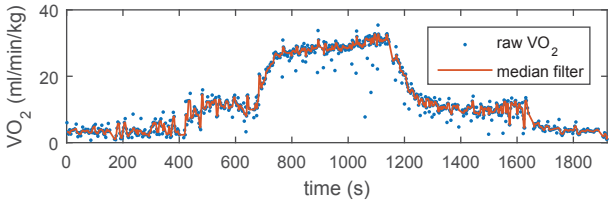

Fig. 6.10 Raw VO_2 measurement and filtered measurement of participant 1

therefore be expressed as a 300 order FIR model:

$$\begin{aligned} y[n] &= g[1]u[n-1] + g[2]u[n-2] + \cdots + g[300]u[n-300] \\ &= \sum_{i=1}^{300} g[i]u[n-i]. \end{aligned} \tag{6.27}$$

As we mentioned before, since this study is focused on the onset, we only took the measurements from $t = 420$ (starting walking at 3 km/h) to $t = 1120$ (finishing running at 8 km/h), which is 700 measurements in total. As the order of the FIR is 300, while the walking period only has 240 measurements (4 $mins$ walking), we cloned 200 measurements of walking and inserted it into the selected 700 measurements. Therefore, the data records were extended from 700 to 900. Hence, the input $u[i]$ is defined as follows, $u[i] = 0,\ i = 1, 2, \cdots, 420$; $u[i] = 1,\ i = 421, 422, \cdots, 900$. With these 900 measurements, firstly, we removed the offset which is the average value of the initial 420 outputs. Then, the proposed nonparametric kernel based estimation was applied to estimate the IR model by using stable spline kernel ($c = 1$, $\lambda = 0.978$). During the estimation, the coefficients γ and α for the $\mathcal{L}_1$ and $\mathcal{L}_2$ norm were set to 4 and 10 respectively. As a comparison to classic method, we also used system identification toolbox from Maltab to estimate the model. We used ARX model with AIC for model

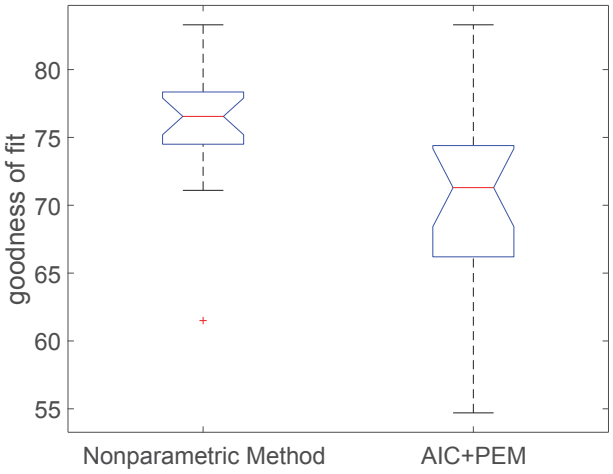

Fig. 6.11 Results comparison for proposed method and classic method

selection [106]. Then the system was estimated by PEM based on the model that selected by AIC. The fit ratios (NRMSE) were calculated and recorded in Table 6.4. For a fair comparison, only the $\hat{y}$ from samples 301 to 900 of the selected $900s$ samples was compared for both method as the initial value of $\hat{y}$ of nonparametric method started from $301s$.

The results are reported in Table 6.4 and the box plot is given in Fig. 6.11. From Table 6.4, it can be seen that the proposed method can significantly outperform the classic method in most of the cases. It also has higher goodness-of-fit and less standard deviation. Actually, the results in Table 6.4 show that the proposed method is very effective when the system has level of noise.

Table 6.4 Goodness-of-fit

Subject	Nonparametric	AIC + PEM	AIC
Participant 1	83.3%	83.3%	11
Participant 2	77.0%	67.4%	7
Participant 3	61.5%	54.7%	12
Participant 4	75.3%	65.4%	7
Participant 5	74.7%	61.0%	4
Participant 6	81.1%	73.7%	8
Participant 7	81.7%	80.1%	13
Participant 8	82.2%	80.6%	11
Participant 9	78.3%	74.5%	12
Participant 10	72.6%	63.6%	10
Participant 11	74.3%	65.1%	9
Participant 12	72.9%	71.0%	13
Participant 13	71.1%	67.0%	17
Participant 14	77.8%	74.3%	15
Participant 15	76.6%	74.1%	17
Participant 16	76.5%	71.6%	11
Participant 17	78.0%	76.0%	11
Participant 18	78.4%	72.1%	11
Participant 19	76.3%	69.4%	10
Participant 20	76.4%	70.8%	13
average	76.0%	71.4%	-
standard deviation	5.72%	7.24%	-

Particularly, Fig. 6.12-(a) shows the estimations based on PEM and the proposed method for one participant. The figure clearly shows that the model response of the proposed method fits better to the original measurements, especially for the transient stage.

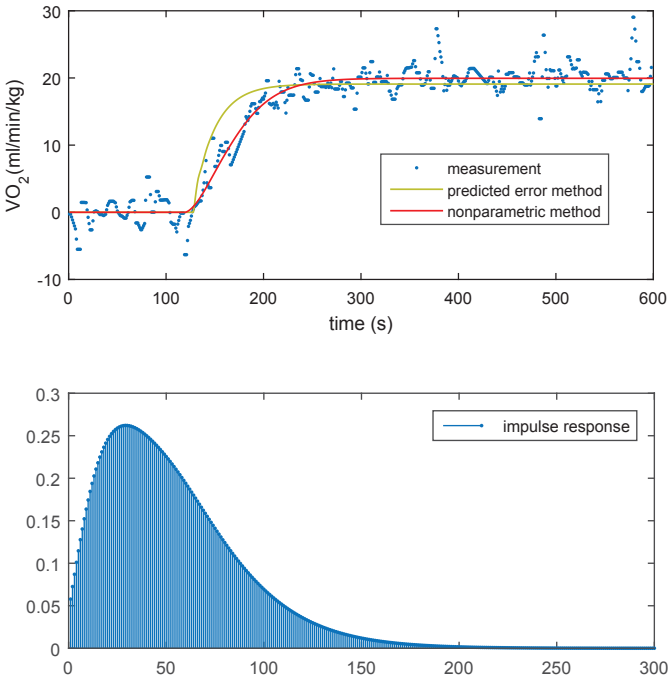

Fig. 6.12 (a) Estimated response for one participant with PEM and nonparametric and (b) the estimated impulse for the participant

Fig. 6.13 shows the estimated impulse responses for all twenty participants. Although the values of the impulse responses are slightly different, the patterns of the responses among participant are similar. This figure also shows that dynamic VO_2 response to exercise of these twenty participants should be described by a higher order model instead of a simple first order transfer function as the starting point of the identified impulse response is non-zero. Furthermore, from these results, it shows that the impact of time delay in Eq.(6.1) is negligible, which is similar as reported in [107]. The average impulse response is also shown in Fig. 6.13. Based on the estimated average impulse response model, we calculated the predicted average VO_2 output, and then compared it with the experimental data, which is shown in Fig. 6.14. It can be observed that the estimation fits *properly* with the experimental data without over-fitting.

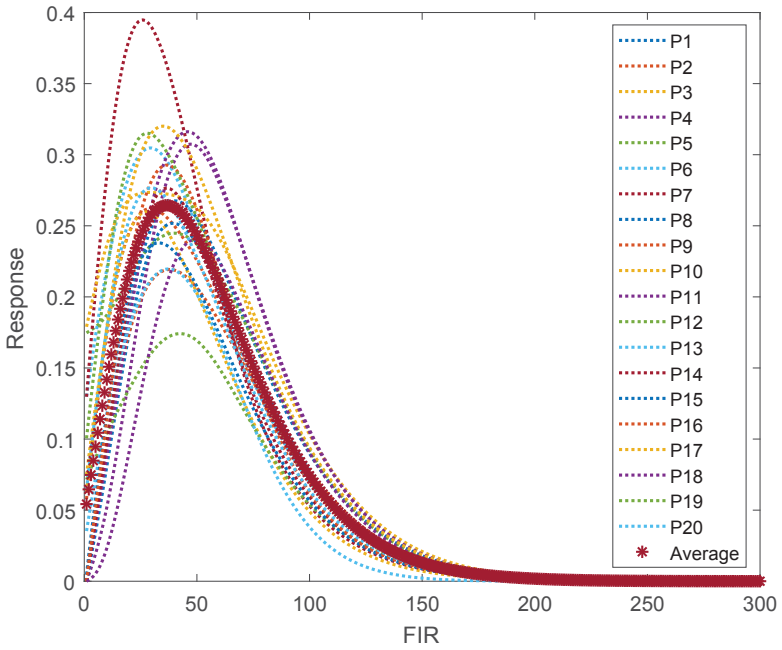

Fig. 6.13 Average IR and individual IR from twenty participants.

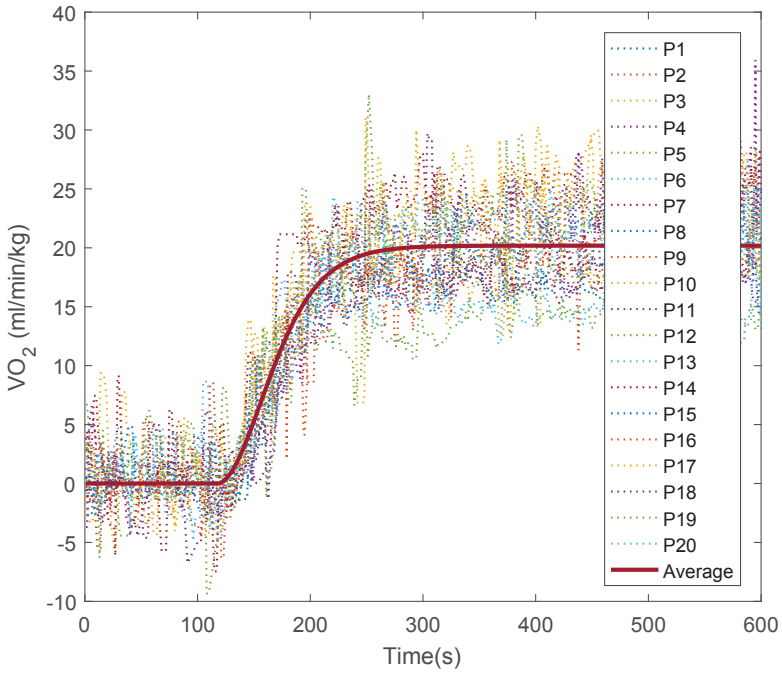

Fig. 6.14 Comparison between estimated VO_2 and measurements from twenty participants.

6.5 Summary

This chapter aims to establish a dynamic model of VO_2 response to jogging exercise. Similar to most human physiological system modelling, the major difficulty for the modelling of dynamic cardiorespiratory response is due to the fact that the experimental data is often short and with low-SNR (signal to noise ratio). Under this limitation, by now, the models of VO_2 response are often simplified as a simple parametric model, e.g., the first order linear time invariant model. Only recently, the kernel based nonparametric modelling approaches [41, 78, 80, 103] have been developed for the modelling of system with short-recorded and low-SNR data. Intrigued by this revolutionary technique, this study developed a kernel based modelling method in order to reliably estimate the impulse response model of oxygen uptake. To well utilise the prior knowledge for the model identification, several kernel functions have been exploited and tested using different numerical simulations and experiments, and the stable spline kernel was chosen as it can achieve expected results. With stable spline kernel, the proposed estimation method was tested experimentally with 20 participants. The obtained results showed that the goodness-of-fit of the proposed method can significantly exceed the classical modelling approaches, e.g., predicted error method. We conclude that the kernel based nonparametric modelling method is an effective method for the estimation of the impulse response of VO_2. We believe the proposed kernel based modelling approaches together with the identified FIR model will be valuable tools for the dynamic estimation and regulation of cardiorespiratory response during exercises.

Chapter 7

Conclusions and Future Work

7.1 Conclusions

In this section, we summarise the contributions of the dissertation first. Based on that, we conclude the thesis. The research in this dissertation address several challenging parameter estimation problems with the respect to calibration of the MEMS type tri-axial accelerometer and dynamic modelling of oxygen uptake response to exercise. The main contributions of this thesis are four-fold:

- We have proposed a G-optimal experimental design for a special second-order model with spherical constraint. Then, the model of the tri-axial accelerometer is linearised to implement the proposed experimental design. Based on the linearised model, an iterative and recursive estimation method is proposed to estimate the unknown parameter and remove the bias caused by linearisation.
- We have proposed an online iterative and recursive parameter estimation method for the online calibration of the tri-axial accelerometer. A damping term is included to further reduce the parameter variation caused by noise.
- For the automatic model selection during online estimation, we have explored and modified a penalised expectation maximum algorithm based on recursive least square estimation. A $\mathcal{L}_1$ norm is included as penalty to remove the un-

wanted parameters. The proposed algorithm is well performed with affordable computational complexity.

- For the oxygen uptake response to exercise, a nonparametric modelling technique has been proposed. With the kernel-based estimation method, an additional $\mathcal{L}_1$ norm is added to form a special elastic net which can shrink the number of unknown parameters. The selection and tuning of the kernel can reflect the prior information and reduce the demand of comprehensive input signal.

In Chapter 1, a brief introduction to the related works and a brief overview of interesting problems in the related topics have been provided.

In Chapter 2, some basic knowledge in parameter estimation and related topics are reviewed. Particularly, experimental design, expectation maximum algorithm, kernel based estimation method, etc., have been reviewed.

In Chapter 3, a six-orientation G-optimal experimental scheme has been proposed for a specific second-order model with three factors. To apply this experimental scheme for auto-calibration, a linearised model of tri-axial accelerometer and an iterative algorithm have been proposed to solve the unknown parameters. Furthermore, the region of convergence is proven for the proposed iterative algorithm. Then, intensive simulations and experiments were carried out for the performance verification.

Based on the simulation results, it can be concluded that the proposed algorithm can achieve accurate estimation within three iterations for most cases. The mean error and standard deviation of the estimation are small under different initial conditions. Several experiments were performed for the proposed calibration method using analog and digital MEMS accelerometers. After implementing the proposed method, the errors of the estimated responses are calculated and analysed. The results clearly indicate that the vector sum of three axes can be accurately estimated with the proposed calibration algorithm. With the advantage of the G-optimal experimental design, the overall estimated response are also minimised.

In chapter 4, a linearisation method of the 6-parameter tri-axial accelerometer model has been introduced for online auto-calibration. To solve the unknown parameters of the linearised model in real-time, a modified damped recursive least square estimation

method has been proposed. The extra $\mathcal{L}_2$ norm damping penalty term can help to reduce the variation caused by noise, and the proposed iterative estimation can also remove the bias caused by linearisation.

Simulations and experiments have been performed to verify the performance. Based on the simulation results, it can be concluded that the proposed calibration method can achieve the desired accuracy within 150 iterations for most cases. The simulation results have also proved that the estimated response is unbiased with small standard deviation related to noise level. Last but not least, the simulation results have indicated that the proposed method could track the varying parameters rapidly, generally within 50 measurements. A self-designed health monitoring device with an IMU module embedded is used to implement the experiment of proposed online calibration method. The errors between the estimated orientations and the reference orientations are calculated and analysed. The experimental results have also indicated that the proposed online calibration approach could accurately estimate the response after calibration.

In chapter 5, to simplify the online estimation with automatic model selection process, a linearisation method for 9-parameter tri-axial model has been investigated and presented for auto-calibration. A modified sparse least square estimation method is explored to solve the unknown parameters while insignificant parameters are automatically removed during online calibration. Furthermore, the proposed calibration method can also track the variation of parameters caused by daily drift and temperature variation.

Simulations and experiments have been carried out to verify the performance of the proposed method. Based on the simulation results, it has been proved that the proposed calibration method can achieve accurate estimation within 50 iterations for most cases with a small mean error and standard deviation of the estimated response. More importantly, the results from simulation also indicate that the proposed method can correctly identify the parameters which are set to zero at the beginning. Experiments has been performed for the proposed calibration method with a self-designed health monitoring device with an IMU embedded. The error between estimated response and reference response have been calculated and analysed. The results show that the proposed algorithm can automatically select models. Besides, the proposed calibration

approach can accurately estimate the vector sum of the three axes in the whole measurement region.

In chapter 6, a dynamic model of VO_2 response to treadmill exercise based on non-parametric modelling method has been established. Similar to most human physiological system modelling, the major difficulties of modelling the dynamic cardiorespiratory response are the noise of experimental data and relatively short input without enough stimulations. Due to this limitation, the models of VO_2 response are often simplified as a simple parametric model, such as the first-order linear time invariant model.

Inspired by the novel kernel based estimation method [41, 78, 80] for impulse response with short-recorded data and limited input signal variation, this study has developed a kernel based modelling method to estimate the impulse response model of oxygen uptake by including an extra penalty to form the special elastic net. This can reduce the number of unknown parameter, and remove those parameters caused by noise. Furthermore, to utilised the prior knowledge of the cardiorespiratory response model, several kernel functions have been exploited and tested on a vast number of simulations and experiments. It can be observed that, a well tuned stable spline kernel is able to obtain the best results. The proposed estimation method are also tested experimentally with a total of 20 healthy participants. The results from the participants have showed that the goodness-of-fit of the proposed method can significantly exceed the benchmark modelling approaches (prediction error method). Therefore, the kernel based nonparametric modelling method is a novel and efficient approach for estimation of the impulse response of VO_2 and it will be a valuable tool for the dynamic system estimation and regulation of cardiorespiratory response during exercises.

7.2 Future Work

Interesting directions for future work are presented in the following.

- In Chapter 3, for offline parameter estimation, we considered G-optimal experimental design for the linearised model. In the future, depending on various applications, D-optimal experimental design and V-optimal experimental design

can also be good ideas to investigate. A more challenging topic is to develop a G-optimal experimental design for nonlinear model directly.

- In Chapter 4 and 5, for online parameter estimation of accelerometer calibration, an expectation maximum algorithm based recursive least square estimation method was proposed to achieve online estimation with automatic model selection. However, this model selection is based on the $\mathcal{L}_1$ norm which can cause slight bias of the estimated parameters. In the future, the modification method with sparsity that do not base on the $\mathcal{L}_1$ norm may further improve the accuracy of estimated response.

- In Chapter 6, we utilised the prior information based on tuning kernels. In the future, the optimum kernel can be solved directly based on previous experiments. It may further improve the goodness-of-fit of the estimated response. Furthermore, it is also possible to extend the online kernel based estimation method to this cardiorespiratory response. We believe that if the optimum kernel is combined with the online kernel based estimation method, the accuracy of the estimated response can be further improved.

Appendix A

Proof of Theorem 3.1

Proof For a special second-order model which is shown in Eq.(3.2):

$$y = \sum_{i=1}^{3} \beta_i x_i + \sum_{i=1}^{3} \beta_{ii} x_i^2 + \epsilon. \tag{A.1}$$

Let us recall the model matrix $\boldsymbol{X}$ (3.7) of experimental scheme (3.6) for the model (A.1). Then, according to [17], to prove the G-optimality, we need to know that the maximum SPV of (3.5) is equal to the number of unknown parameters. For experimental scheme (3.6), the SPV of (A.1) can be expressed as:

$$\begin{aligned} d(\boldsymbol{x}, \boldsymbol{\xi}_n) &= \tfrac{n \cdot var(\hat{y}(\boldsymbol{x}))}{\sigma^2} = n \cdot \boldsymbol{f}^T(\boldsymbol{x})(\boldsymbol{X}^T\boldsymbol{X})^{-1}\boldsymbol{f}(\boldsymbol{x}) \\ &= 3x_1^2 + 3x_2^2 + 3x_3^2 + 3x_1^4 + 3x_2^4 + 3x_3^4 \\ &= 3(x_1^2 + x_2^2 + x_3^2) + 3(x_1^2 + x_2^2 + x_3^2)^2 \\ &\quad -6(x_1^2x_2^2 + x_1^2x_3^2 + x_2^2x_3^2). \end{aligned} \tag{A.2}$$

For (A.2), in the design region $(x_1^2 + x_2^2 + x_3^2) = 1$, the sum of the first two terms is 6 and it is constant. Furthermore, the last term $-6(x_1^2x_2^2 + x_1^2x_3^2 + x_2^2x_3^2)$ is non-positive and it has minimum value 0 when x_1, x_2 or x_3 is equal to 1. Thus, the maximum value of $d(\boldsymbol{x}, \boldsymbol{\xi}_n)$ is 6 which is equal to the number of unknown parameters. It proves that the experimental scheme (3.6) is G-optimal. ∎

Appendix B

Proof of Theorem 3.2

Proof To prove $\hat{\boldsymbol{\beta}}$ is convergent, let us recall (3.1). The model of the 6-parameter accelerometer can be rewritten as:

$$\begin{aligned} \boldsymbol{A} &= \boldsymbol{S}(\boldsymbol{V}+\boldsymbol{O}) \\ &= \boldsymbol{S}\boldsymbol{V}+\boldsymbol{B}, \end{aligned} \tag{B.1}$$

where $\boldsymbol{B} = [b_x, b_y, b_z]^T$ is the product of $\boldsymbol{S}$ and $\boldsymbol{O}$.

For the ith measurement, the auto-calibration model for (B.1) can be expressed as:

$$g^2 = \sum_{j=x,y,z} S_j^2 v_{j,i}^2 + \sum_{j=x,y,z} 2S_j b_j v_{j,i} + \sum_{j=x,y,z} b_j^2 + \varepsilon_i, \tag{B.2}$$

where $\sum\limits_{j=x,y,z} b_j^2$ is the neglected term $\boldsymbol{\gamma}$ from (3.18).

If we suppose that the value of local gravity is 1g, for the kth iteration, we have:

$$\sum_{j=x,y,z} \hat{S}_j^{2(k)} v_{j,i}^2 + \sum_{j=x,y,z} 2\hat{S}_j^{(k)} \hat{b}_j^{(k)} v_{j,i} = 1 - \sum_{j=x,y,z} \hat{b}_j^{2(k)}. \tag{B.3}$$

Then, assuming that we have an experiment with n observations, we have (B.4) and (B.5), in which the symbol "†" stands for pseudo inverse, i.e., $A^\dagger = (A^T A)^{-1} A^T$. As $\boldsymbol{\beta}$ is identifiable, the pseudo inverse in (B.4) and (B.5) is unique.

$$\begin{bmatrix} \hat{S}_x^{2(k)} \\ \hat{S}_y^{2(k)} \\ \hat{S}_z^{2(k)} \\ 2\hat{S}_x^{(k)}\hat{b}_x^{(k)} \\ 2\hat{S}_y^{(k)}\hat{b}_y^{(k)} \\ 2\hat{S}_z^{(k)}\hat{b}_z^{(k)} \end{bmatrix} = \begin{bmatrix} V_{x,1}^2 & V_{y,1}^2 & V_{z,1}^2 & V_{x,1} & V_{y,1} & V_{z,1} \\ \vdots & \vdots & \vdots & \vdots & \vdots & \vdots \\ \vdots & \vdots & \vdots & \vdots & \vdots & \vdots \\ \vdots & \vdots & \vdots & \vdots & \vdots & \vdots \\ \vdots & \vdots & \vdots & \vdots & \vdots & \vdots \\ V_{x,n}^2 & V_{y,n}^2 & V_{z,n}^2 & V_{x,n} & V_{y,n} & V_{z,n} \end{bmatrix}^{\dagger} \begin{bmatrix} 1 - \sum_{j=x,y,z} \hat{b}_j^{2(k-1)} \\ \vdots \\ \vdots \\ \vdots \\ \vdots \\ 1 - \sum_{j=x,y,z} \hat{b}_j^{2(k-1)} \end{bmatrix} \tag{B.4}$$

$$\begin{bmatrix} S_x^2 \\ S_y^2 \\ S_z^2 \\ 2S_x b_x \\ 2S_y b_y \\ 2S_z b_z \end{bmatrix} = \begin{bmatrix} V_{x,1}^2 & V_{y,1}^2 & V_{z,1}^2 & V_{x,1} & V_{y,1} & V_{z,1} \\ \vdots & \vdots & \vdots & \vdots & \vdots & \vdots \\ \vdots & \vdots & \vdots & \vdots & \vdots & \vdots \\ \vdots & \vdots & \vdots & \vdots & \vdots & \vdots \\ \vdots & \vdots & \vdots & \vdots & \vdots & \vdots \\ V_{x,n}^2 & V_{y,n}^2 & V_{z,n}^2 & V_{x,n} & V_{y,n} & V_{z,n} \end{bmatrix}^{\dagger} \begin{bmatrix} 1 - \sum_{j=x,y,z} b_j^2 \\ \vdots \\ \vdots \\ \vdots \\ \vdots \\ 1 - \sum_{j=x,y,z} b_j^2 \end{bmatrix} \tag{B.5}$$

Let us consider the x-axis first; the other two axes are similar. For $\hat{S}_x, \hat{b}_x$ (S_x, b_x), we have the following relationship for the kth iteration if we divide (B.5) by (B.4):

$$\begin{bmatrix} \hat{S}_x^{2(k)} \\ \hat{S}_x^{(k)}\hat{b}_x^{(k)} \end{bmatrix} = \frac{1 - \sum_{j=x,y,z} \hat{b}_j^{2(k-1)}}{1 - \sum_{j=x,y,z} b_j^2} \begin{bmatrix} S_x^2 \\ S_x b_x \end{bmatrix}. \tag{B.6}$$

From (B.6), we have:

$$\begin{aligned} \hat{b}_x^{2(k)} &= \left(\frac{1 - \sum_{j=x,y,z} \hat{b}_j^{2(k-1)}}{1 - \sum_{j=x,y,z} b_j^2} \right)^2 \frac{S_x^2 b_x^2}{\hat{S}_x^{2(k)}} \\ &= \left(\frac{1 - \sum_{j=x,y,z} \hat{b}_j^{2(k-1)}}{1 - \sum_{j=x,y,z} b_j^2} \right)^2 \frac{1 - \sum_{j=x,y,z} b_j^2}{1 - \sum_{j=x,y,z} \hat{b}_j^{2(k-1)}} b_x^2 \\ &= \frac{1 - \sum_{j=x,y,z} \hat{b}_j^{2(k-1)}}{1 - \sum_{j=x,y,z} b_j^2} b_x^2. \end{aligned} \tag{B.7}$$

If the values of b_x, b_y, b_z are correctly estimated, then the parameters can be solved by (3.17). Let us consider the overall value b_x, b_y and b_z as a block and replace $\sum b_j^2$ by γ. Based on (B.7), we can easily obtain the following relationship:

$$\hat{\gamma}^{(k)} = \frac{1-\hat{\gamma}^{(k-1)}}{1-\gamma}\gamma, \tag{B.8}$$

$$\hat{\gamma}^{(k)}(1-\gamma) = (1-\hat{\gamma}^{(k-1)})\gamma, \tag{B.9}$$

$$\hat{\gamma}^{(k)} - \hat{\gamma}^{(k)}\gamma = \gamma - \hat{\gamma}^{(k-1)}\gamma, \tag{B.10}$$

$$\hat{\gamma}^{(k)} = \gamma + \hat{\gamma}^{(k)}\gamma - \hat{\gamma}^{(k-1)}\gamma. \tag{B.11}$$

For $\hat{\gamma}^{(k-1)}$, we also have:

$$\hat{\gamma}^{(k-1)} = \gamma + \hat{\gamma}^{(k-1)}\gamma - \hat{\gamma}^{(k-2)}\gamma. \tag{B.12}$$

Substracting (B.11) by (B.12), we have:

$$\hat{\gamma}^{(k)} - \hat{\gamma}^{(k-1)} = (\hat{\gamma}^{(k)}\gamma - \hat{\gamma}^{(k-1)}\gamma) - (\hat{\gamma}^{(k-1)}\gamma - \hat{\gamma}^{(k-2)}\gamma), \tag{B.13}$$

$$(\hat{\gamma}^{(k)} - \hat{\gamma}^{(k-1)}) - \gamma(\hat{\gamma}^{(k)} - \hat{\gamma}^{(k-1)}) = -\gamma(\hat{\gamma}^{(k-1)} - \hat{\gamma}^{(k-2)}), \tag{B.14}$$

$$(\hat{\gamma}^{(k)} - \hat{\gamma}^{(k-1)})(1-\gamma) = -\gamma(\hat{\gamma}^{(k-1)} - \hat{\gamma}^{(k-2)}), \tag{B.15}$$

$$(\hat{\gamma}^{(k)} - \hat{\gamma}^{(k-1)}) = \frac{-\gamma}{1-\gamma}(\hat{\gamma}^{(k-1)} - \hat{\gamma}^{(k-2)}). \tag{B.16}$$

From (B.16), we can have the relationship between $(\hat{\gamma}^{(k)} - \hat{\gamma}^{(k-1)})$ and $(\hat{\gamma}^{(2)} - \hat{\gamma}^{(1)})$

$$(\hat{\gamma}^{(k)} - \hat{\gamma}^{(k-1)}) = (\frac{-\gamma}{1-\gamma})^{k-1}(\hat{\gamma}^{(1)}\gamma - \hat{\gamma}^{(0)}). \tag{B.17}$$

From (B.17), we can see the iterative calibration method proposed above is convergent if $0 \leqslant \gamma < 0.5$.

For any γ within the region of convergence, from (B.8), it is also implicitly shown that the estimated $\hat{\gamma}$ is damping around the true value of γ. For example, if $\hat{\gamma}^{(k-1)}$ is

less than γ, $\frac{1-\hat{\gamma}^{(k-1)}}{1-\gamma}$ is greater than 1. Then, based on (B.8), we have $\hat{\gamma}^{(k)}$ greater than γ, and vice versa. That is, we have either $\hat{\gamma}^{(k-1)} \leq \gamma \leq \hat{\gamma}^{(k)}$ or $\hat{\gamma}^{(k-1)} \geq \gamma \geq \hat{\gamma}^{(k)}$.

Therefore, we can draw the conclusion that $\hat{\gamma}^{(k)}$ is convergent to the true value of γ if $0 \leqslant \gamma < 0.5$. ∎

References

[1] M. Yuwono, B. D. Moulton, S. W. Su, B. G. Celler, H. T. Nguyen, *et al.*, "Unsupervised machine-learning method for improving the performance of ambulatory fall-detection systems," *Biomedical Engineering OnLine*, vol. 11, no. 9, 2012.

[2] S. W. Su, L. Wang, B. G. Celler, A. V. Savkin, and Y. Guo, "Modelling and control for heart rate regulation during treadmill exercise," in *Proc. 2006 28th Annual International Conference of the IEEE Engineering in Medicine and Biology Society*, pp. 4299–4302, IEEE, 2006.

[3] S. W. Su, B. G. Celler, A. V. Savkin, H. T. Nguyen, T. M. Cheng, Y. Guo, and L. Wang, "Transient and steady state estimation of human oxygen uptake based on noninvasive portable sensor measurements," *Medical & biological engineering & computing*, vol. 47, no. 10, pp. 1111–1117, 2009.

[4] O. Postolache, J. M. D. Pereira, V. Viegas, L. Pedro, P. S. Girão, R. Oliveira, and G. Postolache, "Smart walker solutions for physical rehabilitation," *IEEE Instrumentation and Measurement Magazine*, vol. 18, no. 5, pp. 21–30, 2015.

[5] S. Zihajehzadeh, T. J. Lee, J. K. Lee, R. Hoskinson, and E. J. Park, "Integration of mems inertial and pressure sensors for vertical trajectory determination," *IEEE Transactions on Instrumentation and Measurement*, vol. 64, no. 3, pp. 804–814, 2015.

[6] D. A. Grejner-Brzezinska, C. K. Toth, H. Sun, X. Wang, and C. Rizos, "A robust solution to high-accuracy geolocation: Quadruple integration of gps, imu, pseudolite, and terrestrial laser scanning," *IEEE Transactions on instrumentation and measurement*, vol. 60, no. 11, pp. 3694–3708, 2011.

[7] R. Zhao, D. Wang, R. Yan, K. Mao, F. Shen, and J. Wang, "Machine health monitoring using local feature-based gated recurrent unit networks," *IEEE Transactions on Industrial Electronics*, 2017.

[8] M. Carminati, G. Ferrari, R. Grassetti, and M. Sampietro, "Real-time data fusion and mems sensors fault detection in an aircraft emergency attitude unit based on kalman filtering," *IEEE sensors journal*, vol. 12, no. 10, pp. 2984–2992, 2012.

[9] H. B. Rossiter, "Exercise: kinetic considerations for gas exchange," *Comprehensive Physiology*, 2011.

[10] A. V. Hill, C. Long, and H. Lupton, "Muscular exercise, lactic acid, and the supply and utilisation of oxygen," *Proceedings of the Royal Society of London. Series B, Containing Papers of a Biological Character*, vol. 97, no. 681, pp. 84–138, 1924.

[11] I. Frosio, F. Pedersini, and N. A. Borghese, "Autocalibration of mems accelerometers," *IEEE Transactions on Instrumentation and Measurement*, vol. 58, no. 6, pp. 2034–2041, 2009.

[12] M. Glueck, D. Oshinubi, P. Schopp, and Y. Manoli, "Real-time autocalibration of mems accelerometers," *IEEE Transactions On Instrumentation and Measurement*, vol. 63, no. 1, pp. 96–105, 2014.

[13] S.-h. P. Won and F. Golnaraghi, "A triaxial accelerometer calibration method using a mathematical model," *IEEE Transactions on Instrumentation and Measurement*, vol. 59, no. 8, pp. 2144–2153, 2010.

[14] Z. Syed, P. Aggarwal, C. Goodall, X. Niu, and N. El-Sheimy, "A new multi-position calibration method for mems inertial navigation systems," *Measurement Science and Technology*, vol. 18, no. 7, p. 1897, 2007.

[15] A. I. Khuri and S. Mukhopadhyay, "Response surface methodology," *Wiley Interdisciplinary Reviews: Computational Statistics*, vol. 2, no. 2, pp. 128–149, 2010.

[16] D. C. Montgomery, *Design and analysis of experiments*. John Wiley & Sons, 2005.

[17] R. H. Myers, D. C. Montgomery, and C. M. Anderson-Cook, *Response surface methodology: process and product optimization using designed experiments*. John Wiley & Sons, 2003.

[18] C. R. Rojas, J. S. Welsh, G. C. Goodwin, and A. Feuer, "Robust optimal experiment design for system identification," *Automatica*, vol. 43, no. 6, pp. 993–1008, 2007.

[19] D. Jurman, M. Jankovec, R. Kamnik, and M. Topič, "Calibration and data fusion solution for the miniature attitude and heading reference system," *Sensors and Actuators A: Physical*, vol. 138, no. 2, pp. 411–420, 2007.

[20] L. Ye and S. W. Su, "Experimental design and its posterior efficiency for the calibration of wearable sensors," *Journal of Intelligent Learning Systems and Applications*, vol. 7, no. 01, p. 11, 2015.

[21] L. Ye and S. W. Su, "Optimum experimental design applied to mems accelerometer calibration for 9-parameter auto-calibration model," in *Proc. 2015 37th Annual International Conference of the IEEE Engineering in Medicine and Biology Society (EMBC)*, pp. 3145–3148, IEEE, 2015.

[22] L. Ye, Y. Guo, and S. Su, "An efficient auto-calibration method for triaxial accelerometer," *IEEE Transactions on Instrumentation and Measurement*, vol. 66, no. 9.

[23] Z. Wu, Z. Wang, and Y. Ge, "Gravity based online calibration for monolithic triaxial accelerometers' gain and offset drift," in *Proceedings of 2012 the 4th World Congress on Intelligent Control and Automation*, vol. 3, pp. 2171–2175, IEEE, 2002.

[24] InvenSense, "Mpu 9150 datasheet," 2013.

[25] P. Batista, C. Silvestre, P. Oliveira, and B. Cardeira, "Accelerometer calibration and dynamic bias and gravity estimation: Analysis, design, and experimental evaluation," *IEEE Transactions on Control Systems Technology*, vol. 19, no. 5, pp. 1128–1137, 2011.

[26] T. Beravs, J. Podobnik, and M. Munih, "Three-axial accelerometer calibration using kalman filter covariance matrix for online estimation of optimal sensor orientation," *IEEE Transactions on Instrumentation and Measurement*, vol. 61, no. 9, pp. 2501–2511, 2012.

[27] S. Bonnet, C. Bassompierre, C. Godin, S. Lesecq, and A. Barraud, "Calibration methods for inertial and magnetic sensors," *Sensors and Actuators A: Physical*, vol. 156, no. 2, pp. 302–311, 2009.

[28] I. Frosio, F. Pedersini, and N. A. Borghese, "Autocalibration of triaxial mems accelerometers with automatic sensor model selection," *IEEE Sensors Journal*, vol. 12, no. 6, pp. 2100–2108, 2012.

[29] K. P. Burnham and D. R. Anderson, *Model selection and multimodel inference: a practical information-theoretic approach*. Springer Science & Business Media, 2003.

[30] K. P. Burnham and D. R. Anderson, "Multimodel inference: understanding aic and bic in model selection," *Sociological methods & research*, vol. 33, no. 2, pp. 261–304, 2004.

[31] S. Mukhopadhyay and P. Sircar, "Parametric modelling of ecg signal," *Medical and Biological Engineering and computing*, vol. 34, no. 2, pp. 171–174, 1996.

[32] L. Lu, L. Hamzaoui, B. Brown, B. Rigaud, R. Smallwood, D. Barber, and J. Morucci, "Parametric modelling for electrical impedance spectroscopy system," *Medical and Biological Engineering and Computing*, vol. 34, no. 2, pp. 122–126, 1996.

[33] C.-C. Lin, C.-M. Chen, I.-F. Yang, and T.-F. Yang, "Automatic optimum order selection of parametric modelling for the evaluation of abnormal intra-qrs signals in signal-averaged electrocardiograms," *Medical and Biological Engineering and Computing*, vol. 43, no. 2, pp. 218–224, 2005.

[34] S. W. Su, L. Wang, B. G. Celler, and A. V. Savkin, "Oxygen uptake estimation in humans during exercise using a hammerstein model," *Annals of biomedical engineering*, vol. 35, no. 11, pp. 1898–1906, 2007.

[35] S. W. Su, L. Wang, B. G. Celler, A. V. Savkin, and Y. Guo, "Identification and control for heart rate regulation during treadmill exercise," *IEEE Transactions on Biomedical Engineering*, vol. 54, no. 7, pp. 1238–1246, 2007.

[36] D. Pearce and H. Milhorn Jr, "Dynamic and steady-state respiratory responses to bicycle exercise," *Journal of Applied Physiology*, vol. 42, no. 6, pp. 959–967, 1977.

[37] B. J. Whipp, S. A. Ward, N. Lamarra, J. A. Davis, and K. Wasserman, "Parameters of ventilatory and gas exchange dynamics during exercise," *Journal of Applied Physiology*, vol. 52, no. 6, pp. 1506–1513, 1982.

[38] D. Essfeld, U. Hoffmann, and J. Stegemann, "Vo2 kinetics in subjects differing in aerobic capacity: investigation by spectral analysis," *European journal of applied physiology and occupational physiology*, vol. 56, no. 5, pp. 508–515, 1987.

[39] U. Hoffmann, D. Eßfeld, H.-G. Wunderlich, and J. Stegemann, "Dynamic linearity of vo2 responses during aerobic exercise," *European journal of applied physiology and occupational physiology*, vol. 64, no. 2, pp. 139–144, 1992.

[40] B. Babadi, N. Kalouptsidis, and V. Tarokh, "SPARLS: The sparse RLS algorithm," *IEEE Transactions on Signal Processing*, vol. 58, no. 8, pp. 4013–4025, 2010.

[41] G. Pillonetto and G. De Nicolao, "A new kernel-based approach for linear system identification," *Automatica*, vol. 46, no. 1, pp. 81–93, 2010.

[42] G. Pillonetto, A. Chiuso, and G. De Nicolao, "Prediction error identification of linear systems: a nonparametric gaussian regression approach," *Automatica*, vol. 47, no. 2, pp. 291–305, 2011.

[43] L. M. Roylance and J. B. Angell, "A batch-fabricated silicon accelerometer," *IEEE Transactions on Electron Devices*, vol. 26, no. 12, pp. 1911–1917, 1979.

[44] S. Kal, S. Das, D. Maurya, K. Biswas, A. R. Sankar, and S. Lahiri, "Cmos compatible bulk micromachined silicon piezoresistive accelerometer with low off-axis sensitivity," *Microelectronics Journal*, vol. 37, no. 1, pp. 22–30, 2006.

[45] J.-C. Yu, C. Lee, W. Kuo, and C. Chang, "Modeling analysis of a triaxial microaccelerometer with piezoelectric thin-film sensing using energy method," *Microsystem technologies*, vol. 17, no. 4, pp. 483–493, 2011.

[46] M. Mehran and S. Mohajerzadeh, "High sensitivity nanostructure incorporated interdigital silicon based capacitive accelerometer," *Microelectronics Journal*, vol. 46, no. 2, pp. 166–173, 2015.

[47] C.-H. Liu and T. W. Kenny, "A high-precision, wide-bandwidth micromachined tunneling accelerometer," *Journal of microelectromechanical systems*, vol. 10, no. 3, pp. 425–433, 2001.

[48] B. Mezghani, F. Tounsi, A. A. Rekik, F. Mailly, M. Masmoudi, and P. Nouet, "Sensitivity and power modeling of cmos mems single axis convective accelerometers," *Microelectronics Journal*, vol. 44, no. 12, pp. 1092–1098, 2013.

[49] X. Yun and E. R. Bachmann, "Design, implementation, and experimental results of a quaternion-based kalman filter for human body motion tracking," *IEEE Transactions on Robotics*, vol. 22, no. 6, pp. 1216–1227, 2006.

[50] L. Chang, F. Zha, and F. Qin, "Indirect kalman filtering based attitude estimation for low-cost attitude and heading reference systems," *IEEE/ASME Transactions on Mechatronics*, vol. 22, no. 4, pp. 1850–1858, 2017.

[51] Q. Cai, N. Song, G. Yang, and Y. Liu, "Accelerometer calibration with nonlinear scale factor based on multi-position observation," *Measurement Science and Technology*, vol. 24, no. 10, p. 105002, 2013.

[52] E.-H. Shin and N. El-Sheimy, "A new calibration method for strapdown inertial navigation systems," *Zeitschrift für Vermessungswesen.–2002.–Zfv*, vol. 127, no. 1, pp. 41–50, 2002.

[53] I. Skog and P. Händel, "Calibration of a mems inertial measurement unit," in *XVII IMEKO World Congress*, pp. 1–6, 2006.

[54] H. Zhang, Y. Wu, W. Wu, M. Wu, and X. Hu, "Improved multi-position calibration for inertial measurement units," *Measurement Science and Technology*, vol. 21, no. 1, p. 015107, 2010.

[55] W. Fong, S. Ong, and A. Nee, "Methods for in-field user calibration of an inertial measurement unit without external equipment," *Measurement Science and Technology*, vol. 19, no. 8, p. 085202, 2008.

[56] G. Panahandeh, I. Skog, and M. Jansson, "Calibration of the accelerometer triad of an inertial measurement unit, maximum likelihood estimation and cramer-rao bound," in *Proc. International Conference Indoor Positioning Indoor Navigation*, pp. 1–6, IEEE, 2010.

[57] P. Schopp, H. Graf, W. Burgard, and Y. Manoli, "Self-calibration of accelerometer arrays," *IEEE Transactions on Instrumentation and Measurement*, vol. 65, no. 8, pp. 1913–1925, 2016.

[58] F. Camps, S. Harasse, and A. Monin, "Numerical calibration for 3-axis accelerometers and magnetometers," in *Proc IEEE International Conference on Electro/Information Technology*, pp. 217–221, IEEE, 2009.

[59] D. Tedaldi, A. Pretto, and E. Menegatti, "A robust and easy to implement method for imu calibration without external equipments," in *Proc IEEE International Conference on Robotic Automation*, pp. 3042–3049, IEEE, 2014.

[60] M. Glueck, A. Buhmann, and Y. Manoli, "Autocalibration of mems accelerometers," in *Proc. 2012 IEEE International Instrumentation and Measurement Technology Conference (I2MTC)*, pp. 1788–1793, IEEE, 2012.

[61] J. Pan, C. Zhang, and Q. Cai, "An accurate calibration method for accelerometer nonlinear scale factor on a low-cost three-axis turntable," *Measurement Science and Technology*, vol. 25, no. 2, p. 025102, 2014.

[62] A. Atkinson, A. Donev, and R. Tobias, *Optimum experimental designs, with SAS*. Oxford Univ. Press, UK, 2007.

[63] E. A. Wan and R. Van Der Merwe, "The unscented kalman filter for nonlinear estimation," in *Adaptive Systems for Signal Processing, Communications, and Control Symposium 2000. AS-SPCC. The IEEE 2000*, pp. 153–158, Ieee, 2000.

[64] R. Zhang, F. Hoflinger, and L. M. Reind, "Calibration of an imu using 3-d rotation platform," *IEEE sensors Journal*, vol. 14, no. 6, pp. 1778–1787, 2014.

[65] R. Tibshirani, "Regression shrinkage and selection via the lasso," *Journal of the Royal Statistical Society. Series B (Methodological)*, pp. 267–288, 1996.

[66] H. Zou and T. Hastie, "Regularization and variable selection via the elastic net," *Journal of the Royal Statistical Society: Series B (Statistical Methodology)*, vol. 67, no. 2, pp. 301–320, 2005.

[67] T. K. Moon, "The expectation-maximization algorithm," *IEEE Signal processing magazine*, vol. 13, no. 6, pp. 47–60, 1996.

[68] M. A. Figueiredo and R. D. Nowak, "An em algorithm for wavelet-based image restoration," *IEEE Transactions on Image Processing*, vol. 12, no. 8, pp. 906–916, 2003.

[69] S. J. McGregor, M. A. Busa, J. A. Yaggie, and E. M. Bollt, "High resolution mems accelerometers to estimate vo2 and compare running mechanics between highly trained inter-collegiate and untrained runners," *PLoS One*, vol. 4, no. 10, p. e7355, 2009.

[70] D. A. Blythe and F. J. Király, "Prediction and quantification of individual athletic performance of runners," *PloS one*, vol. 11, no. 6, p. e0157257, 2016.

[71] J. G. Pelarigo, L. Machado, R. J. Fernandes, C. C. Greco, and J. P. Vilas-Boas, "Oxygen uptake kinetics and energy system's contribution around maximal lactate steady state swimming intensity," *PloS one*, vol. 12, no. 2, p. e0167263, 2017.

[72] D. R. Bassett Jr and E. T. Howley, "Limiting factors for maximum oxygen uptake and determinants of endurance performance," *Medicine & Science in Sports & Exercise*, vol. 32, no. 1, p. 70, 2000.

[73] D. C. Poole and A. M. Jones, "Oxygen uptake kinetics," *Comprehensive Physiology*, 2012.

[74] J. A. Zoladz, B. Grassi, J. Majerczak, Z. Szkutnik, M. Korostyński, M. Grandys, W. Jarmuszkiewicz, and B. Korzeniewski, "Mechanisms responsible for the acceleration of pulmonary vo2 on-kinetics in humans after prolonged endurance training," *American Journal of Physiology-Regulatory, Integrative and Comparative Physiology*, vol. 307, no. 9, pp. R1101–R1114, 2014.

[75] P. Rich, "The molecular machinery of keilin's respiratory chain," 2003.

[76] J. Sharma, *Exercise physiology: health fitness and performance*. Horizon book, 2015.

[77] L. Ljung, "Prediction error estimation methods," *Circuits, Systems and Signal Processing*, vol. 21, no. 1, pp. 11–21, 2002.

[78] G. Pillonetto, F. Dinuzzo, T. Chen, G. De Nicolao, and L. Ljung, "Kernel methods in system identification, machine learning and function estimation: A survey," *Automatica*, vol. 50, no. 3, pp. 657–682, 2014.

[79] A. J. Smola and B. Schölkopf, "A tutorial on support vector regression," *Statistics and computing*, vol. 14, no. 3, pp. 199–222, 2004.

[80] T. Chen, H. Ohlsson, and L. Ljung, "On the estimation of transfer functions, regularizations and gaussian processes—revisited," *Automatica*, vol. 48, no. 8, pp. 1525–1535, 2012.

[81] T. Chen, M. S. Andersen, L. Ljung, A. Chiuso, and G. Pillonetto, "System identification via sparse multiple kernel-based regularization using sequential convex optimization techniques," *IEEE Transactions on Automatic Control*, vol. 59, no. 11, pp. 2933–2945, 2014.

[82] S. Bonettini, A. Chiuso, and M. Prato, "A scaled gradient projection method for bayesian learning in dynamical systems," *SIAM Journal on Scientific Computing*, vol. 37, no. 3, pp. A1297–A1318, 2015.

[83] P. D. Tao and L. T. H. An, "Convex analysis approach to dc programming: Theory, algorithms and applications," *Acta Mathematica Vietnamica*, vol. 22, no. 1, pp. 289–355, 1997.

[84] A. L. Yuille and A. Rangarajan, "The concave-convex procedure," *Neural computation*, vol. 15, no. 4, pp. 915–936, 2003.

[85] S. Boyd and L. Vandenberghe, *Convex optimization*. Cambridge university press, 2004.

[86] X. Li and Z. Li, "A new calibration method for tri-axial field sensors in strapdown navigation systems," *Measurement Science and Technology*, vol. 23, no. 10, p. 105105, 2012.

[87] F. Höflinger, J. Müller, R. Zhang, L. M. Reindl, and W. Burgard, "A wireless micro inertial measurement unit (imu)," *IEEE Transactions on Instrumentation and Measurement*, vol. 62, no. 9, pp. 2583–2595, 2013.

[88] R. Ghodssi and P. Lin, *MEMS materials and processes handbook*, vol. 1. London: Springer-Verlag, 2011.

[89] M. Sipos, P. Paces, J. Rohac, and P. Novacek, "Analyses of triaxial accelerometer calibration algorithms," *IEEE Sensors Journal*, vol. 12, no. 5, pp. 1157–1165, 2012.

[90] D. Nemec, A. Janota, M. Hruboš, and V. Šimák, "Intelligent real-time mems sensor fusion and calibration," *IEEE Sensors Journal*, vol. 16, no. 19, pp. 7150–7160, 2016.

[91] C. Zengqiang, L. Maoqiong, and Y. Zhuzhi, "Convergence and stability of recursive damped least square algorithm," *Applied mathematics and mechanics*, vol. 21, no. 2, pp. 237–242, 2000.

[92] L. Ye, S. W. Su, D. Lei, and H. T. Nguyen, "An online recursive autocalibration of triaxial accelerometer," in *Engineering in Medicine and Biology Society (EMBC), 2016 IEEE 38th Annual International Conference of the*, pp. 2038–2041, IEEE, 2016.

[93] M. Pedley, "High precision calibration of a three-axis accelerometer," *Freescale Semiconductor Application Note, Document Number: AN4399, Rev*, vol. 1, 2013.

[94] C. Bishop, "Pattern recognition and machine learning (information science and statistics), 1st edn. 2006. corr. 2nd printing edn," *Springer, New York*, 2007.

[95] A. C. of Sports Medicine, *Guidelines for exercise testing and prescription*. Williams & Wilkins, 1991.

[96] W. Van der Walt and C. Wyndham, "An equation for prediction of energy expenditure of walking and running.," *Journal of Applied Physiology*, vol. 34, no. 5, pp. 559–563, 1973.

[97] A. M. Nevill and R. L. Holder, "Modelling maximum oxygen uptake-a case-study in non-linear regression model formulation and comparison," *Applied Statistics*, pp. 653–666, 1994.

[98] D. Abe, K. Yanagawa, and S. Niihata, "Effects of load carriage, load position, and walking speed on energy cost of walking," *Applied ergonomics*, vol. 35, no. 4, pp. 329–335, 2004.

[99] A. N. Tikhonov, V. I. Arsenin, and F. John, *Solutions of ill-posed problems*, vol. 14. Winston Washington, DC, 1977.

[100] J. A. Schrack, E. M. Simonsick, and L. Ferrucci, "Comparison of the cosmed k4b2 portable metabolic system in measuring steady-state walking energy expenditure," *PloS one*, vol. 5, no. 2, p. e9292, 2010.

[101] A. E. Hoerl and R. W. Kennard, "Ridge regression: Biased estimation for nonorthogonal problems," *Technometrics*, vol. 12, no. 1, pp. 55–67, 1970.

[102] S.-J. Kim, K. Koh, M. Lustig, S. Boyd, and D. Gorinevsky, "An interior-point method for large-scale l1-regularized least squares," *IEEE journal of selected topics in signal processing*, vol. 1, no. 4, pp. 606–617, 2007.

[103] T. Chen and L. Ljung, "On kernel design for regularized lti system identification," *arXiv preprint arXiv:1612.03542*, 2016.

[104] T. Chen and L. Ljung, "Implementation of algorithms for tuning parameters in regularized least squares problems in system identification," *Automatica*, vol. 49, no. 7, pp. 2213–2220, 2013.

[105] G. Oetken, T. Parks, and H. Schussler, "New results in the design of digital interpolators," *IEEE Transactions on Acoustics, Speech, and Signal Processing*, vol. 23, no. 3, pp. 301–309, 1975.

[106] H. Bozdogan, "Model selection and akaike's information criterion (AIC): The general theory and its analytical extensions," *Psychometrika*, vol. 52, no. 3, pp. 345–370, 1987.

[107] J. Hagberg, R. Hickson, A. Ehsani, and J. Holloszy, "Faster adjustment to and recovery from submaximal exercise in the trained state," *Journal of Applied Physiology*, vol. 48, no. 2, pp. 218–224, 1980.